U.S. DEPARTMENT OF COMMERCE
National Technical Information Service

PB-296 095

A Lagrangian Approach to Modeling Air Pollutant Dispersion: Development and Testing in the Vicinity of a Roadway

Systems Applications, Inc, San Rafael, CA

Prepared for

Environmental Sciences Research Lab, Research Triangle Park, NC

Apr 79

United States
Environmental Protection
Agency

Environmental Sciences Research
Laboratory
Research Triangle Park NC 27711

EPA-600/4-79-023
April 1979

Research and Development

PB 296095

EPA

A Lagrangian Approach to Modeling Air Pollutant Dispersion

Development and Testing in the Vicinity of a Roadway

REPRODUCED BY
NATIONAL TECHNICAL
INFORMATION SERVICE
U.S. DEPARTMENT OF COMMERCE
SPRINGFIELD, VA. 22161

RESEARCH REPORTING SERIES

Research reports of the Office of Research and Development, U.S. Environmental Protection Agency, have been grouped into nine series. These nine broad categories were established to facilitate further development and application of environmental technology. Elimination of traditional grouping was consciously planned to foster technology transfer and a maximum interface in related fields. The nine series are:

1. Environmental Health Effects Research
2. Environmental Protection Technology
3. Ecological Research
4. Environmental Monitoring
5. Socioeconomic Environmental Studies
6. Scientific and Technical Assessment Reports (STAR)
7. Interagency Energy-Environment Research and Development
8. "Special" Reports
9. Miscellaneous Reports

This report has been assigned to the ENVIRONMENTAL MONITORING series. This series describes research conducted to develop new or improved methods and instrumentation for the identification and quantification of environmental pollutants at the lowest conceivably significant concentrations. It also includes studies to determine the ambient concentrations of pollutants in the environment and/or the variance of pollutants as a function of time or meteorological factors.

This document is available to the public through the National Technical Information Service, Springfield, Virginia 22161.

TECHNICAL REPORT DATA
(Please read Instructions on the reverse before completing)

1. REPORT NO. EPA-600/4-79-023	2.
3. RECIPIENT'S ACCESSION NO. PB296095	
4. TITLE AND SUBTITLE A LAGRANGIAN APPROACH TO MODELING AIR POLLUTANT DISPERSION Development and Testing in the Vicinity of a Roadway	5. REPORT DATE April 1979 6. PERFORMING ORGANIZATION CODE
7. AUTHOR(S) R. G. Lamb, H. Hogo, L. E. Reid	8. PERFORMING ORGANIZATION REPORT NO.
9. PERFORMING ORGANIZATION NAME AND ADDRESS Systems Applications, Inc. 950 Northgate Drive San Rafael, CA 94903	10. PROGRAM ELEMENT NO. 1AA815B CA-033 (FY-78) 11. CONTRACT/GRANT NO. 68-02-2733
12. SPONSORING AGENCY NAME AND ADDRESS Environmental Sciences Research Laboratories - RTP, NC Office of Research and Development U. S. Environmental Protection Agency Research Triangle Park, NC 27711	13. TYPE OF REPORT AND PERIOD COVERED Final 3/78 - 9/78 14. SPONSORING AGENCY CODE EPA/600/09
15. SUPPLEMENTARY NOTES	

16. ABSTRACT

A microscale roadway dispersion model based on Lagrangian diffusion theory has been developed and tested. The model incorporates similarity expressions for the mean wind and turbulence energy in the atmospheric boundary layer, through which the effects of wind shear and atmospheric stability are taken into account, and a parameterization of vehicle wake turbulence. Through simple modifications, the model can be structed to treat particle settling, deposition, and resuspension, as well as buoyancy of the effluent material. Calm winds, winds parallel to the roadway, flows around depressed or elevated roadways, shallow mixed layers, and transient of spatially variable meteorological conditions can all be explicity taken into account within the framework of the modeling approach.

The model was tested by applying it to the 30-minute experimental periods reported in the General Motors sulfate study. Of the 1040 predicted values of the mean concentration of an inert material (SF_6), half were found to be within +30 percent of the measured values. The overall correlation coefficient was 0.91. The computer time (but not core storage) required by the model is directly proportional to the distance between the farthest receptor and the road. For the studies reported the model requires on the average 20 seconds of CPU time on the CDC 7600 to simulate each of the 30-minute General Motors experiments.

17. KEY WORDS AND DOCUMENT ANALYSIS

a. DESCRIPTORS	b. IDENTIFIERS/OPEN ENDED TERMS	c. COSATI Field/Group
*Air pollution *Roads *Atmospheric diffusion *Mathematical models Lagrangian functions Development Tests		13B 04A 12A 14B

18. DISTRIBUTION STATEMENT RELEASE TO PUBLIC	19. SECURITY CLASS *(This Report)* UNCLASSIFIED 20. SECURITY CLASS *(This page)* UNCLASSIFIED	21. NO. OF PAGES 117 22. PRICE PCA06/A01

EPA Form 2220-1 (9-73)

EPA-600/4-79-023
April 1979

A LAGRANGIAN APPROACH TO MODELING AIR POLLUTANT DISPERSION
Development and Testing in the Vicinity of a Roadway

by

R. G. Lamb, H. Hogo, and L. E. Reid
Systems Applications, Inc.
950 Northgate Drive
San Rafael, California 94903

Contract No. 68-02-2733

Project Officer

R. E. Eskridge
Meteorology and Assessment Division
Environmental Sciences Research Laboratory
Research Triangle Park, North Carolina 27711

ENVIRONMENTAL SCIENCES RESEARCH LABORATORY
OFFICE OF RESEARCH AND DEVELOPMENT
U.S. ENVIRONMENTAL PROTECTION AGENCY
RESEARCH TRIANGLE PARK, NORTH CAROLINA 27711

DISCLAIMER

This report has been reviewed by the Environmental Science Research Laboratory, U.S. Environmental Protection Agency, and approved for publication. Approval does not signify that the contents necessarily reflect the views and policies of the U.S. Environmental Protection Agency, nor does mention of trade names or commercial products constitute endorsement or recommendation for use.

ABSTRACT

We have developed and demonstrated a microscale roadway dispersion model based on Lagrangian diffusion theory. The model incorporates similarity expressions for the mean wind and turbulence energy in the atmospheric boundary layer, through which the effects of wind shear and atmospheric stability are taken into account; a parameterization of vehicle wake turbulence; and provisions for predicting the turbulence quantities required to simulate second-order chemical reactions. Through simple modifications, the model can be structured to treat particle settling, deposition, and resuspension, as well as buoyancy of the effluent material. Calm winds, winds parallel to the roadway, flows around depressed or elevated roadways, shallow mixed layers, and transient or spatially variable meteorological conditions can all be explicitly taken into account within the framework of our modeling approach. The model requires minimum computer core storage and fairly small execution times. It is not based on finite difference equations, and therefore, it is free of the truncation errors and computational stability and convergence problems that models based on those methods encounter.

We demonstrated the model by applying it to 52 of the 30-minute experimental periods reported in the GM sulfate study. Of the 1040 predicted values of the mean concentration of an inert material (SF_6), we found half of them to be within ±30 percent of the measured values. The overall correlation coefficient was 0.91. The monitoring sites treated ranged in distance from 2 to 100 meters from the edge of the roadway. The computer time (but not core storage) required by our model is directly proportional to the distance between the farthest receptor and the road. For the studies reported here, the model required on the average 20 seconds of CPU time on the CDC 7600 to simulate each of the 30-minute GM experiments.

One finding from our tests of the model is that vehicle wake turbulence is important in dispersing material near the roadway, especially under stable atmospheric conditions. The great improvement in the accuracy of the predicted concentrations achieved by adding just a simple parameterization of the wake indicates that concentration levels close to the road are relatively insensitive to the intensity of ambient turbulence.

Further refinement and testing of this model is planned to improve the wake turbulence parameterization, to evaluate in more detail the accuracy of the method used to simulate ambient turbulence effects under combined light wind and very unstable situations, to incorporate the nonlinear chemical reaction simulation capability, to make the simple modifications necessary to simulate fugitive dust dispersion, and to optimize the computer code.

CONTENTS

Abstract iii

Illustrations vi

Tables viii

I. Introduction 1

II. Formulation of the Model 7

A. General Formulation 7

B. Determining the Function J and Its Time Integral 13

C. Application to Photochemical Pollutants 18

III. Model Testing 21

IV. Meteorological Inputs to the Model 27

V. Results of Preliminary Model Validation Experiments 52

A. Simulations That Neglect Wake Effects 52

B. Simulations That Include a Simple Parameterization of Wake Effects 55

VI. Summary 68

Appendices

A. A Scheme for Simulating Particle Pair Motions in Turbulent Fluid 69

B. User's Guide to the Lagrangian Highway Model 91

References 104

ILLUSTRATIONS

Number		Page
1	Schematic Illustration of the Relationship Between the Lagrangian and Eulerian Approaches to Turbulent Diffusion	4
2	Coordinate System Used in the Roadway Model To Compute Concentrations at an Arbitrary Receptor Site.	8
3	Schematic Illustration of Some of the Parameters Required and the Method Used To Calculate p	15
4	Example of the Dependence of $\overline{J}^K$ on the Number of Realizations K. . .	17
5	Sample Particle Trajectories with $\bar{u}$ = 3.0, $\overline{u'^2}$ = 1, and $\overline{w'^2}$ = 0.6 (MKS Units)	22
6	The Root-Mean-Square Particle Dispersion Component σ_x as a Function of Travel Time for Two Values of the Integral Time Scale T	23
7	Comparison of Roadway Model Predicted Cross-Wind Integrated Concentration with Gaussian Plume Formula Predictions at a Distance of 100 m Downwind of a Point Source at 50 m Elevation . . .	24
8	Comparison of Roadway Model Predicted Cross-Wind Integrated Concentrations with Gaussian Plume Formula Predictions at a Distance of 100 m Downwind of a Point Source at 5 m Elevation. . . .	25
9	Coordinate System Used To Express Mean Wind and Turbulence Velocities	29
10	Observed Versus Predicted Mean Wind Speed	36
11	Observed Versus Predicted Values of $\overline{u'^2}^{1/2}$ and $\overline{w'^2}^{1/2}$	39
12	Observed Versus Predicted Values of u' = $\overline{u'^2}^{1/2}$ and w' = $\overline{w'^2}^{1/2}$ . . .	42
13	Observed Versus Predicted Values of u' and w'.	44
14	Plots of the Ratio of the Wind Speed at 10.5 and 1.5 Meters and the Drag Coefficient $u_*/\bar{u}(10.5)$ Given by Similarity Theory as Functions of 1/L.	47

Number		Page
15	Comparison of the u_* and 1/L Values of Table 1 with Those Derived Using the WSR Method	49
16	Comparison of Observed SF_6 Concentrations with Those Simulated by the Roadway Model with Vehicle Wake Turbulence Neglected: All Experiments Included	54
17	Comparison of Observed SF_6 Concentrations with Those Simulated by the Roadway Model with Vehicle Wake Turbulence Neglected: Data Points for Day 295 ($\bar{u} < 1$ m/sec, $R_i > 0.25$) Omitted	56
18	Comparison of Observed SF_6 Concentrations with Those Predicted by the Roadway Model with Wake Turbulence Effects Parameterized: All Experiments (1100 Data Points) Included	59
19	Comparison of Observed SF_6 Concentrations with Those Predicted by the Roadway Model with Wake Turbulence Effects Parameterized: Results Displayed for Stably Stratified Flows Only (580 Data Points)	61
20	Comparison of Observed SF_6 Concentrations with Those Predicted by the Roadway Model with Wake Turbulence Effects Parameterized: Results Displayed for Unstably Stratified Flows Only (520 Data Points)	62
21	Comparison of Observed Peak SF_6 Concentrations for Each of the 55 GM Experiments with the Values Predicted by the Model (Wake Effects Included)	64
22	Distribution of Fractional Error	67
A-1	Streamwise Component $(\overline{\ell^2} - \ell 0)_x^{2\,1/2}$ of the rms Separation of Simulated Particle Motions Under the Conditions $\bar{u}$ - 3.0, $u'^2 = 1$, and $w'^2 = 0.6$ for Two Values of the Parameter a_0	89

TABLES

Number		Page
1	Estimated Values of u_* and L for the GM Experiment Periods (z_0 - 5 cm) and the Angle $\bar{\theta}$ of the Mean Wind Relative to the Road.	33
2	Model Performance Statistics	66
B-1	Format for Card 1	93
B-2	Format for Cards 3 and 4	94
B-3	Format for the Monitor Site Cards.	96
B-4	Format for the First Meteorological Data Card.	96
B-5	Format for the Second Meteorological Data Card	98
B-6	Format for the Source Location Card.	98
B-7	Format for the Miscellaneous Data Cards.	99
B-8	Sample Input Deck Used in the GM Simulations	100

I INTRODUCTION

The General Motors (GM) Sulfate Dispersion Experiment conducted in late 1975 and reported by Cadle et al. in 1976 revived interest in roadway diffusion modeling. The study not only raised a controversy about the adequacy of existing roadway models, but also collected a unique set of turbulence and concentration data in a roadway environment under well-monitored conditions. The work described in this report is in part an indirect outgrowth of the GM study: Although the basic theory of the model described here was developed several years ago, it was implemented and tested under contract to EPA as part of the roadway model development activity at EPA that the GM study encouraged.

Prior to 1976, the most widely used model for performing environmental impact assessments of roadways was HIWAY, a model based on the Gaussian plume formula (Zimmerman and Thompson, 1975). Comparisons made by Chock (1977) of the predictions of HIWAY and concentration values measured during the GM study revealed that HIWAY seriously overpredicted concentrations, especially during stable, light wind conditions. The generally poor performance of HIWAY was not surprising, considering the host of simplifying assumptions inherent in the Gaussian plume formula on which it is based. In addition to neglect of streamwise diffusion, an assumption that is invalid during light winds, other simplifying assumptions include neglect of vehicle wake turbulence, dismissal of wind shear effects, and use of interpolation to obtain values for the dispersion parameters σ_y and σ_z from some arbitrarily chosen initial value at the source and the values measured approximately 100 meters downwind. Furthermore, the plume formula is not applicable under nonsteady or spatially inhomogeneous situations, it cannot describe dispersion that occurs around depressed or elevated roads, and it is limited to the treatment of inert pollutants.

Seeking to develop roadway models free of the restrictions inherent in the Gaussian plume formula, many investigators have turned to the diffusion equation. Among these are Danard (1972), Ragland and Pierce (1973), Egan, Epstein, and Keefe (1973), and Eskridge and Demerjian (1977). However, the diffusion equation is not a rigorously sound basis for multipoint or line source models. In deriving the K-theory diffusion equation from basic principles, one must assume that the smallest length scale of the spatial variation in the mean concentration distribution is much larger than the Lagrangian integral length scale of the turbulence (see, for example, Lamb, 1973).

The effects of this assumption and the limitation it imposes can be seen clearly in the special case of stationary, homogeneous turbulence. In this case, the eddy diffusivity K is a constant and the diffusion equation can be solved analytically. Its solution for a point source has the standard Gaussian form with $\sigma^2 = 2Kt$, where $t = x/\bar{u}$, x is distance downwind from the source, and $\bar{u}$ is the mean (uniform) wind speed. This expression is consistent with Taylor's (1921) classical result for diffusion at large distances from a source, but it is at odds with the observed, theoretically derivable relationship $\sigma^2 = \overline{u'^2}\, t^2$ that applies when t is small. Here, $\overline{u'^2}$ is the variance of the turbulent velocity fluctuations. Thus, the assumption of smooth concentration fields invoked in the derivation of the diffusion equation implicitly filters out the turbulence processes that are important during the initial period of diffusion from a point source and that are responsible for the $\sigma^2 \sim t^2$ relationship cited above. By assuming that the diffusivity K is a function of travel time t, viz., $K = 1/2\ \overline{u'^2}\, t$, one can make the diffusion equation compatible with the observed behavior of point source dispersion. But this modification can be used only if a single point or line source is present. Otherwise, no unique value of K(t) or K(x) exists.

Teske and Lewellen (1978) have developed a roadway model using a second-order turbulence closure technique. It is not clear to what extent this approach circumvents the problem just cited. Two disadvantages of

diffusion models based on second-order turbulence closure is that they are complicated and costly to operate. Also, they suffer from several problems that any model based on finite difference methods incurs. One of these is that when the winds are very light or are blowing parallel to the road, the pseudo-diffusion associated with many finite difference forms of the diffusion equation can spread material over much larger areas than ambient and vehicle wake turbulence together are capable of doing. Finite difference schemes that minimize pseudo-diffusion do so at increased costs in computer time and storage requirements. A second problem with finite difference models is that the number of grid points required, and hence the computer time needed, increases with the square of the width of the region treated. This occurs because the top of the model must be at least several times the maximum value of σ_z for the area of interest, and as we pointed out above, $\sigma_z \sim x$ initially. As a result, it is difficult to achieve the fine spatial resolution needed around the roadway without making the core and machine time requirement of the model excessive. Also, it is awkward to apply finite difference methods to areas having complex shapes, such as those of elevated and depressed roadways. Finally, one must always bear in mind that the finite difference equation is a model of the differential equation it represents and, unless care is taken, under some conditions the finite difference equation might possess solutions that are radically different from any of those of the diffusion equation.

All of the problems discussed above can be circumvented by casting the roadway model in Lagrangian form. Figure 1, which is taken from Lamb (1978a), illustrates the way in which this approach is related to the Gaussian plume and K-theory models discussed above. The theoretical aspects of the model are developed in Chapter II. We discuss below several important features of the Lagrangian approach that make it ideally suited to simulating diffusion and even some chemical reactions over short distances (up to several hundred meters) from point or line sources.

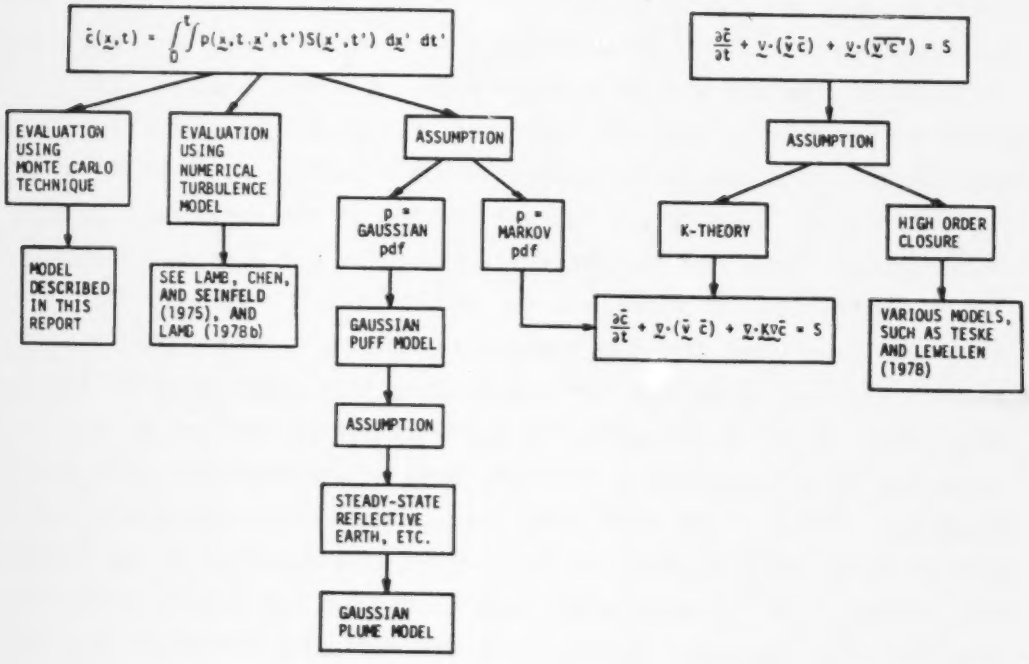
$\bar{c}(\underline{x},t) = \int_0^t \int p(\underline{x},t,\underline{x}',t')S(\underline{x}',t')\, d\underline{x}'\, dt'$
EVALUATION USING MONTE CARLO TECHNIQUE
MODEL DESCRIBED IN THIS REPORT
EVALUATION USING NUMERICAL TURBULENCE MODEL
SEE LAMB, CHEN, AND SEINFELD (1975), AND LAMB (1978b)
ASSUMPTION
p = GAUSSIAN pdf
GAUSSIAN PUFF MODEL
ASSUMPTION
STEADY-STATE REFLECTIVE EARTH, ETC.
GAUSSIAN PLUME MODEL
p = MARKOV pdf
$\frac{\partial \bar{c}}{\partial t} + \underline{v}\cdot(\bar{\underline{v}}\,\bar{c}) + \underline{v}\cdot(\overline{\underline{v}'c'}) = S$
ASSUMPTION
K-THEORY
HIGH ORDER CLOSURE
$\frac{\partial \bar{c}}{\partial t} + \underline{v}\cdot(\bar{\underline{v}}\,\bar{c}) + \underline{v}\cdot\underline{K}\underline{v}\bar{c} = S$
VARIOUS MODELS, SUCH AS TESKE AND LEWELLEN (1978)

FIGURE 1. SCHEMATIC ILLUSTRATION OF THE RELATIONSHIP BETWEEN THE LAGRANGIAN AND EULERIAN APPROACHES TO TURBULENT DIFFUSION

First, Lagrangian models require no grid network; as few or as many receptor points as desired can be used, and these can be arbitrarily distributed in any configuration over the area of interest. The computer core needs are therefore minimal. Also, the absence of a grid network and of finite differencing schemes makes the computational task of modeling dispersion around elevated or depressed roadways (or even that of modeling transport and diffusion in complex terrain) relatively simple.

Secondly, the Lagrangian approach is essentially free of the restricting assumptions (mentioned earlier) that hinder the plume and K-theory models in certain instances. The roadway model we develop here can explicitly account for the following effects: wind shear; particle settling, deposition, and resuspension; buoyancy of the effluent; calm winds or flows parallel to the roadway; vehicle wake turbulence; atmospheric stability; and time or space variability in the meteorological or source emissions conditions. The temporal evolution of the dispersion from the $\sigma^2 \sim t^2$ regime to that of $\sigma^2 \sim t$ described above is also properly duplicated.

Thirdly, when used in conjunction with the closure approximation developed by Lamb and Shu (1978), the Lagrangian roadway model can treat pollutant species such as NO, NO_2, O_3, and others, taking into account the effects on chemical reaction rates of turbulence-induced concentration fluctuations.

Finally, this particular modeling approach utilizes readily measurable Eulerian turbulence statistics, primarily the variances of the velocity fluctuations, rather than Lagrangian statistics like the σ parameter used in puff and plume models. In this report, we show that available empirical-theoretical expressions for the vertical profiles of mean wind and the required velocity variances are accurate enough for obtaining good concentration predictions through this modeling technique using only the friction velocity u_*, the Monin-Obukov length L, and an estimate of the Lagrangian integral time scale of the turbulence as input parameters.

The remainder of this report discusses the formulation of the model (Chapter II), testing of the model through comparisons of its prediction with those of another model (Chapter II), the meteorological inputs to the model, and the results of our preliminary model validation experiments. Appendix A describes a scheme for simulating particle pair motions in turbulent fluid that is the heart of the roadway model. Appendix B describes the input variables required by the model.

II FORMULATION OF THE MODEL

This chapter discusses the theoretical formulation of the roadway model and its application to photochemical pollutants.

A. GENERAL FORMULATION

For simplicity, the roadway model is cast in a two-dimensional form. The process by which this is achieved is illustrated in Figure 2. For a roadway link of sufficient length (to be established later), oriented as shown in Figure 2, the mean concentration at the receptor shown in the figure is given by:

$$\langle c(x,0,z,t) \rangle = \int_0^t \int_{-\infty}^{\infty} p(x,0,z,t|x_s,y',z_s,t') S(y',t')\, dy'\, dt' \quad , \qquad (1)$$

where z_s is the effective height of the vehicle emissions; x_s denotes the location of the road in the chosen frame (only a single lane of traffic is considered here); S is the function describing the distribution of vehicle emissions; and $p(\underset{\sim}{r},t|\underset{\sim}{r}_s,t')$ is the probability density that a particle released at $\underset{\sim}{r}'$ at time t' will be found at the point $\underset{\sim}{r}$ at time t. In Lamb (1978a), Eq. (1) is derived from basic Lagrangian principles. Note that Eq. (1) is the generalized form of the solution of the inhomogeneous, ensemble-averaged mass continuity equation of an inert substance, and p is the Green's function of that equation. For traffic of uniform speed v_s, we have:

$$S(y',t') = \sum_{n=1}^{N} Q_n \delta(y' - y_{0n} - v_n t') \quad , \qquad (2)$$

where Q_n is the emissions rate (mass/time) of the n-th vehicle; N is the total number of vehicles operating on the link; y_{0n} is a random variable representing the position at t = 0 of the n-th vehicle; $v_n = v_s$ if the

n-th vehicle is moving toward +y, $v_n = -v_s$ otherwise; and δ is the delta function.

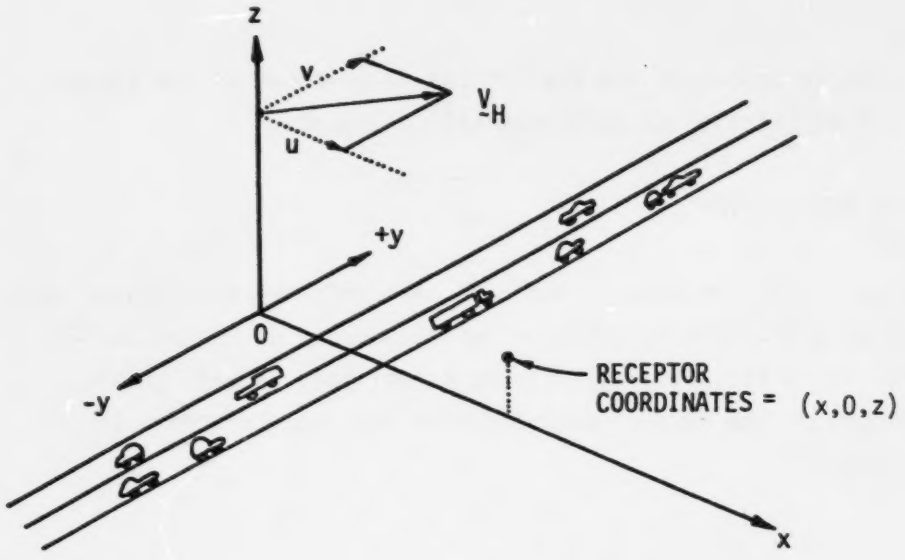

$\underset{\sim}{V}_H$ = mean wind vector

u = component of $\underset{\sim}{V}_H$ normal to roadway

v = component of $\underset{\sim}{V}_H$ parallel to roadway

0 = coordinate origin; y axis parallel to road with receptor lying in x-z plane

FIGURE 2. COORDINATE SYSTEM USED IN THE ROADWAY MODEL TO COMPUTE CONCENTRATIONS AT AN ARBITRARY RECEPTOR SITE

Owing to the symmetry of the roadway about the x-z plane, we can assume that the component of diffusion parallel to the roadway is negligible, in which case,

$$p(x,0,z,t|x_s,y',z_s,t') = p(x,z,t|x_s,z_s,t')\delta[y' + (t - t')v] \quad , \qquad (3)$$

where v is the component of the mean wind parallel to the road (see Figure 2). Substituting Eqs. (2) and (3) into Eq. (1) and evaluating the y' integral, we obtain

$$\langle c(x,0,z,t)\rangle = \sum_{n=1}^{N} Q_n \int_0^t p(x,z,t|x_s,z_s,t')\delta[t'(v - v_n) - tv - y_{0n}]\, dt' \quad . \tag{4}$$

Let $\xi = (v - v_n)t' = V_n t'$. Then Eq. (4) can be written in the form:

$$\langle c(x,0,z,t)\rangle = \sum_{n=1}^{N} Q_n \int_0^{V_n t} p\left(x,z,t|x_s,z_s,\frac{\xi}{V_n}\right)\delta(\xi - vt - y_{0n})\frac{d\xi}{V_n}$$

$$= \sum_{n=1}^{N} \frac{Q_n}{|V_n|} J_n \quad , \tag{5a}$$

where

$$J_n(x,z,t|x_s,z_s) = \begin{cases} p\left(x,z,t|x_s,z_s,\dfrac{vt + y_{0n}}{V_n}\right) & , \quad \text{if } 0 \le vt + y_{0n} \le V_n t \text{ and } V_n \ge 0, \text{ or if } 0 \ge vt + y_{0n} \ge V_n t \text{ and } V_n < 0; \\ 0 & , \quad \text{otherwise.} \end{cases} \tag{5b}$$

To arrive at Eq. (5a), we made use of the following well-known property of the delta function:

$$\int_a^b f(x)\delta(x - x_0)dx = f(x_0) \quad , \quad a < x_0 < b \quad .$$

It is perhaps instructive to comment briefly on the physical meaning of Eq. (5). The delta function in this equation is the effective source strength function. Keeping in mind that $\delta(\xi)$ is nonzero only when $\xi = 0$ and that y_{0n} is a random sequence describing vehicle locations at t = 0,

we see that the source function S in our roadway model is a random sequence of instantaneous point sources distributed in time in a manner determined by the combination of vehicle and wind speed components v_n and v. For example, if v = 0, i.e., if the winds are either calm or blowing perpendicular to the road, then the delta function in Eq. (5) is nonzero only when $t'v_n + y_{0n} = 0$. By definition of y_{0n}, this occurs only at the instant t' when the n-th vehicle passes through the x-z plane of the receptor. This obvious result occurs because, when v = 0 and the roadway is symmetric about the receptor plane, only those pollutants released in that plane can, in effect, influence that receptor. As a second example, suppose that all vehicles are stopped, $v_n = 0$, but $v \neq 0$. In this case, the delta function in Eq. (5) is nonzero, for a given t, when $(t - t')v = -y_{0n}$. In other words, emissions released at time t' from the n-th vehicle affect the receptor at the time $t = t' - (y_{0n}/v)$ when those emissions pass through the receptor plane.

Consider the special case where $V_n = v - v_n = 0$, which represents the situation where the speed and direction of the n-th vehicle are identical to those of the wind component parallel to the roadway. In this case, the $\langle c \rangle$ equation is best obtained from Eq. (4) rather than from the transformed Eq. (5). We then have:

$$\left\langle c(x,0,z,t) \right\rangle = \sum_{n=1}^{N} Q_n \delta (v_n t + y_{0n}) \int_0^t p(x,z,t|x_s,z_s,t')\, dt' \quad . \qquad (6)$$

This is simply the superposition of N two-dimensional plumes (recall that we are neglecting diffusion in the y-direction), each located at the y-position of its source at time t, i.e., at $y = y_{0n} + v_n t$. The n-th plume passes through the receptor plane y = 0 at time $t = -y_{0n}/v_n$. This relationship reveals the obvious result that, if the vehicles are northbound, i.e., v_n (= v) > 0, then only those whose initial locations are south of the receptor plane, i.e., $y_{0n} < 0$, will affect concentrations at the monitoring site.

In most problems of interest, it is the time-averaged concentration near the roadway that is of concern. The averaging time T should be long

compared with the time scales of mixing and transport from the road to the farthest monitor, but short compared with the smallest time scale of temporal changes in the vehicle flow rate and meteorology; otherwise the time-averaged concentration would depend on the length of the averaging interval. A time average is denoted by an overbar ($\bar{}$) and defined as:

$$\langle \bar{c}(x,z,t) \rangle \equiv \frac{1}{T} \int_{t-(T/2)}^{t+(T/2)} \langle c(x,z,t') \rangle \, dt' \quad . \tag{7}$$

The dependence of $\langle \bar{c} \rangle$ on t is a consequence of the dependence of c on vehicle flow rate and meteorology, which are functions of the time of day, t. From here on, we drop the reference to t in $\langle \bar{c} \rangle$ since, for a given constant set of external conditions, $\bar{c}$ is independent of time. Substituting Eq. (5) into (7), we obtain:

$$\langle \bar{c}(x,z) \rangle = \sum_{n=1}^{N} \frac{Q_n}{T|v - v_n|} \int_0^T J_n(x,z,t) \, dt \quad . \tag{8}$$

Recall that N is the total number of vehicles operating on the roadway. In most cases, not all of these vehicles will influence the concentration at the given receptor sites. For example, if the mean wind is perpendicular to the highway, then only those vehicles that pass through the receptor plane contribute to the concentration levels observed. However, if the vehicles are all stopped or moving very slowly and if there exists a sizable component of the wind parallel to the roadway, many more vehicles than those that pass through the receptor plane will affect concentrations at the designated sites. Barring this and similar cases, we can reduce Eq. (8) to the form:

$$\langle \bar{c}(x,z) \rangle = \sum_{m=1}^{M} \frac{\dot{n}_m Q_m}{|v - v_m|} \int_0^\infty J(x,z,t'|x_{sm},z_{sm}) \, dt' \quad , \tag{9}$$

where $\dot{n}_m$ is the flow rate (vehicles/time) of vehicles of type m, all of which have the same emission rate Q_m, speed v_m, and location (x_{sm},z_{sm}) in the receptor plane. For example, automobiles in one lane might represent the group designated by m = 1, trucks in that lane might constitute m = 2, autos in another lane might be represented by m = 3, and so on. [To obtain Eq. (9), note that the number N of vehicles that pass through the receptor plane in a period T is $N = \sum_{m=1}^{M} \dot{n}_m T$.]

Equation (9) is identical to that of the mean concentration produced by M steady, continuous line sources of strengths $\dot{n}_m Q_m (|v - v_m|)^{-1}$. The dependence of the effective line source strength on the wind speed component v is noteworthy because it has not been taken into account in previous line source roadway models. The error produced by this omission is small in cases of light winds where $|v_s| >> |v|$; but on congested roadways or in situations where there is a strong component of the wind parallel to the road, errors of 20 percent or larger can result in the $\langle\bar{c}\rangle$ estimates if v is neglected in the source strength calculation.

Looking back over the steps that led to Eq. (5), we find that this equation becomes invalid if a significant fraction of the emissions that affect the receptor arise from portions of the roadway that are not parallel to the y-axis. A condition on the length of roadway that must be straight in the vicinity of the receptor to render Eq. (5) accurate can be derived as follows. Let

$$T_L \equiv \min\left(\frac{|x_R - x_s|}{u_c} \ , \ \frac{|z_R - z_s|}{w_c}\right) \ , \qquad (10)$$

where (x_R,z_R) denotes the receptor coordinates,

$$u_c = \frac{d}{dt}(\bar{x} + \sigma_x) \ , \qquad (11a)$$

$$w_c = \frac{d}{dt}(\bar{z} + \sigma_z) \ , \qquad (11b)$$

and $(\bar{x},\bar{z})$ is the centroid of an instantaneous cloud of emissions and σ_x and σ_z are (roughly) the cloud dimensions. [See, for example, Monin and Yaglom

(1971) for similarity theory expressions for $\bar{x}$, $\bar{z}$, σ_x, and σ_z.] Under these definitions, T_L is a measure of the time required for material released at (x_s, z_s) to reach the receptor (x_R, z_R) through the combined actions of transport and diffusion. Thus, the roadway in the vicinity of the receptor must be straight for a distance L_s that satisfies the condition

$$L_s >> vT_L \quad , \tag{12}$$

because otherwise significant quantities of material could reach the receptor from points whose projection on the receptor plane are different from the assumed point (x_s, z_s). Subject to this constraint, Eq. (8) can be used as the basis of a roadway model in general situations, and Eq. (9) can be used in cases in which the vehicle and wind speed components are such that the line source approximation is valid [see the discussion preceding Eq. (9)].

B. DETERMINING THE FUNCTION J AND ITS TIME INTEGRAL

The kernel p that enters in the definition of J [see Eq. (5b)] is the probability density that a material particle released at the point (x_s,z_s) at a specified time, say t', will be at the point (x,z) at the later time t. In situations in which the meteorology is quasi-steady, as we have already assumed, the turbulence can be considered to be stationary, in which case the kernel p is a function only of the travel time $\tau = t - t'$ and not of t and t' jointly. In this case, by virtue of the definition of p, the quantity $p(x,z,\tau|x_s,z_s,0)\,dx\,dz$ is equal to the fraction of all realizations of the turbulence in which a particle released at (x_s,z_s) is located after a travel time τ in the box of dimensions (dx,dz) centered at (x,z). That is,

$$p(x,z,\tau|x_s,z_s,0) = \lim_{K\to\infty} \frac{1}{K\,dx\,dz} \sum_{k=1}^{K} \phi_k(x,z,\tau|x_s,z_s) \quad , \tag{13a}$$

where

$$\phi_k(x,z,\tau|x_s,z_s) = \begin{cases} 1 \ , & \text{if a particle released at } (x_s,z_s) \text{ is in the box } (dx,dz) \text{ centered at } (x,z) \text{ after a travel time } \tau \text{ on realization k;} \\ 0 \ , & \text{otherwise.} \end{cases} \tag{13b}$$

Combining Eqs. (13a) and (5b) and integrating with respect to τ, we obtain:

$$\int_0^T J(x,z,\tau|x_s,z_s)\, d\tau = \lim_{K\to\infty} \frac{1}{K\, dx\, dz} \sum_{k=1}^{K} \Delta t_k(x,z|x_s,z_s;T) \quad , \qquad (14)$$

where $\Delta t_k(x,z|x_s,z_s;T)$ is the total time spent during the period T by a particle released at (x_s,z_s) on realization k in the box (dx,dz) centered at (x,z).

Equation (14) provides an operational procedure for implementing the roadway model numerically: If the random turbulence velocity fields could be simulated by a Monte Carlo type of process, then particles could be released at any desired locations (x_s,z_s) in the simulated flows, their motions could be tracked, and Eq. (14) could be evaluated computationally. The resulting values could then be used in either Eq. (8) or Eq. (9) to compute mean concentrations at any desired locations.

We can illustrate the method in more detail with the aid of Figure 3. For the given roadway site and meteorological conditions, we specify the profiles of the mean wind $\bar{u}(z)$--note that only the component $\bar{u}$ normal to the roadway affects the kernel p, the profiles of the variances $\overline{u'^2}(z)$ and $\overline{w'^2}(z)$ of the ambient turbulent velocity components in the receptor plane, and the profile of the Lagrangian integral time scale $\mathcal{T}(z)$. The functional forms used for each of these profiles under various meteorological conditions are listed later in Chapter IV. To account for the effects of vehicle wake turbulence, it is also necessary to specify the speed and drag coefficient of the vehicles and certain other parameters descriptive of their wakes. At present, there are no accurate theoretical or empirical descriptions of the wake turbulence generated by automobiles moving along a roadway. Consequently, only approximations of the wake effects can be incorporated into the dispersion model. The method we have chosen is to express the variances of the lateral and vertical components of the wake turbulence velocities as functions

of the energy dissipated by drag forces on the vehicle and distance from the vehicle and then to estimate the integral time scale T_{wake} of the wake turbulence. The last quantity and the prescribed wake velocity variances are then used to simulate particle dispersion by the wake in the same manner (described later) in which the velocity and time scale properties of the ambient turbulence depicted in Figure 3 are used to describe dispersion by boundary layer turbulence. The technique is described below.

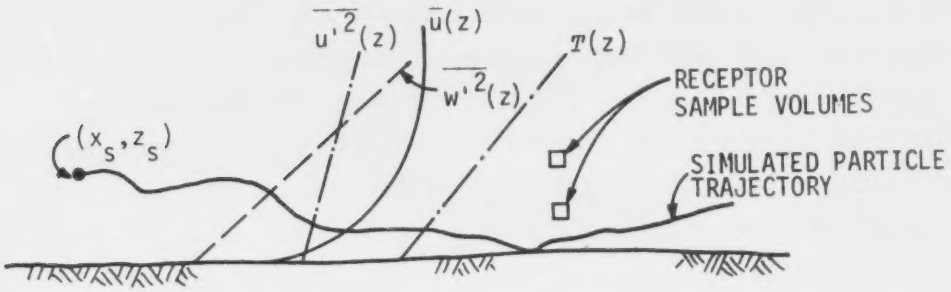

FIGURE 3. SCHEMATIC ILLUSTRATION OF SOME OF THE PARAMETERS REQUIRED AND THE METHOD USED TO CALCULATE p

Let (x_s, z_s) be the release point at which we wish to evaluate the density function p. A particle is released from this point at time $\tau = 0$. In the atmosphere, it acquires velocity components $u_p(\tau)$ and $w_p(\tau)$ that are given by:

$$u_p(\tau) = \frac{\partial x_p(\tau)}{\partial t} = \bar{u}[z_p(\tau)] + u'[z_p(\tau),\tau] + u''(\tau) \quad , \tag{15a}$$

$$w_p(\tau) = \frac{\partial z_p(\tau)}{\partial t} = w'[z_p(\tau),\tau] + w''(\tau) \quad , \tag{15b}$$

where (x_p, z_p) denotes the projection of the particle's coordinates on the receptor plane; $\bar{u}$ is the mean wind speed component normal to the roadway

(depicted in Figure 3); u' and w' are random velocities representing the ambient turbulence; and u" and w" are random velocities representing the vehicle wake turbulence. If there is a nonzero mean vertical wind component $\bar{w}$ or if the particle is positively or negatively buoyant, Eq. (15b) must be modified accordingly.

In the numerical simulation, the random velocity components u' and w' are generated at each time step by an algorithm, described in detail in Appendix A, that utilizes the variance profiles $\overline{u'^2}$ and $\overline{w'^2}$ and the Lagrangian time scale $\mathcal{T}$ of the ambient turbulence. The random wake velocities u" and w" are generated by the same process, except in this case the energy and Lagrangian time scales of the wake turbulence are used. (Further details are given in Chapter V.) Once values for all the random velocity components have been specified, these are used together with the given mean wind profile $\bar{u}$ in Eq. (15) to calculate the particle trajectory $[x_p(\tau), z_p(\tau)]$ for $0 \leq \tau \leq T$. As mentioned earlier, the integrating time period T must be large enough for any particle to pass just beyond the location of the most remote monitor.

At those sites at which the predicted particle trajectory passes through the sample volume (dx,dz) of a monitor, the time Δt_1 that the particle spends in that volume is determined. Here the subscript 1 signifies that this is the first realization of the turbulence processes.

All of the steps outlined above are now repeated, starting with the release of a new particle at (x_s, z_s) and using a new set of random velocity components u', w', u", and w" that are uncorrelated with the first set. From the new realization of the particle trajectory, we determine the residence time Δt_2 in each receptor's sample volume. By continuing this process K times, we obtain the sequence of Δt_k values required in Eq. (14) to evaluate the time integral of J that enters into the equation for the mean concentration. To determine how many realizations K are needed to render a finite sum (over K realizations) an acceptable approximation of the infinite sum of Eq. (14), we use a method in which intermediate approximations of the J integral are stored and analyzed for trends that reveal convergence.

Specifically, let

$$\overline{J}^K = \frac{1}{K\ dx\ dz} \sum_{k=1}^{K} \Delta t_k \quad , \tag{16}$$

represent the estimate of the J integral given by K realizations of the particle trajectories. Figure 4 shows how $\overline{J}^K$ might vary with K. The estimate usually varies rapidly as K increases from zero, but it becomes increasingly steady as K becomes large and $\overline{J}^K$ converges to the true value of the J integral. As a measure of the variability of $\overline{J}^K$ at realization K, we use the standard deviation $\sigma_J(K)$ of the n + 1 values $\overline{J}^K$, $\overline{J}^{K-\Delta K}$, ..., $\overline{J}^{K-n\Delta K}$, where n is any integer greater than 2 (we use 5) and ΔK is some sampling interval in K (we use ΔK = 100). We consider that $\overline{J}^K$ is an acceptable approximation of the true value of the J integral when $\sigma_J(K) \leq \lambda \overline{J}^K$, where λ is some fraction, e.g., λ = 0.01. In our studies with n = 5 and ΔK = 100, we have found that the convergence condition $\sigma_J(K) \leq \lambda \overline{J}^K$ is satisfied within K = 500 realizations at points near the core of a point source plume, while K = 2500 may be necessary to satisfy the criteria at the edge of the plume where $\overline{J}^K$ is only one-tenth the centerline value or less. We have also found that a great reduction in the computer time required by the model can be achieved with virtually no loss of accuracy by setting λ = 0.5 rather than 0.01. (We were surprised to find that by using λ = 1.0, the overall performance of the model simulations of the GM experimental data deteriorated by only 15 percent, as measured by the change in the rms error, while the computer time required dropped to 1/30 of that necessary to run the model using λ = 0.05.)

The value of $\overline{J}^K$ derived from carrying out this procedure for each monitoring site is used in either Eq. (8) or Eq. (9) for the J integral to obtain the mean concentration. Chapter III discusses the agreement between the prediction of this model and those of the Gaussian plume formula for the meteorological conditions under which the latter is known to apply.

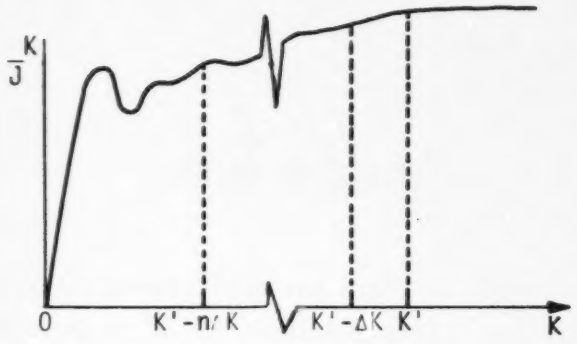

FIGURE 4. EXAMPLE OF THE DEPENDENCE OF $\overline{J}^K$ ON THE NUMBER OF REALIZATIONS K. The difference between $\overline{J}^K$ and the time value of the time integral of J is estimated from (n + 1) moving of $\overline{J}^K$ as described in the text.

C. APPLICATION TO PHOTOCHEMICAL POLLUTANTS

The roadway model can be applied to photochemical pollutants by using the closure technique developed in Lamb and Shu (1978). To facilitate this operation, we assume that pollutants are either pseudo-inert or infinitely fast reacting. This division is prompted by the fact that, in most cases of interest, T is of the order of several minutes, which is a long time compared with the reaction time of species such as NO, O_3, and sulfates around a roadway, but a short time compared with other species such as hydrocarbons. The category a given species falls into must be decided case by case, but we anticipate that around roadways, NO, O_3, and sulfates can generally be treated as infinitely fast reacting. In this case, the equations governing the mean concentrations of these species are (from Lamb and Shu, 1978):

$$\overline{c}_{NO}(\underline{r},t) = \max\left\{0\ ,\ \left[\overline{c}_{INO}(\underline{r},t) - \zeta_{NO}(\underline{r},t)\chi_{O_3}(\underline{r},t)\right]\right\} \tag{17}$$

$$\overline{c}_{O_3}(\underline{r},t) = \chi_{O_3}(\underline{r},t) - \overline{c}_{INO}(\underline{r},t) + \overline{c}_{NO}(\underline{r},t) \quad , \tag{18}$$

$$\overline{c}_{SO_4}(\underline{r},t) = \overline{c}_{ISO_4}(\underline{r},t) \quad . \tag{19}$$

Equation (19) assumes that sulfate is emitted by motor vehicles rather than formed in the atmosphere through the oxidation of SO_2. Here χ_{O_3} is the ambient ozone concentration, assumed to be given; $\bar{c}_{INO}$ is the mean concentration of NO in the absence of any chemical reactions [$\bar{c}_{INO}$ can be calculated direcely from Eq. (8) or Eq. (9)]; and ζ_{NO} is a mixing parameter, which we approximate by (see Table 1 of Lamb and Shu, 1978):

$$\zeta_{NO}(\underline{r},t) \doteq \frac{\bar{c}^2_{INO}(\underline{r},t)}{\overline{c^2_{INO}(\underline{r},t)}} \quad . \tag{20}$$

In Eqs. (17) through (20), $\underline{r} = (x,z)$ denotes the receptor location.

In summary, Eq. (8) is the roadway model equation for the mean concentrations of all pseudo-inert pollutants. This same equation is also used to compute quantities like $\bar{c}_{INO}$ that enter in Eqs. (17) through (20). The model equations for NO, O_3, and sulfate, which we consider to be rapid reactants, are Eqs. (17) and (19). Similar equations can be written for other rapid reactants. The evaluation of Eqs. (17) and (19) requires that the mixing parameter ζ be determined.

The Lagrangian theory from which Eq. (8) was derived (Lamb, 1978a) also provides an expression for c^2 that can be used to evaluate ζ. We have:

$$\overline{c^2}(\underline{r},t) = Q^2 \sum_{n=1}^{N}\sum_{m=1}^{N}\int_0^t\int_0^t p_2(x,z,t;x,z,t|x_s,z_s,t';x_s,z_s,t'') \cdot\left[\delta\ t'(v - v_{sn}) - tv - y_{On}\right]\cdot\delta\left[t''(v - v_{sm}) - tv - y_{Om}\right] dt'\ dt'' \quad , \tag{21}$$

where p_2 is the joint probability density for the displacements of a pair of particles. Note that p is a marginal density of p_2 in that the former can be obtained by integrating p_2 with respect to the position coordinates of one particle over all space. The method described earlier for

determining the J integral can be used to obtain the integrals over p_2 in Eq. (21). However, in this case we must release pairs of particles from the source point (x_s, z_s) and determine the total times that both particles are simultaneously within the sample volumes of each receptor. The algorithm described in Appendix A that we use to generate the random velocity components u', w', u", and w" of single particles can also be used to simulate the velocities of pairs of particles where motions are correlated. In this role, the algorithm requires (in addition to the turbulence velocity variance profiles and Lagrangian integral time scale) the energy dissipation rate profile $\varepsilon(z)$ of the ambient turbulence and comparable information for the vehicle wakes. Some results of particle pair simulations and mean square concentration prediction are presented in Chapter III, but applications of the roadway model to photochemical pollutants were not treated further in this study.

III MODEL TESTING

Since the model described in the previous chapter is somewhat new, it is appropriate to compare its predictions with those of other diffusion models in current use. In particular, by comparing the predictions of our model with concentration estimates obtained from the Gaussian plume formula for situations in which this formula is known to apply (namely, under conditions with no wind shear, steady meteorology and source emission rate, no chemical conversion or deposition, and so on), we can verify our approach as being basically sound. This chapter discusses these verification efforts.

We set the model up to simulate dispersion from a point source in a uniform flow (no shear) of speed $\bar{u}$ = 3.0 m/sec over a flat surface. The variances of the ambient turbulence velocities were set to $\overline{u'^2}$ = 1 m^2/sec^2 and $\overline{w'^2}$ = 0.61 m^2/sec^2. Figure 5 shows 20 simulated particle trajectories from a source 50 m high for each of two values of the time scale T. Note that as $T \to 0$, the value representative of Brownian motion, the trajectories acquire the erratic character associated with molecular scale movement. The root-mean-square (rms) particle dispersion component σ_x corresponding to the cases presented in Figures 5(a) and 5(b) are plotted in Figure 6. It is evident that the $\sigma \sim t$ and $\sigma \sim t^{1/2}$ regimes predicted for short and long travel times t, respectively, by Taylor (1921) are reproduced by the scheme we use to generate the turbulence velocities. The predicted profiles of mean, cross-wind integrated concentration under the same conditions such as those shown in Figures 5(a) and 5(b) are shown in Figure 7 along with the corresponding values given by the Gaussian plume formula. A similar comparison is given in Figure 8 for a source height of 5 m. The excellent agreement between the model and

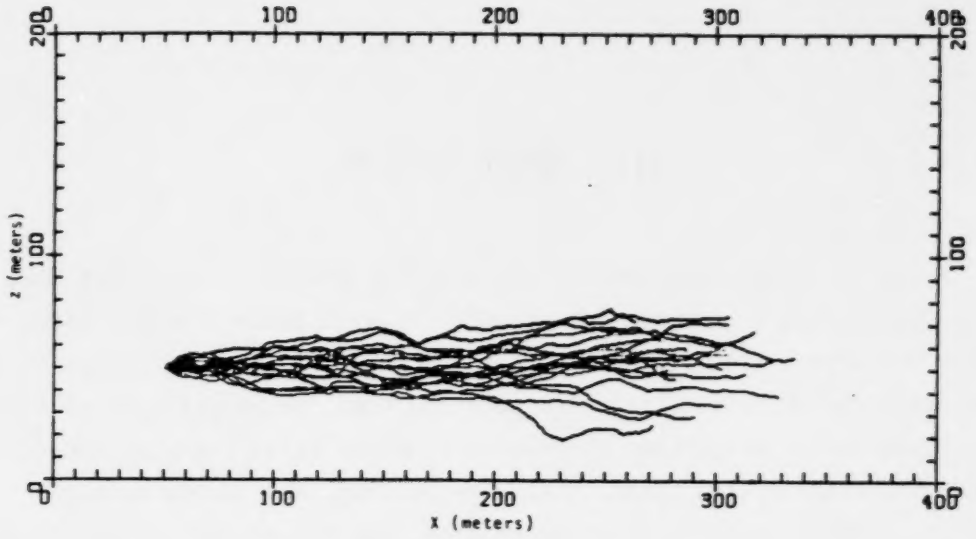

(a) T = 3 Seconds

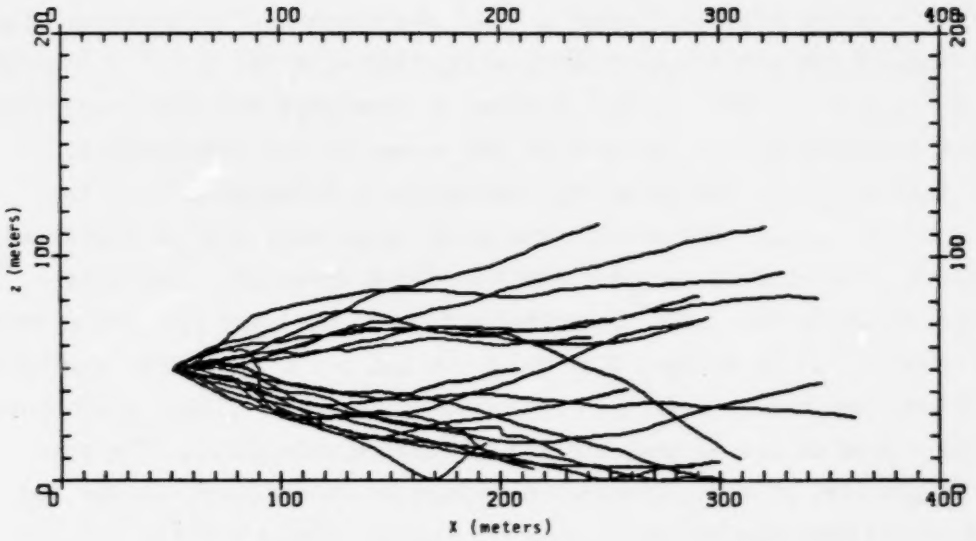

(b) T = 30 Seconds

FIGURE 5. SAMPLE PARTICLE TRAJECTORIES WITH $\bar{u}$ = 3.0, $\overline{u'^2}$ = 1, AND $\overline{w'^2}$ = 0.6 (MKS UNITS)

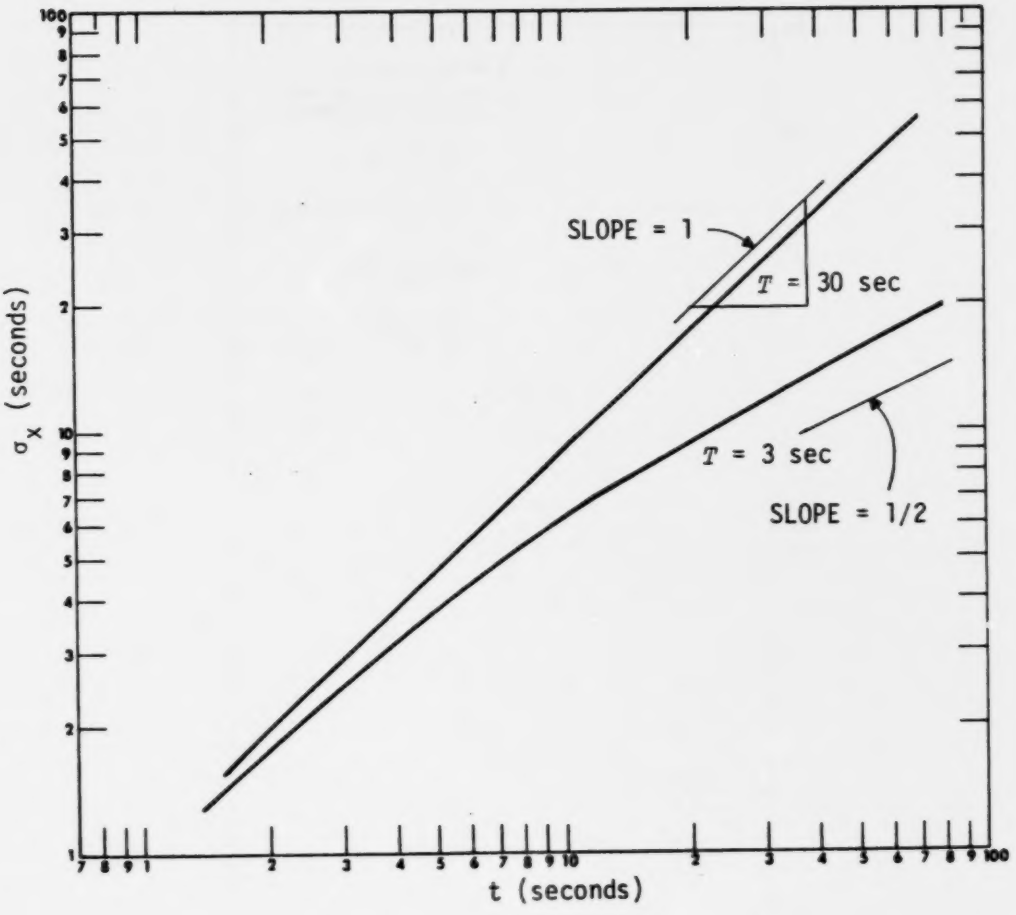

FIGURE 6. THE ROOT-MEAN-SQUARE PARTICLE DISPERSION COMPONENT σ_x AS A FUNCTION OF TRAVEL TIME FOR TWO VALUES OF THE INTEGRAL TIME SCALE T

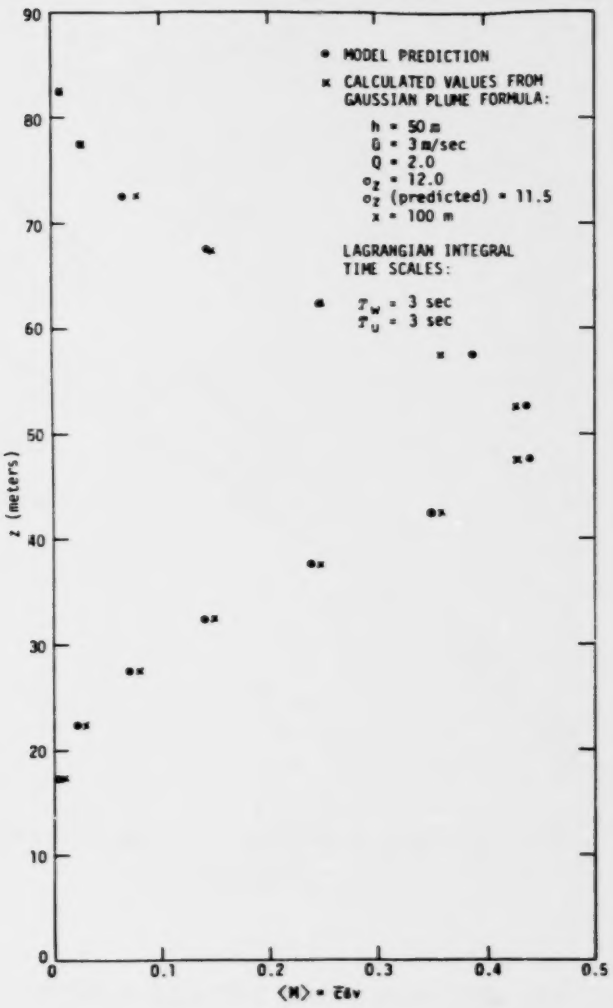

FIGURE 7. COMPARISON OF ROADWAY MODEL PREDICTED CROSS-WIND INTEGRATED CONCENTRATION WITH GAUSSIAN PLUME FORMULA PREDICTIONS AT A DISTANCE OF 100 m DOWNWIND OF A POINT SOURCE AT 50 m ELEVATION

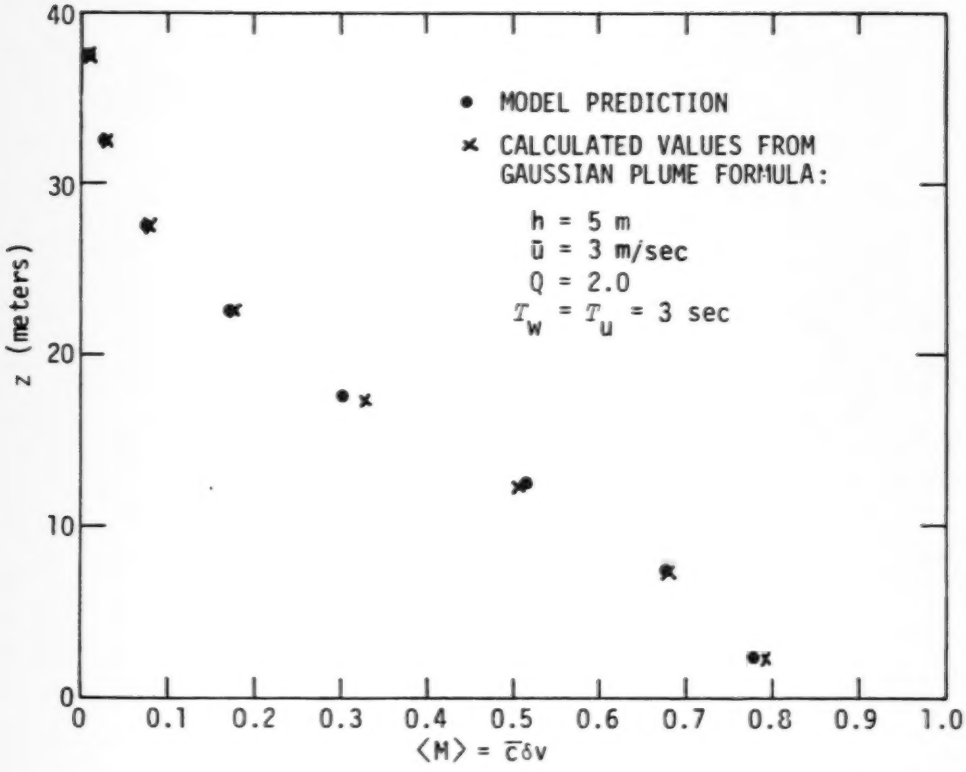

FIGURE 8. COMPARISON OF ROADWAY MODEL PREDICTED CROSS-WIND INTEGRATED CONCENTRATIONS WITH GAUSSIAN PLUME FORMULA PREDICTIONS AT A DISTANCE OF 100 m DOWNWIND OF A POINT SOURCE AT 5 m ELEVATION

plume formula predictions is evidence of the validity of our diffusion modeling approach inasmuch as the plume formula predictions are correct under the conditions used in this simulation.

IV METEOROLOGICAL INPUTS TO THE MODEL

Unlike the GM study in which extensive measurements were made of turbulence quantities, most applied pollution dispersion studies must rely on a limited set of available observations. For this reason, rather than use the GM turbulence data directly in the roadway model, we utilize theoretical-empirical expressions for the quantities required that can be evaluated given only the local values of surface roughness z_0, Obukhov length L, and mean wind speed $\bar{u}_{10}$ at 10 m. This chapter discusses these expressions in detail and compares the values they yield with those from the GM wind and turbulence data.

In Chapter II, we indicated that the model requires profiles of the mean wind component $\bar{u}(z)$ normal to the roadway, the profile $\overline{u'^2}(z)$ of the same component of the turbulent velocity variance, the profile of the vertical turbulent velocity variance $\overline{w'^2}(z)$, and the Lagrangian integral time scale T of the turbulence. The last quantity is difficult to measure because it cannot be obtained directly from turbulence velocity observations made at fixed points. Draxler (1976) has inferred approximate values for T from diffusion data collected at a number of sites. His estimates of T are of the order of 100 sec for the horizontal velocity component under both stable and unstable conditions. His suggested values for the time scale of the vertical velocity fluctuations are 60 sec under unstable conditions, and 30 sec for stably stratified flows. We found that the model predictions agreed better with the observations at the most remote sampling sites (where concentrations are most sensitive to T) if integral time scale values of only one-half those suggested by Draxler were used for the vertical velocity fluctuations. Thus, in all of our simulations, we used

$$T_u = 100 \text{ sec} \quad ,$$

$$T_w = \begin{cases} 30 \text{ sec} & , \quad \text{if} \quad L < 0 \ ; \\ 10 \text{ sec} & , \quad \text{if} \quad L \geq 0 \ , \end{cases}$$

where L is the Monin-Obukhov length.

To formulate the profiles of $\bar{u}$, $\overline{u'^2}$, and $\overline{w'^2}$, we must first express the direction of the mean wind in the coordinate system shown in Figure 9. Recall that in our model $\bar{u}$ and u' are wind components normal to the roadway, regardless of the orientation of the road. Keep in mind, too, that the component $\bar{v}$ of the wind parallel to the highway enters only the source strength term [see Eq. (8) or Eq. (9)] and that the corresponding turbulence component v' does not enter at all. This occurs because of our assumption of symmetry of the roadway with respect to the receptor plane.

The expression for $\bar{u}(z)$ is the following:

$$\bar{u}(z) = \frac{u_*}{k} g(z,L,z_0) \sin \bar{\theta} \quad , \tag{22}$$

where u_* is the friction velocity, k = 0.4 is the von Karman constant, L is the Monin-Obukhov length, z_0 is the surface roughness, and $\bar{\theta}$ is the mean wind direction in the roadway coordinates shown in Figure 9. The form of the function g is determined from similarity theory and depends on the sign of L as follows [from Ragland (1973)]:

$$1/L = 0: \quad g = \ell n\left(\frac{z + z_0}{z_0}\right) \quad ; \tag{23}$$

$$L > 0: \quad g = \ell n\left(\frac{z + z_0}{z_0}\right) + \text{MIN}\left(5.2 \frac{z}{L}, 5.2\right) \quad , \quad z \leq 6L \quad ; \tag{24}$$

$$L < 0: \quad g = 2\left(\tan^{-1} \psi - \tan^{-1} \psi_0\right) + \ell n\left[\frac{(\psi - 1)(\psi_0 + 1)}{(\psi + 1)(\psi_0 - 1)}\right] \quad ; \tag{25}$$

where

$$\psi = \left(1 - 15\,\frac{z + z_0}{L}\right)^{1/4} \quad , \tag{26a}$$

$$\psi_0 = \left(1 - 15\,\frac{z_0}{L}\right)^{1/4} \quad . \tag{26b}$$

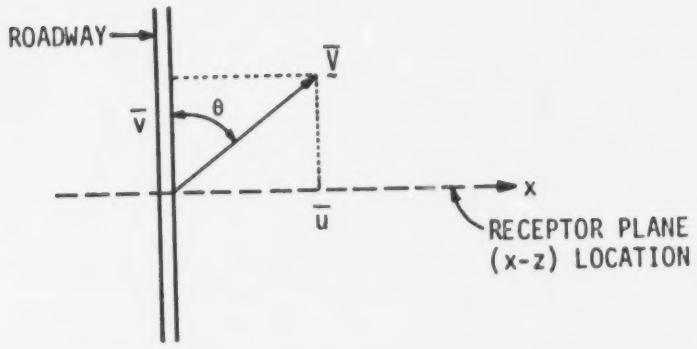

FIGURE 9. COORDINATE SYSTEM USED TO EXPRESS MEAN WIND AND TURBULENCE VELOCITIES

The expressions for $\overline{u'^2}(z)$ and $\overline{w'^2}(z)$ are derived from the semi-empirical formulation of Binkowski (1978). He gives expressions for the rms vertical velocity fluctuation σ_w and the fluctuating components σ_v and σ_u normal and parallel, respectively, to the direction of the mean wind. Translating these formulas into the coordinate system of the roadway shown in Figure 9, we obtain

$$\overline{w'^2}(z) = \sigma_w^2 = u_*^2 \left(\frac{\phi_m - \zeta}{1.2\, f_m}\right)^{2/3} \quad , \quad , \tag{27}$$

$$\overline{u'^2}(z) = [\cos 2\bar{\theta}]^{-1} \cdot \left[\sigma_v^2 + 2\left(\sigma_u^2 - \sigma_v^2\right)\sin^2\bar{\theta}\,\cos^2\bar{\theta} - \left(\sigma_u^2 + \sigma_v^2\right)\sin^2\bar{\theta}\right] \quad , \tag{28}$$

where

$$\sigma_v^2 = \frac{1}{3}\,q^2 - \sigma_w^2\left[0.13\left(\frac{2f_m - 1}{f_m}\right) + 0.08\Gamma\right] \quad , \tag{29a}$$

$$\sigma_u^2 = q^2 - \sigma_w^2 + \sigma_v^2 \quad , \tag{29b}$$

$$q^2 = \sigma_w^2\left[3.0 + 0.75\left(\frac{f_m + 1}{f_m}\right) + 1.8\Gamma\right] \quad , \tag{29c}$$

$$\Gamma = \frac{\zeta}{\phi_m - \zeta} \quad , \tag{29e}$$

$$\phi_m = \begin{cases} (1 - 16\zeta)^{-1/4} & , \quad \zeta < 0 \quad , \\ 1 + 5\zeta & , \quad \zeta \geq 0 \quad , \end{cases} \tag{29f}$$

$$f_m = \begin{cases} 0.4[0.4 + 0.6\exp(4\zeta)] & , \quad \zeta < 0 \quad , \\ 0.4(1.0 + 3.4\zeta - 0.25\zeta^2) & , \quad \zeta \geq 0 \quad , \end{cases} \tag{29f}$$

$$\zeta = \frac{z + z_0}{L} \quad , \tag{29g}$$

and $\bar{\theta}$ is the angle of the mean wind direction shown in Figure 9.

Equations (22) through (26) constitute the bases of the mean wind estimates used in the roadway model, and Eqs. (27) through (29) make up the turbulence velocity variance equations employed. Both sets of equations require as inputs the friction velocity u_*, the Monin-Obukhov length L, and the surface roughness. The remainder of this chapter describes (1) our method of checking the agreement between the values of $\bar{u}$, u'^2, and w'^2 given by Eqs. (22) through (29) and those measured during the GM study, and (2) the derivation of an empirical formula from which estimates of u_* and L can be obtained using wind speed data alone.

To obtain u_* and L values for each of the GM experiment periods, we used u_* and L as fitting parameters to arrive at least-squares fits of the mean wind profiles given by Eqs. (22) through (26) to the GM tower measurements. In the process, we also obtained a value for the surface roughness of the GM site. The following procedure was used.

First, we chose a value of z_0 in the range of values that is reasonable for the terrain surrounding the GM test facility, i.e., $0.01 < z_0 < 0.1$ meter. Then, consideration of the wind data from Towers 1, 5, and 6 only (the other towers are so close to the roadway that they are subject to vehicle wake influences) resulted in a total of nine observations of $\bar{u}$, three at each of the levels of 1.5, 4.5, and 10.5 meters, to which the least squares fitting routine could be applied. Letting ε_n be the difference between the observed value of $\bar{u}$ at station n ($n = 1, 2, \ldots, 9$) and the value calculated from the formula $u = u_\star g(z_n, L, z_0)/k$, we chose $u_\star$ such that the mean error, $\bar{\varepsilon}$, was zero. The following equations were written:

$$\varepsilon_n = \hat{u}_n - \frac{u_\star g_n}{k} \quad , \quad n = 1, \ldots, 9 \quad ; \tag{30}$$

where

$$\hat{u}_n = \text{observation at station n},$$

$$g_n = g(z_n, L, z_0) \quad ,$$

and

$$\bar{\varepsilon} = \frac{1}{9}\sum^{n}\varepsilon_n = 0 \quad ,$$

or

$$\bar{\varepsilon} = \frac{1}{9}\left(\sum^{n}\hat{u}_n - \frac{u_\star}{k}\sum^{n} g_n\right) = 0 \quad ,$$

for given z_0 and L.

Thus,

$$u_\star = k\frac{\sum^{n}\hat{u}_n}{\sum^{n} g_n} \quad . \tag{31}$$

A computer program was set up to solve the $u_\star$ values for each experiment from the initial guess of the surface roughness (z_0). Using the following equation, 100 Monin-Obukhov lengths were generated:

$$L = \exp(X) \quad , \tag{32}$$

where

$$X = 0, 0.1, 0.2, \ldots, 10.0 \quad ,$$

and

$$\text{sign}(L) = \text{sign}(R_i) \quad .$$

where R_i is the Richardson number measured during each experiment. For each of the 100 values of L, we determined u_* from Eq. (31) and the corresponding theoretical value $\bar{u}$ at each of the nine observation sites from Eq. (22), namely,

$$\bar{u}(z) = \frac{u_*}{k} g(z, L, z_0) \quad . \tag{33}$$

The mean square difference $\overline{\varepsilon^2}(L)$ between the observed wind speeds and those given by Eq. (32) for each of the 100 selected values of L was determined by:

$$\overline{\varepsilon^2}(L) = \frac{1}{9} \sum_{n=1}^{9} [\hat{u}_n - \bar{u}(z_n, z_0, L)]^2 \quad . \tag{34}$$

Of the 100 values of L, the best estimate of the true value was taken to be that for which $\overline{\varepsilon^2}$ is a minimum. The minimum values of $\overline{\varepsilon^2}$ for each of the GM experiments were then summed to obtain a "global" error for the chosen value of z_0. The entire process described above was repeated using a different guess for z_0; from the set of global errors obtained, the true value of the surface roughness z_0 was taken to be that corresponding to the minimum global error.

Using the technique outlined above, we found that a surface roughness $z_0 = 0.05$ m gave the best fit of the observed wind data to the similarity profiles. The values of u_* and L that we derived for this surface roughness are listed in Table 1 for each of the GM experiment periods.

TABLE 1. ESTIMATED VALUES OF u_* AND L FOR THE GM EXPERIMENT PERIODS (z_0 = 5 cm) AND THE ANGLE $\bar{\theta}$ OF THE MEAN WIND RELATIVE TO THE ROAD

GM Experiment	Obukhov Length (m)	u_* (m/sec)	$\bar{\theta}$ (rad)
275080	-2.7	0.20	2.50
275083	-2.7	0.29	2.28
275090	-2.7	0.37	2.76
275093	-2.7	0.41	2.81
276081	-270.4	0.20	0.56
276084	-181.2	0.20	0.64
276091	-99.4	0.27	0.83
276094	-90.0	0.30	0.99
279080	16.4	0.09	1.23
279084	24.5	0.09	1.14
279090	-121.5	0.13	1.28
279093	-109.9	0.18	1.23
281080	73.7	0.17	3.96
281083	298.9	0.11	3.86
281090	148.4	0.08	4.76
281093	1.8	0.19	4.85
283081	54.6	0.11	1.25
283085	-20.1	0.10	1.39
283092	-2.7	0.15	1.01
283095	-66.7	0.13	0.64
286081	110.0	0.21	0.19
286084	73.7	0.23	0.33
286091	2.2	0.17	0.41
286094	-330.3	0.25	0.45
290080	812.4	0.19	4.38
290083	181.3	0.18	4.15
290090	601.9	0.19	4.20
290093	1096.6	0.22	4.11
293103	-544.6	0.19	1.58

TABLE 1 (Concluded)

GM Experiment	Obukhov Length (m)	u_* (m/sec)	$\overline{\theta}$ (rad)
293110	-330.3	0.19	1.57
294080	18.2	0.14	0.87
294083	21.0	0.14	0.86
294090	-200.3	0.10	0.63
294093	-66.7	0.13	0.77
295080	4.1	0.01	4.65
295083	18.2	0.04	4.25
295090	3.7	0.03	4.15
295093	2.7	0.02	3.70
296080	134.3	0.23	0.04
296083	181.3	0.25	0.04
296090	244.7	0.28	0.16
296093	-134.3	0.26	0.19
297080	99.5	0.20	0.06
297083	90.0	0.19	0.07
297090	200.3	0.25	6.24
300080	36.6	0.19	0.28
300083	-121.5	0.19	0.43
300090	-200.3	0.21	0.37
300093	-99.5	0.21	0.41
302080	1.8	0.19	2.84
302083	-30.0	0.23	2.97
302090	-36.6	0.28	3.06
302093	-30.0	0.27	3.15
303080	1.5	0.11	2.47
303083	-1.1	0.11	2.97
303090	-1.1	0.14	3.34
303093	-5.0	0.21	3.54

Table 1 also includes the angle $\bar{\theta}$ of the mean wind. Figures 10(a) through 10(c) compare the observed wind speeds at each of the three levels of 1.5, 4.5, and 10.5 meters with the corresponding values obtained from Eqs. (22) through (26) using the u_* and L values shown in Table 1. The observations represent average wind speeds at each level in Towers 1, 5, and 6. A vast majority of the predicted speeds are within ±10 percent of the measured values, indicating that the similarity expressions incorporated in Eqs. (22) through (26) are indeed accurate representations of the wind speed profiles near the ground.

Checking the accuracies of the turbulence velocity variance expressions [Eqs. (27) through (29)] requires some caution because the measured values of these parameters are more sensitive to vehicle wake turbulence than are the mean wind components. Accordingly, we first considered only situations with westerly winds, i.e., wind directions between 250° and 290°, and used only the turbulence data collected at Tower 1, which is farthest west of the roadway. The resulting observed and predicted values of $u' = \overline{u'^2}^{1/2}$ and $w' = \overline{w'^2}^{1/2}$ are displayed in Figures 11(a) and 11(b), respectively. The observed and predicted values of w' agree quite well--60 percent of the predicted values are within ±20 percent of the measurements; but the predicted values of u' are consistently too low by about 35 percent. Almost all of the data points used in Figure 11 are for cases of unstable stratification, and it is during these conditions that the Kansas and Minnesota turbulence data, which Binkowski (1978) used to develop the formulas in Eq. (29), show the largest scatter in the σ_u and σ_v values. In fact, the scatter is sufficiently large that profiles of σ_u and σ_v exist that would be compatible with both the Binkowski and the GM data sets. We have not pursued this point. In the model validation studies (discussed in Chapter V), we simply multiplied all the u' predictions by 1.5 to eliminate the discrepancy shown in Figure 11(a).

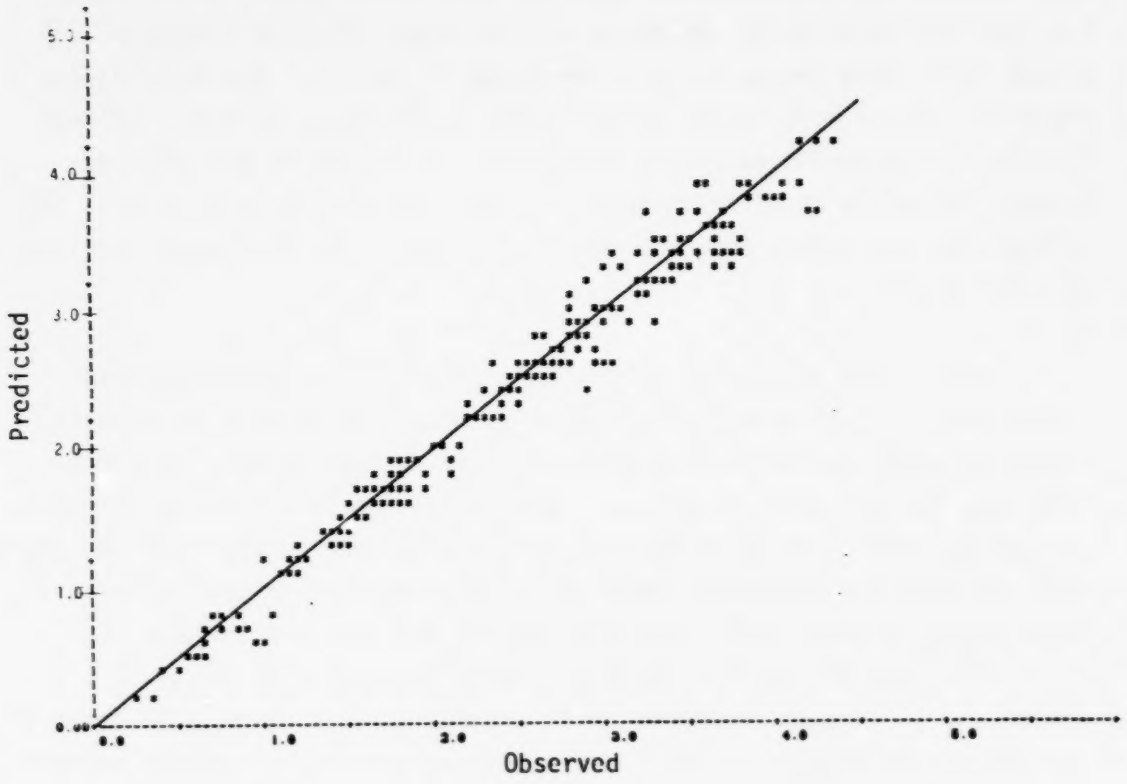

(a) $z = 10.5$ meters ($z_0 = 0.05$ meters)

FIGURE 10. OBSERVED VERSUS PREDICTED MEAN WIND SPEED

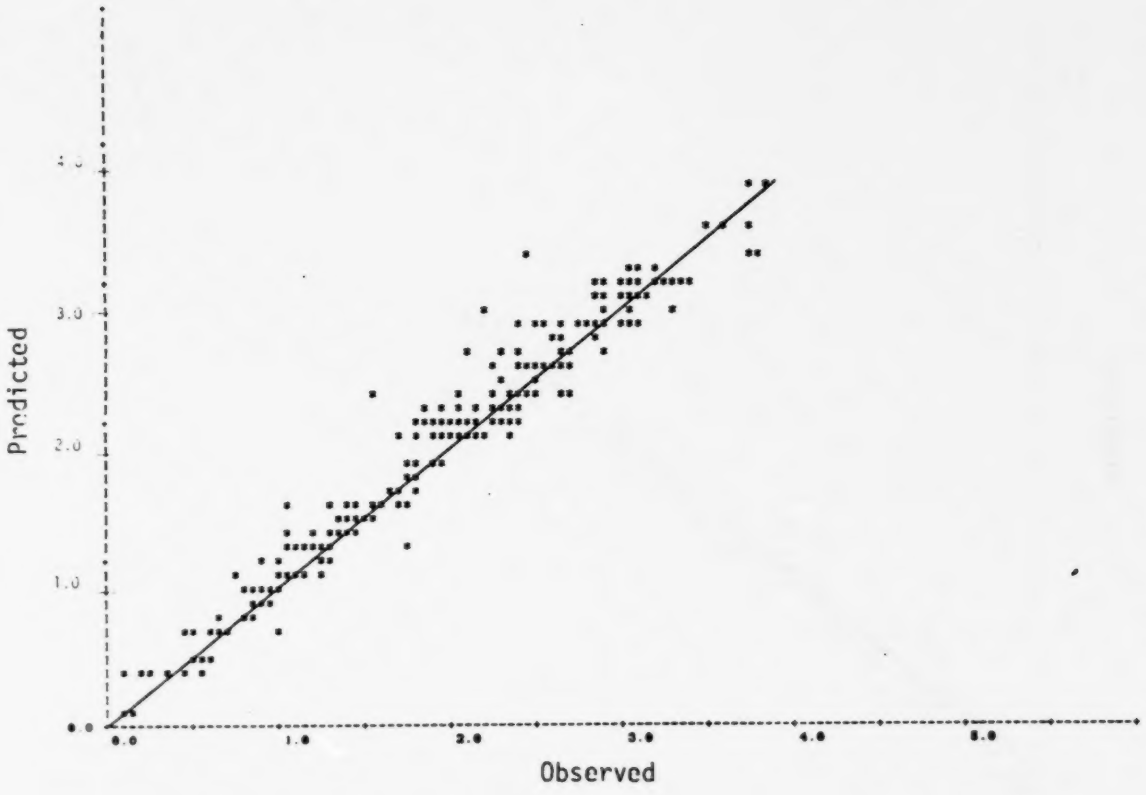

(b) $z = 4.5$ meters ($z_0 = 0.05$ meters)

FIGURE 10 (Continued)

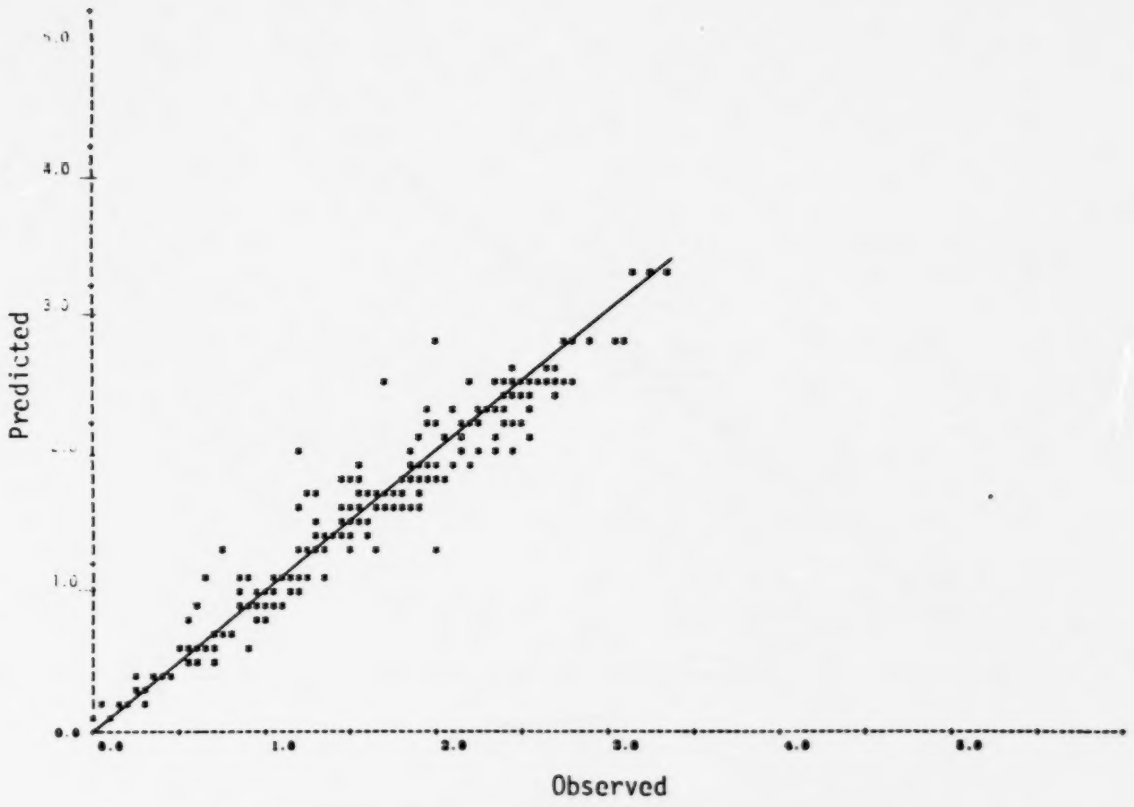

(c) z = 1.5 meters (z_0 = 0.05 meters)

FIGURE 10 (Concluded)

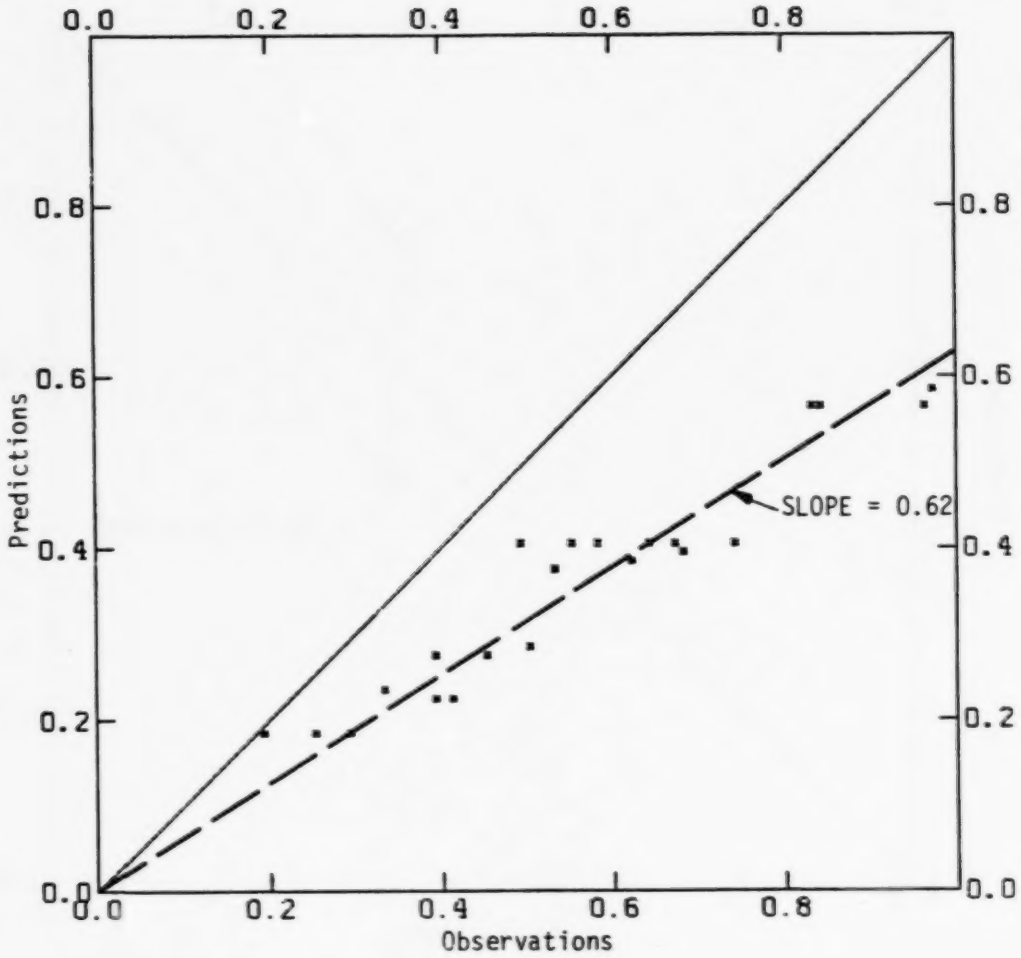

(a) $\overline{u'^2}^{1/2}$

FIGURE 11. OBSERVED VERSUS PREDICTED VALUES OF $\overline{u'^2}^{1/2}$ AND $\overline{w'^2}^{1/2}$. Only cases with wind direction $\bar{\theta}$ in the range $250 < \bar{\theta} < 290$ are represented, and only data from Tower 1 are included.

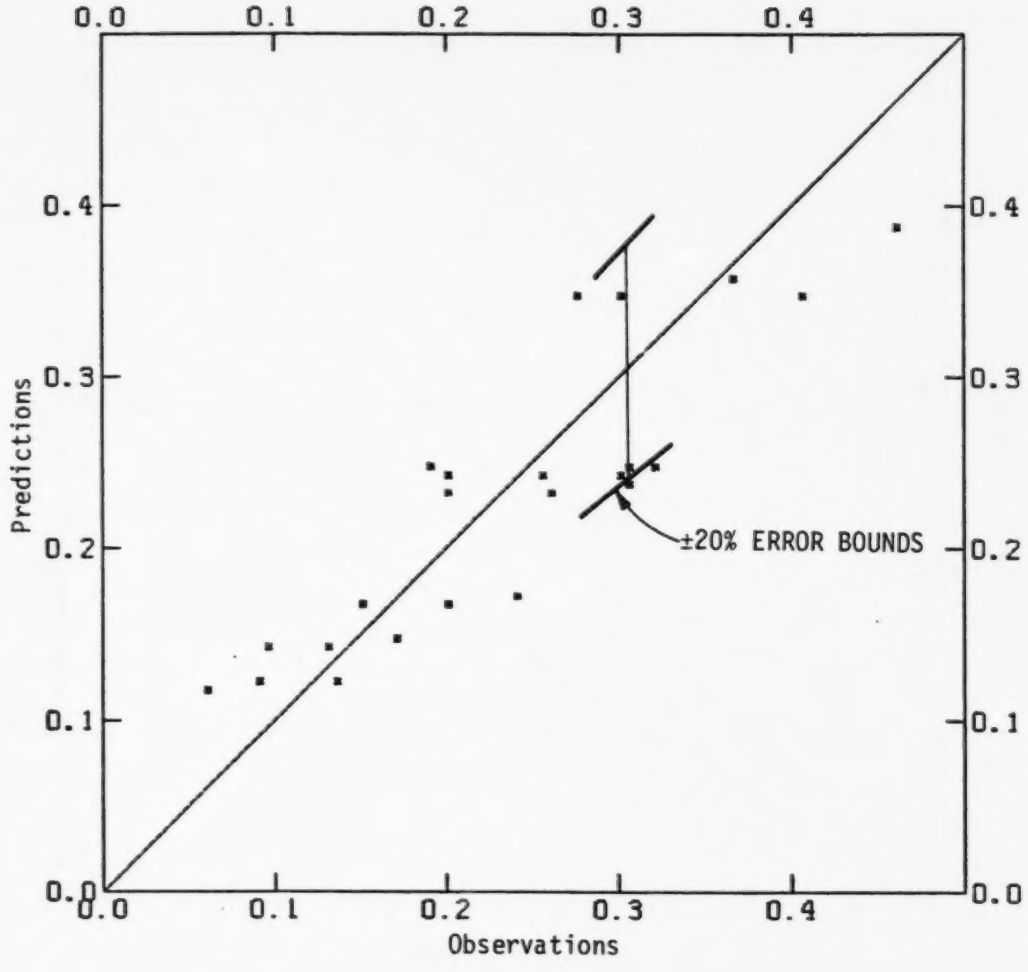

(b) $\overline{w'^2}^{1/2}$

FIGURE 11 (Concluded)

Our efforts to check the accuracies of the variance formulas [Eqs. (27) through (29)] were extended by considering data from Tower 6, the east-most tower, only in cases of wind directions $\bar{\theta}$ in the range of $70° < \bar{\theta} < 110°$. The predicted and observed values of u' and w' are shown in Figures 12(a) and 12(b), respectively. The tendency for the predicted u' value to be too low is again apparent. One noteworthy set of points shown in both figures is that for which the predicted values of u' and w' are near zero--u' = 0.02, w' = 0.01--but the observed values are over 10 times larger. This particular set of points corresponds to a case of extremely stable flow and light winds (Day 295) with a vertical temperature gradient of +1°C per 5 meters and $\bar{u} \simeq 0.4$ m/sec. The large value of u' measured in this case is most likely due to meanders in the local circulation induced by topography and inhomogeneities in surface roughness, and the large w' values observed may be due to horizontal divergence in the circulation, to gravity waves, or to both. In any event, the fluctuating velocities observed are not the result of the mechanical and buoyancy phenomena that generate the turbulence described by similarity theory. Describing the dispersive properties of very stably stratified flows is one of the largest unsolved problems of diffusion modeling.

Finally, we compared the predicted u' and w' values with those measured at Towers 1, 5, and 6 when the wind direction $\bar{\theta}$ fell in either of the sectors $340 < \bar{\theta} < 20$ or $160 < \bar{\theta} < 200$. These comparisons are given in Figures 13(a) and 13(b). The dashed line in Figure 13(a) is the best fit line of the u' values shown in Figure 11(a). It is apparent that with northerly or southerly winds the predicted u' values are not as low as they are for westerly flows. The dependence on wind direction of the discrepancy between the observed and predicted values of u' may be the result of the dependence of σ_u and σ_v on inversion height. Panofsky et al. (1977) have proposed the relationship:

$$\sigma_u = \sigma_v = u_*[12 - h/(2L)]^{1/3} \quad , \quad L < 0 \quad , \qquad (35)$$

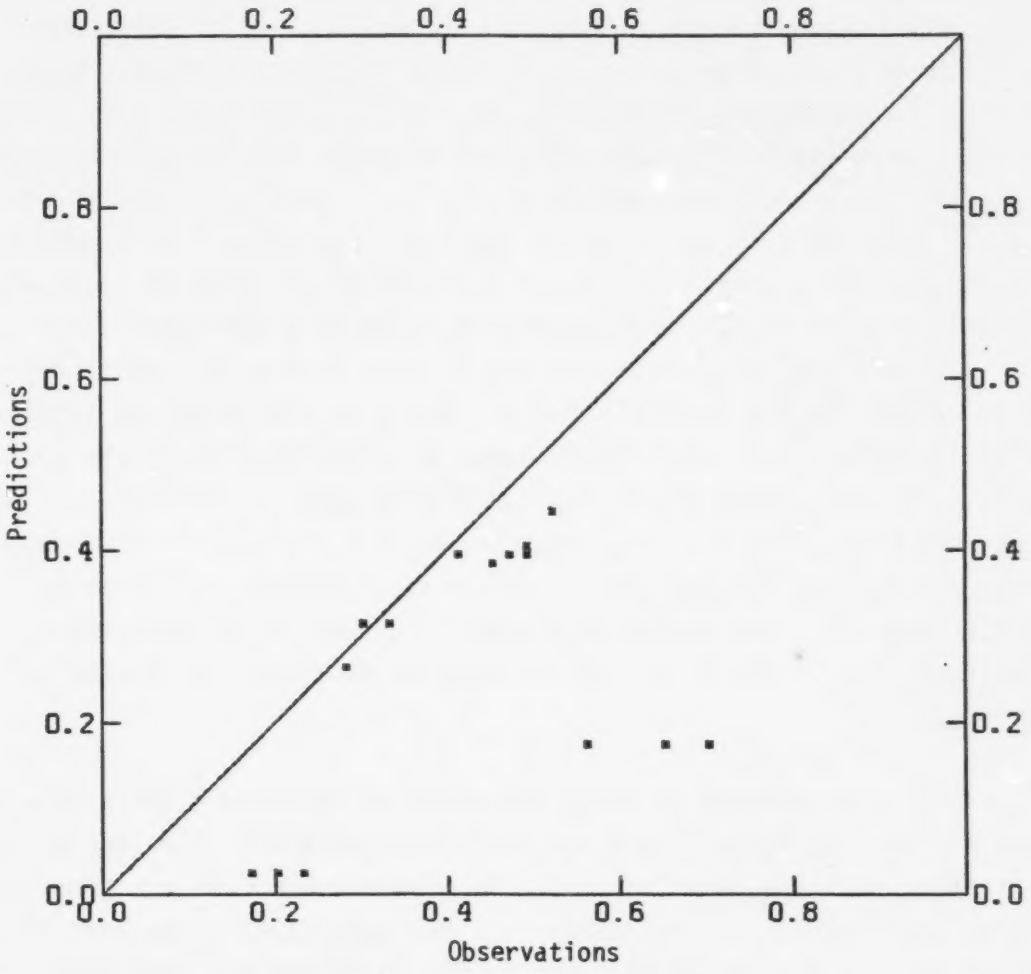

(a) $u' = \overline{u'^2}^{1/2}$

FIGURE 12. OBSERVED VERSUS PREDICTED VALUES OF $u' = \overline{u'^2}^{1/2}$ AND $w' = \overline{w'^2}^{1/2}$. Only cases with wind direction $\bar{\theta}$ in the range $70 < \bar{\theta} < 110$ are represented, and only data from Tower 6 are included.

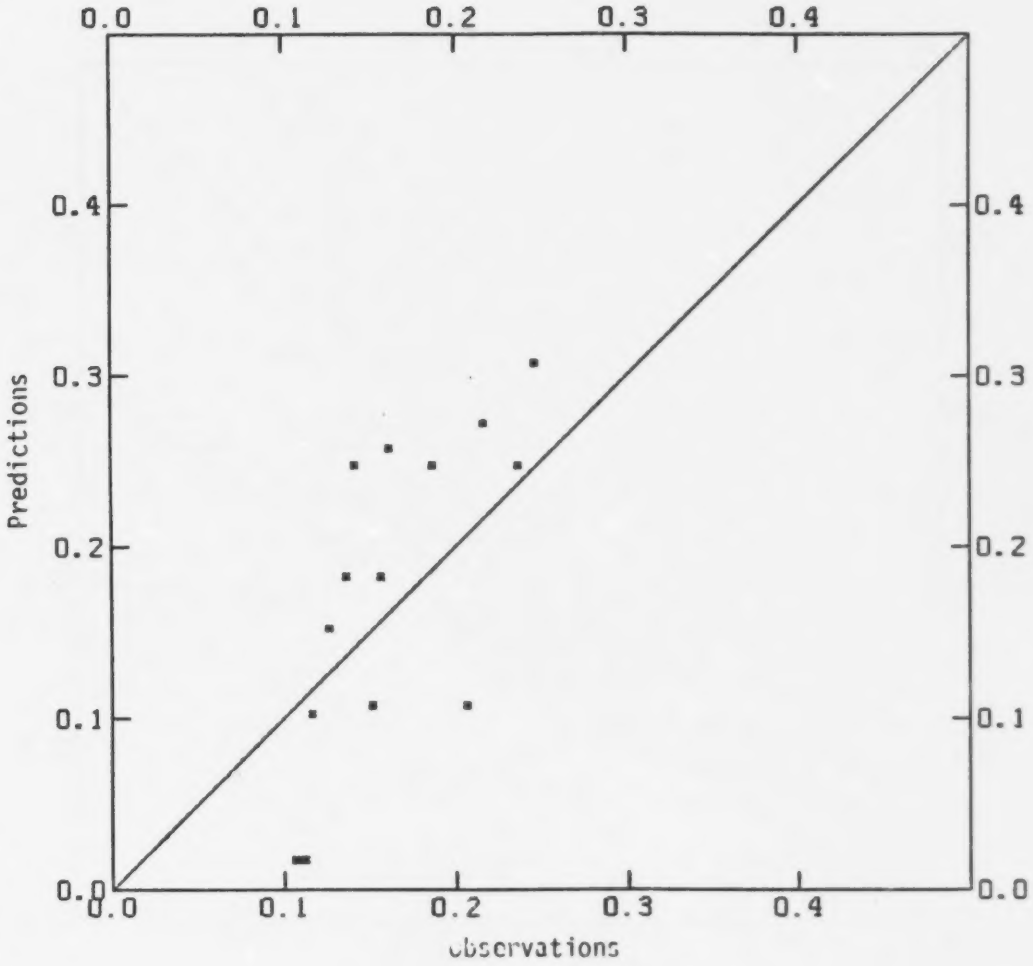

(b) $w' = \overline{w'^2}^{1/2}$

FIGURE 12 (Concluded)

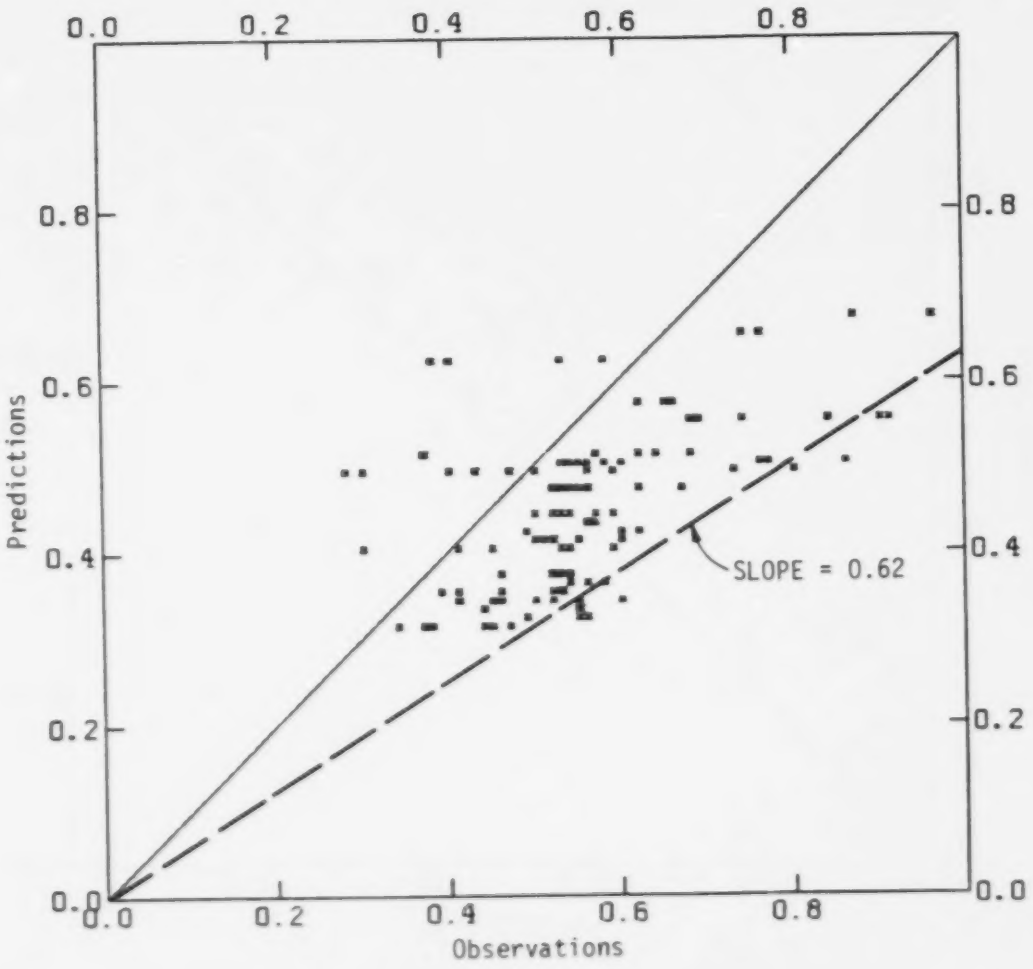

(a) u'

FIGURE 13. OBSERVED VERSUS PREDICTED VALUES OF u' AND w'. Only data for cases with wind direction in the sectors $340 < \bar{\theta} < 20$ and $160 < \bar{\theta} < 200$ are represented, and only measurements from Towers 1, 5, and 6 are included.

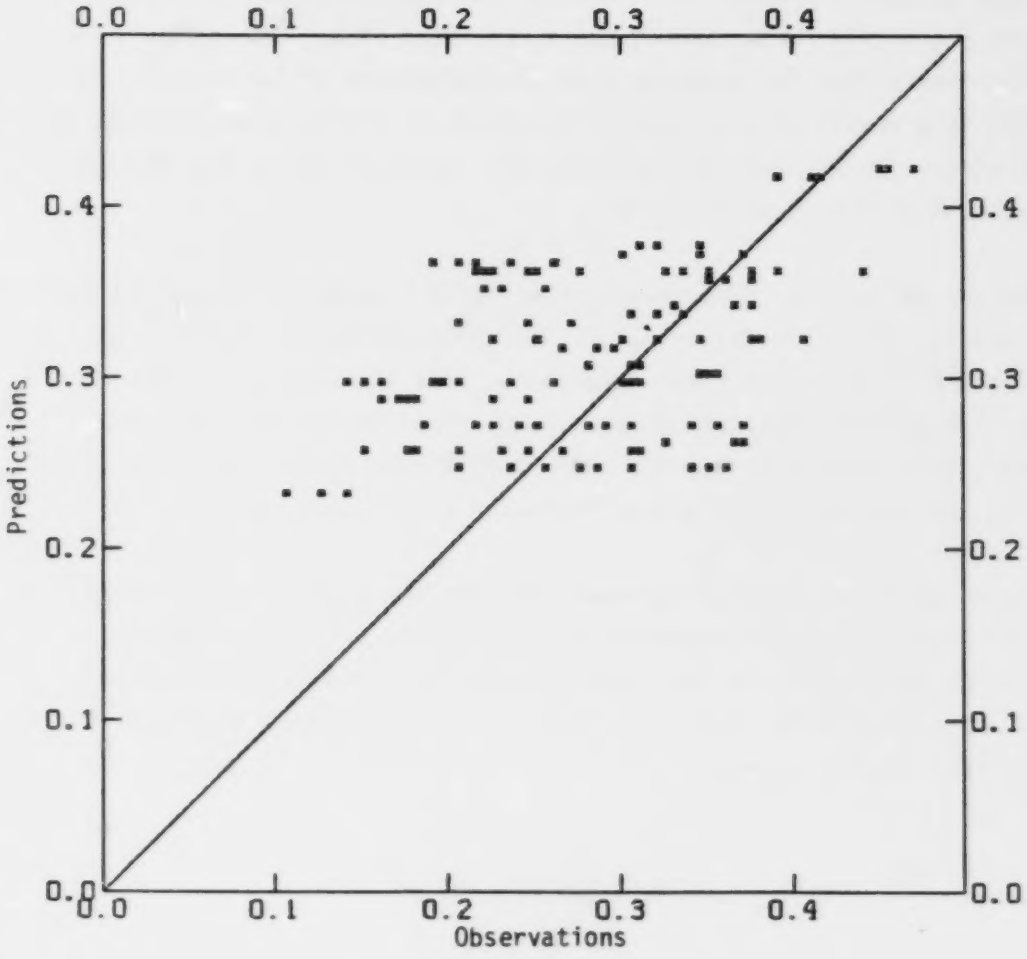

(b) w'

FIGURE 13 (Concluded)

where h is the mixed layer depth or inversion base height. They have found very good agreement between this equation and measured data. Binkowski's formulas [Eq. (29)] for σ_u and σ_v are independent of h. Consequently, it is quite likely that the dependence on wind direction of the accuracy of Eq. (29) is a result of a systematic variation of h with wind direction at the GM site. Since inversion data were not measured during the GM study, we cannot test this hypothesis now.

On the whole, the comparisons presented in Figures 11 through 13 indicate that Eq. (27) provides acceptably accurate estimates of $\overline{w'^2}^{1/2}$ but that the $\overline{u'^2}^{1/2}$ values obtained through Eq. (29) are subject to some uncertainty. We believe that through proper modifications of Eq. (29) or by replacing this formula altogether with Eq. (35), acceptably accurate estimates of the horizontal turbulence variances can also be obtained.

As a result of the good agreement between the $\bar{u}$ values predicted by similarity theory and the measurements (see Figure 10), we decided to explore the possibility of deriving estimates of u_* and L from wind data alone. According to Eq. (22), the ratio of the wind speeds measured at two heights, z_1 and z_2, is:

$$\frac{\bar{u}_1}{\bar{u}_2} = \frac{g(z_1, L, z_0)}{g(z_2, L, z_0)} \quad . \tag{36}$$

For given values of z_1, z_2, and z_0, the right side of Eq. (36) is a unique function of L, at least in the interval $-0.1 \leq 1/L \leq 0.1$. Figure 14 shows a plot of this function for $z_1 = 10.5$, $z_2 = 1.5$, and $z_0 = 5$ cm. Also shown is a plot of the drag coefficient:

$$C_D = \frac{u_*}{\bar{u}_1} = \frac{k}{g(z_1, L, z_0)} \tag{37}$$

obtained from Eqs. (22) through (26). Using the wind speed measurements made at 10.5 and 1.5 meters and the two curves plotted in Figure 14,

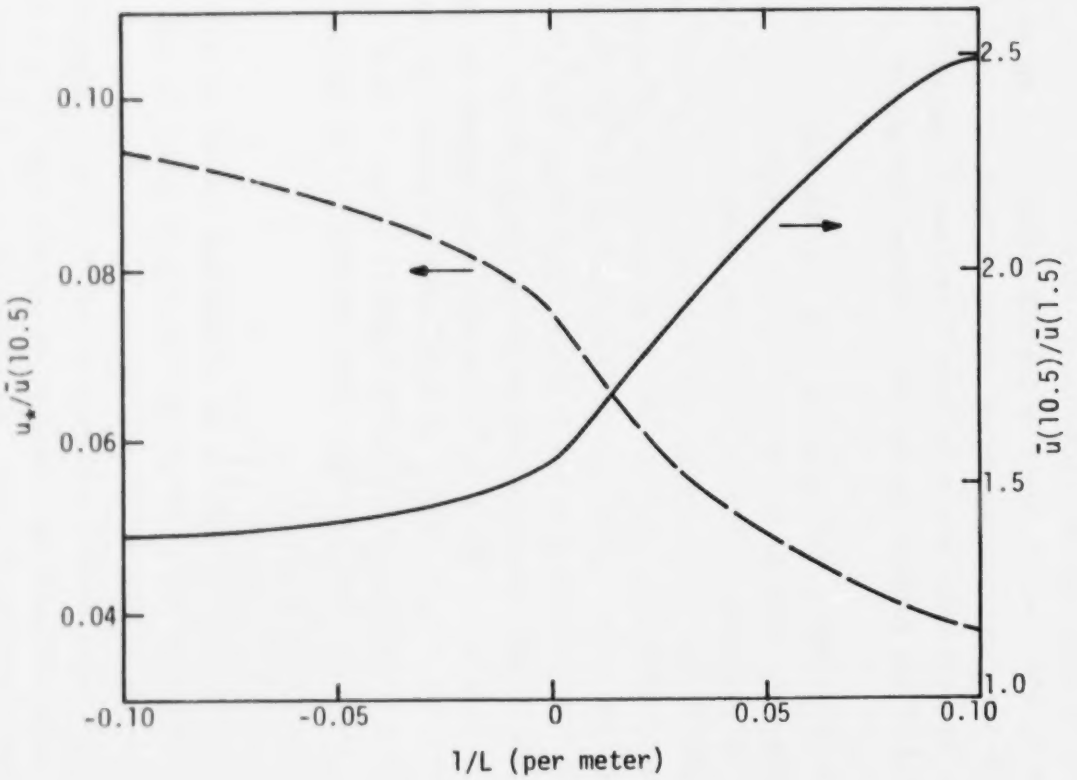

FIGURE 14. PLOTS OF THE RATIO OF THE WIND SPEEDS AT 10.5 AND 1.5 METERS AND THE DRAG COEFFICIENT $u_*/\bar{u}(10.5)$ GIVEN BY SIMILARITY THEORY AS FUNCTIONS OF 1/L. The surface roughness, z_0, is 5 cm.

we can obtain estimates of both u_* and L. For convenience, we refer to this as the wind speed ratio (WSR) method. The technique can be used for any values of z_1, z_2, and z_0 by recomputing the $\bar{u}_1/\bar{u}_2$ and $u_*/\bar{u}_1$ curves. We should also point out that with this method, L = 10 is assumed if $\bar{u}_1/\bar{u}_2$ exceeds the theoretical value at 1/L = 0.1, and L = -10 is assumed if the wind speed ratio is less than the theoretical value at 1/L = -0.1. Figure 15 compares the u_* and L values given by the WSR method for each of the GM experiments with the corresponding values listed in Table 1. In applying the WSR method, we used data from only Tower 1 or Tower 6, depending on which was upwind of the roadway, rather than averages for several towers.

Looking first at the u_* estimates, we find that the two sets of values are in fair agreement: Over 67 percent of the WSR estimates are within ±20 percent of the values given in Table 1. However, there is a distinct tendency for the WSR method to overpredict u_*, a direct result of the method's tendency to predict unstable stratification (for which $u_*/\bar{u}_1$) is large) in situations where the values in Table 1 indicate that stable stratification existed. Recall that in obtaining the L values of Table 1, the sign of L was taken from the Richardson number, which was measured during each of the GM experiments. In general, there is little agreement between the two sets of 1/L values shown in Figure 15(b). In fact, only 60 percent of the values given by the WSR method agree in sign with those in Table 1--only slightly better than the agreement that could be obtained by making random guesses of the sign of L.

A case-by-case examination of the meteorological conditions existing during those periods when the signs of the L values given by the two methods disagree revealed the following findings. On 4 of the 23 occasions for which the signs differ, the sign of the Richardson number measured at Tower 1 was opposite that recorded at Tower 6 some 100 meters away. In 9 of the remaining 19 cases, the temperature stratification was not uniform vertically at the tower from which the wind data used in the WSR method were taken; the sign of the temperature difference between the top two levels of the tower was opposite that between the bottom two levels. The 4 cases in which the Richardson numbers at Towers 1 and 6 had opposite

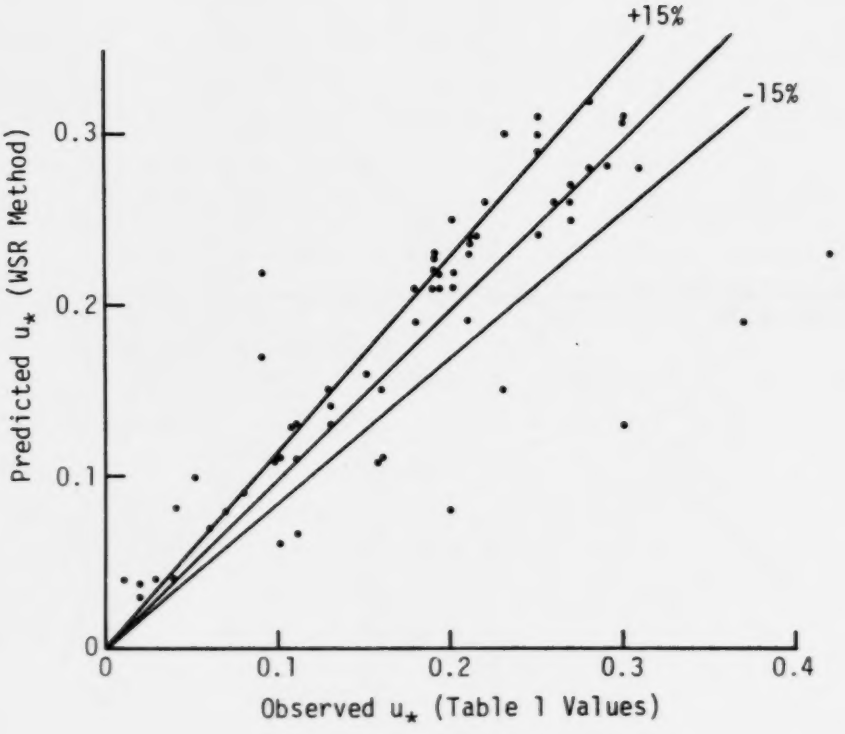

(a) Friction Velocity, u_*

FIGURE 15. COMPARISON OF THE u_* AND 1/L VALUES OF TABLE 1 WITH THOSE DERIVED USING THE WSR METHOD

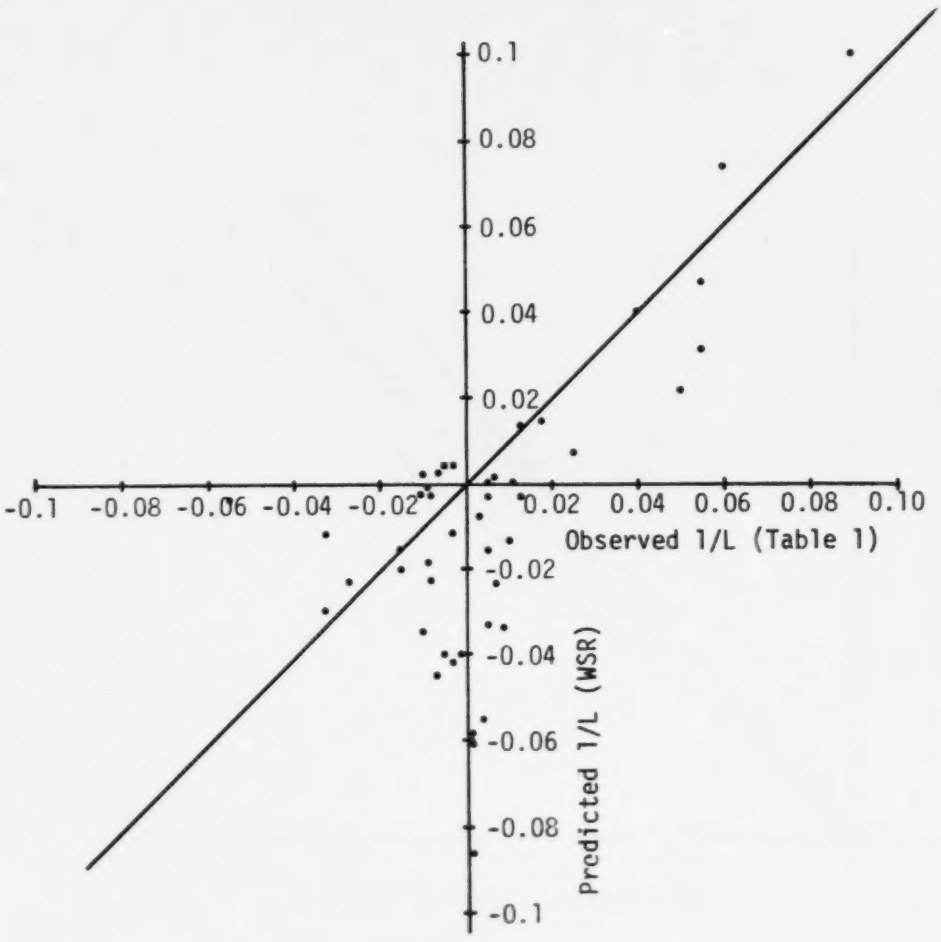

(b) Monin-Obukhov Length, L

FIGURE 15 (Concluded)

signs all occurred on Day 290, when the flow was stably stratified upwind of the roadway during the observation period and unstable downwind. This suggests that the heat from large numbers of automobiles and the release of heat stored in the roadway itself can significantly alter the turbulence locally when the ambient flow is stably stratified. Another possible cause of change in stability downwind of the road is the overturning of the cold air near the ground and the warmer air above by the vehicle wake turbulence. Our finding that the vertical temperature structure near the ground was not uniform in a number of instances in which the two methods of estimating L give radically different results emphasizes the problem of characterizing stability when the vertical temperature profile is nearly isothermal. Chapter V quantitatively examines the magnitude of the errors in mean concentration estimates resulting from uncertainties in the values of u_* and L.

V RESULTS OF PRELIMINARY MODEL VALIDATION EXPERIMENTS

This chapter discusses the SF_6 concentrations predicted by our model for each of the GM experiment periods and compares them with the values actually observed. The roadway used in the GM study is oriented north-south. Instrumented towers were placed 30 and 2 meters west of the roadway; one tower was sited in the roadway median; and additional towers were located at distances of 4, 15, 30, 50, and 100 meters east of the roadway's eastern edge. Thirty-minute averaged SF_6 concentrations were measured at the 1.5, 4.5, and 10.5 meter levels of all towers except those located 50 and 100 meters east of the road, where measurements were made at 1.5 meters only. Thus, a total of 20 SF_6 measurements were made during each experiment. The reader is referred to Cadle et al. (1976) for further details on the GM monitoring network and study conditions.

A. SIMULATIONS THAT NEGLECT WAKE EFFECTS

In previous chapters we detailed all aspects of the roadway model except one--the vehicle wake turbulence parameterization. Most early roadway models ignored the dispersive effects of wake turbulence entirely, but models developed within the last few years have included some means of approximating these effects. Apparently, however, no quantitative modeling studies have ever been performed to establish the actual importance of wake effects to accurate predictions. We performed such a study by exercising our model under the conditions of the GM experiments, with a wake turbulence parameterization omitted entirely. Obtaining good agreement between the simulation results and the measured data would indicate that, at least insofar as the mean concentration of an inert material (SF_6) is concerned, wake effects are minor and can be neglected.

In Figure 16, the SF_6 concentrations predicted by the model with a wake parameterization omitted are compared with the GM data. We emphasize that the only input data used in the model for these calculations were the SF_6 emissions rates reported in Cadle et al. (1976), the u_*, $\overline{\theta}$, and L values given earlier in Table 1, and estimates of the time scales T_w and T_u given on page 28. The only exceptions are the four experiments conducted on Day 295. As we noted earlier in Chapter IV, similarity theory completely failed to duplicate conditions on this extremely calm, stable day. The bulk Richardson's numbers measured during the four experiments conducted on Day 295 ranged between 0.35 and 7.5, which are outside the limit (viz, 0.2) of applicability of the similarity expressions that we use in the model. Consequently, in the simulations of the four experiments conducted on Day 295, we forced the $\overline{u}$, σ_w, and σ_u profiles to agree with the averaged measured values at the 10.5 meter levels of the towers 30 meters east and west of the road. Our justification for altering the input data in this manner lies in the fact that we are concerned here with how well the diffusion model itself performs under various meteorological conditions. Therefore, we are attempting in these validation and testing exercises to minimize errors in the input data as much as possible so that errors in the predicted concentrations will reveal inadequacies in the model itself. We showed in the previous chapter that the similarity expressions that we have incorporated in the diffusion model yield quite accurate mean wind and turbulence profiles given only the local values of the friction velocity and Monin-Obukhov length. However, under extremely stable conditions, namely $R_i > 0.2$, these expressions break down altogether and the profiles they produce are completely unreliable. Consequently, under these conditions one must rely on measured winds and turbulence parameters for reliable estimates. We have adhered to this procedure in our validation studies.

We find in Figure 16 that, with the exception of several of the values predicted for Day 295 (designated by arrows in the figure), the performance of the model with wake effects ignored is not particularly bad. The rms error of the 1100 predicted values is 0.80 ppb (the averaged observed value

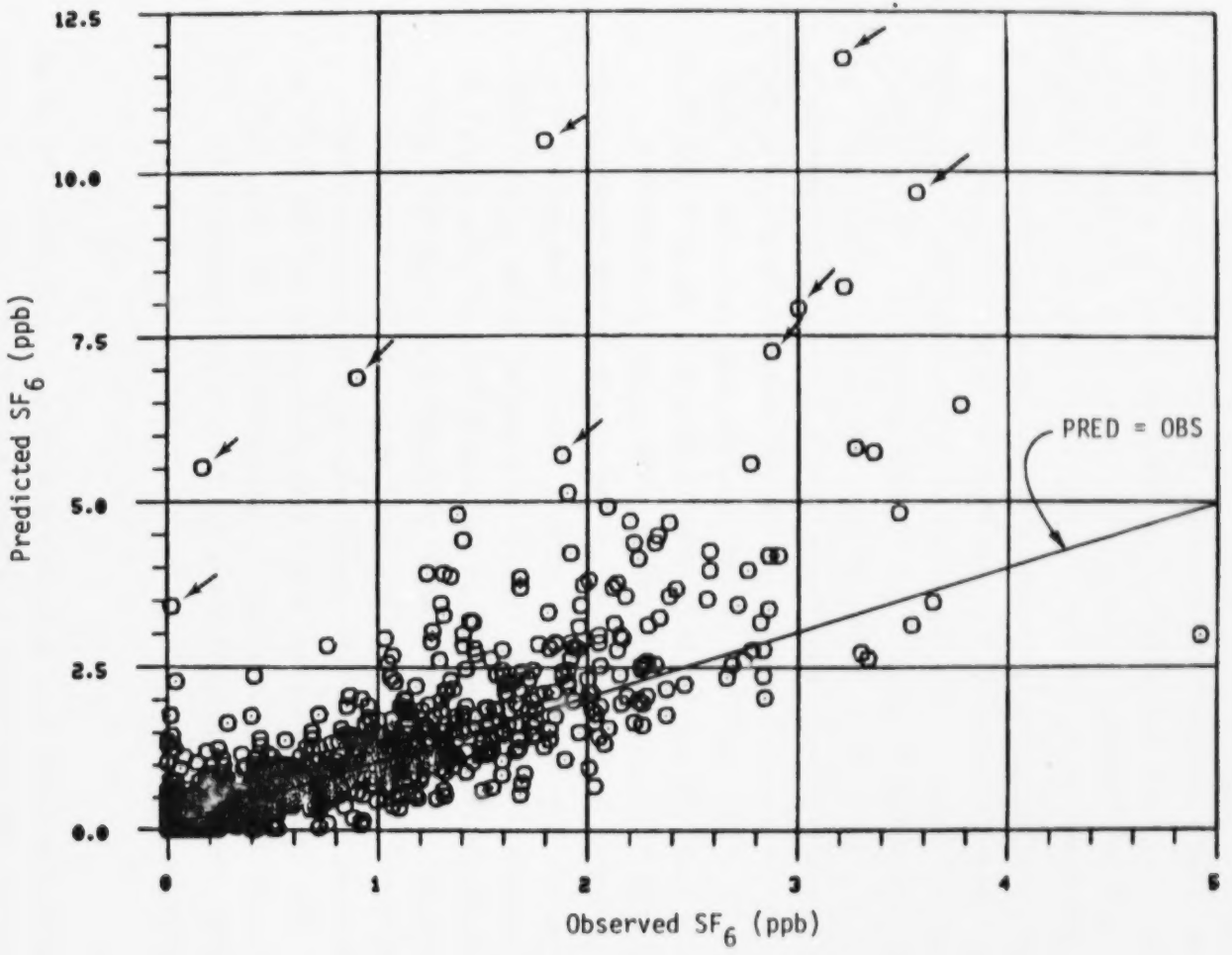

FIGURE 16. COMPARISON OF OBSERVED SF_6 CONCENTRATIONS WITH THOSE SIMULATED BY THE ROADWAY MODEL WITH VEHICLE WAKE TURBULENCE NEGLECTED: ALL EXPERIMENTS INCLUDED. Arrows indicate some of the results for Day 295.

is 0.71), the correlation coefficient $\rho = 0.79$, and the regression line is PRED = 0.07 + 1.27 · OBS. One of the features that sets Day 295 apart from all the others is extremely light winds: $\bar{u} \sim 0.5$ m/sec. On all other days, wind speeds were typically higher than 1.5 m/sec.

Considering the results shown in Figure 16 from this perspective, we speculate that wake effects are apparently most pronounced when wind speeds are less than 1 m/sec, at least when the vehicle speeds are 22 m/sec and higher, as they were in the GM study. This speculation is supported by Figure 17, where we have replotted the results shown in Figure 16 with the 80 values predicted for Day 295 deleted. In this subsample of 1020 points, and with the wake parameterization scheme still omitted, the rms error is $\sigma = 0.53$ ppb, the correlation coefficient $\rho = 0.87$, and the regression line is PRED = 0.07 + 1.16 · OBS.

B. SIMULATIONS THAT INCLUDE A SIMPLE PARAMETERIZATION OF WAKE EFFECTS

At least three quantities are required to model the wake properly: the initial turbulent energy in the wake, the time scale of the energy decay, and the Lagrangian integral time scale of the wake turbulence. Because values are not currently available for any of these parameters, it was necessary to formulate a wake parameterization empirically. Our initial efforts, which are quite primitive, were based on the following assumptions. First, for simplicity, the integral time scale of the wake turbulence was assumed to be zero. (This is tantamount to assuming that the diffusive action of the wake is akin to that of Fickian diffusion.) Second, the initial wake turbulence energy was assumed to be proportional to the work done by the drag force on the motor vehicle; that is,

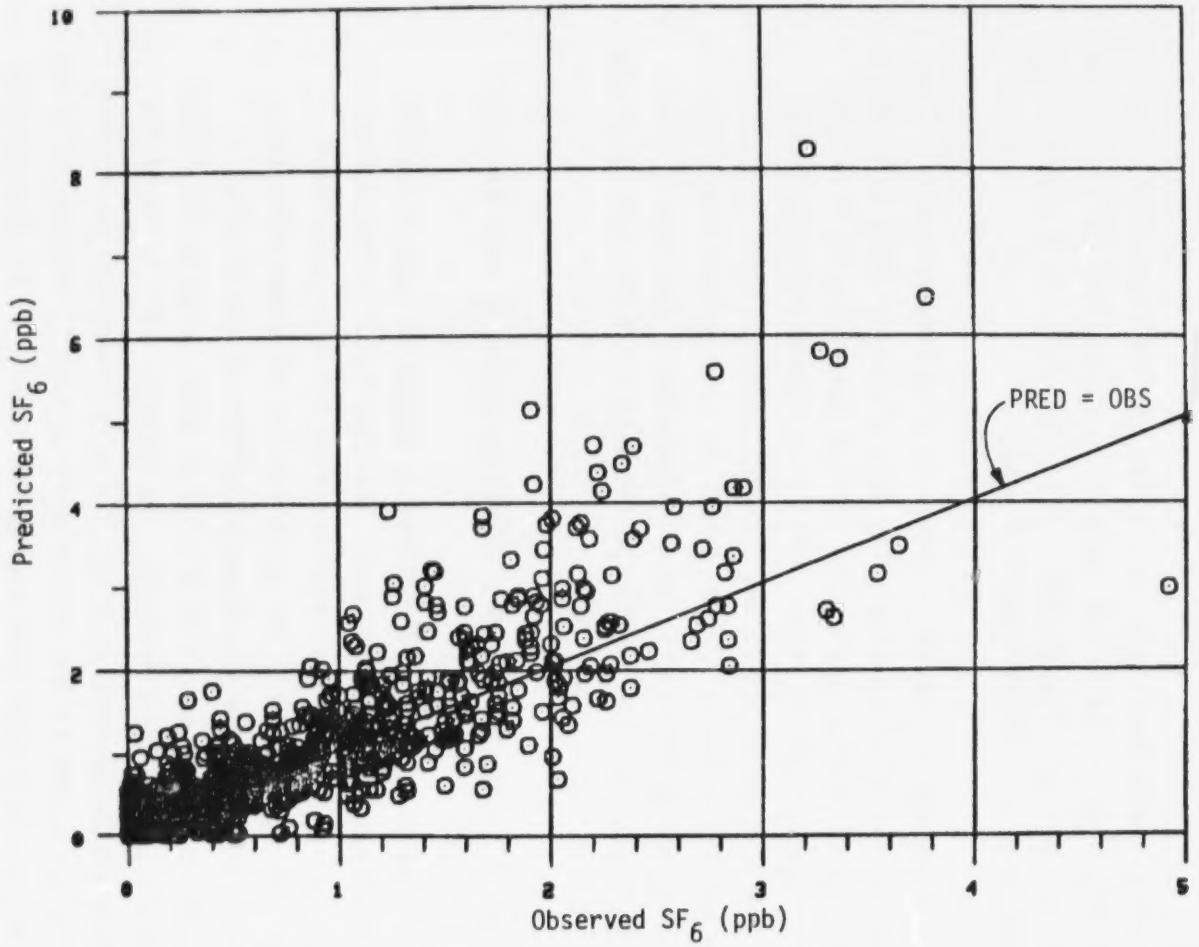

FIGURE 17. COMPARISON OF OBSERVED SF_6 CONCENTRATIONS WITH THOSE SIMULATED BY THE ROADWAY MODEL WITH VEHICLE WAKE TURBULENCE NEGLECTED: DATA POINTS FOR DAY 295 ($\bar{u}$ < 1 m/sec, R_i > 0.25) OMITTED

$$\overline{u''^2_w} = 2\gamma_u^2 C_D V^3 A \quad , \tag{38}$$

$$\overline{w''^2_w} = 2\gamma_w^2 C_D V^3 A \quad , \tag{39}$$

where

C_D = the vehicle drag coefficient,
A = the cross-sectional area of the vehicle,
V = the vehicle speed relative to the air,
γ_u, γ_w = constants,
$\overrightarrow{u''^2_w}, \overrightarrow{w''^2_w}$ = the horizontal and vertical components, respectively, of the initial mean square velocity fluctuations in the wake.

Third, to account for the decay of the wake energy, the wake intensity was assumed to be constant at the level given by Eqs. (38) and (39) for a period of T_w seconds, after which the energy was assumed to drop abruptly to zero and to remain there for all later travel time.

The foregoing description of the wake was incorporated into the stochastic velocity generator used to produce the simulated wake velocity components u" and w" described in Chapter II [see Eq. (15)].

To avoid using γ_u, γ_w, and T_w as devices for "tuning" the model, we attempted to determine values for the first two parameters from the wind and turbulence measurements made at the sites closest to the roadway. We chose

$$\gamma_u = \gamma_w = \gamma \quad ,$$

and then using $C_D = 0.5$, and $A = (2.5\ \text{m})^2$, values chosen somewhat arbitrarily, we selected a value for γ that made Eqs. (38) and (39) yield velocity variances close to those suggested by the wind and turbulence

measurements. Through this process, we found $0.005 < \gamma < 0.01$. Next, to refine the estimate of γ and to obtain a value for T_w, we exercised the model with the wake parameterization included to simulate Experiment 279080. (This period was chosen completely arbitrarily.) We varied the value of γ within the range noted above, and we experimented with various values of T_w to determine which set of values produced concentration predictions in closest agreement with the measured data. We were particularly concerned with reproducing the upstream diffusion that did not occur in the simulation in which the wake was ignored. The following parameter values were selected from these exercises:

$$T_w = 3 \text{ sec} \quad ,$$

$$\gamma = 0.007 \text{ sec}^{1/2}/\text{m}^{3/2} \quad .$$

Using these values in the wake parameterization along with the values of C_D and A given earlier, we incorporated the wake simulation algorithm into the model and then repeated the simulation of all of the GM experiment periods. The source emission rates and the values of u_*, $\bar{\theta}$, L, T_w, and T_u employed in these calculations were identical to those used in the simulations illustrated in Figure 16 in which the wake effects were ignored. Figure 18 shows the results of the comparison of the new calculations (with the wake simulation included) with the observed data.

Comparison of the results presented in Figure 16 and 18 indicates that the wake parameterization scheme, as simple as it is, has improved the accuracy of the model predictions considerably. The correlation coefficient of the new results is very high ($\rho = 0.91$), and 53 percent of the 1100 predicted concentrations are within ±30 percent of the measured values (as illustrated later in Figure 22). The rms error $\sigma = 0.33$ and the regression line is PRED = 0.13 + 0.91 · OBS. In the course of testing the wake parameterization scheme, we discovered that while the overall performance of the model was greatly improved with the scheme included, there were a number of simulation periods in which the model performed considerably

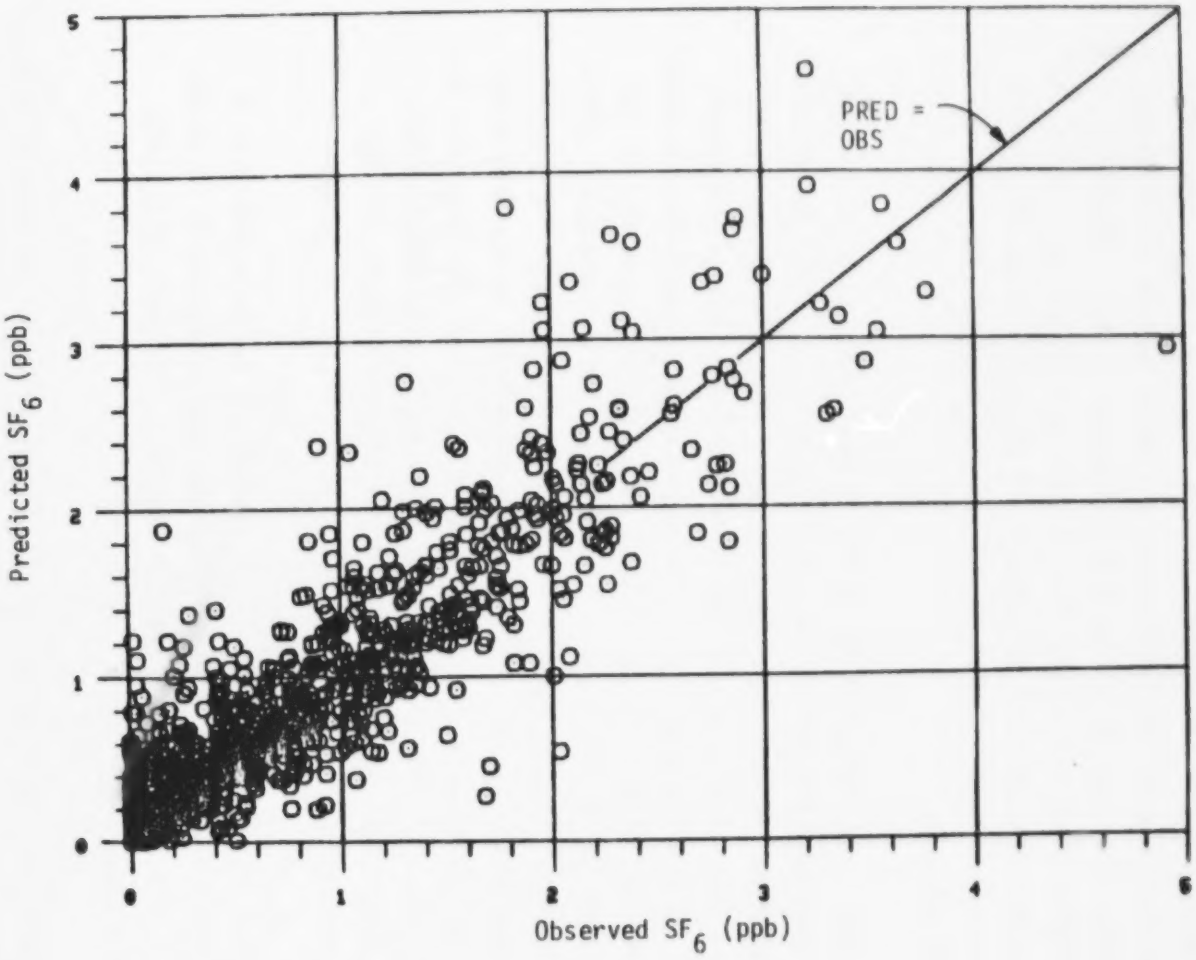

FIGURE 18. COMPARISON OF OBSERVED SF_6 CONCENTRATIONS WITH THOSE PREDICTED BY THE ROADWAY MODEL WITH WAKE TURBULENCE EFFECTS PARAMETERIZED: ALL EXPERIMENTS (1100 DATA POINTS) INCLUDED

better with the wake parameterization omitted. On seeking an explanation of this finding, we discovered that in all cases in which the model performed better with the wake effects ignored, the mean wind direction $\overline{\theta}$ was within about $\pm 10°$ of the roadway, namely, $|\sin \overline{\theta}| < 0.2$. The number of cases involved (13 of the 55 GM study periods), the high correlation with wind direction, and the difference in the rms error of the model realized between simulations made with and without the wake parameterization were strong evidence that the phenomenon in question was not merely a chance event, but rather the result of some physical process associated with the vehicle wake.

After examining the condition of the GM experiment more closely, we concluded, with some confidence, that the process in question is the so-called "slipstream" phenomenon. The vehicles in the GM experiment were spaced only a few vehicle lengths apart, so that each vehicle was within the wake of the one ahead of it, except when the mean wind component normal to the roadway was strong enough to force each vehicle's wake out of the path of the vehicle immediately behind. When the vehicles are well within each other's wakes, the air speed relative to each vehicle is considerably lower than that which a single vehicle would experience in the same meteorological conditions. Thus, with close vehicle spacing, the drag work done by each vehicle, and hence the intensity of turbulence in the wake produced, are lower than that which would occur if each vehicle were not within the wakes of others.

To account for this phenomenon, we set the air velocity relative to each vehicle to 1/10 of its nominal value when the wind angle $\overline{\theta}$ is in the range $|\sin \overline{\theta}| < 0.2$. The model results displayed in Figure 18 include this modification.

In order to analyze the model's capabilities further, we have plotted in Figures 19 and 20 scatter diagrams of predicted versus observed concentrations for stable and unstable conditions separately. These figures reveal a tendency for the model to overpredict slightly in stably

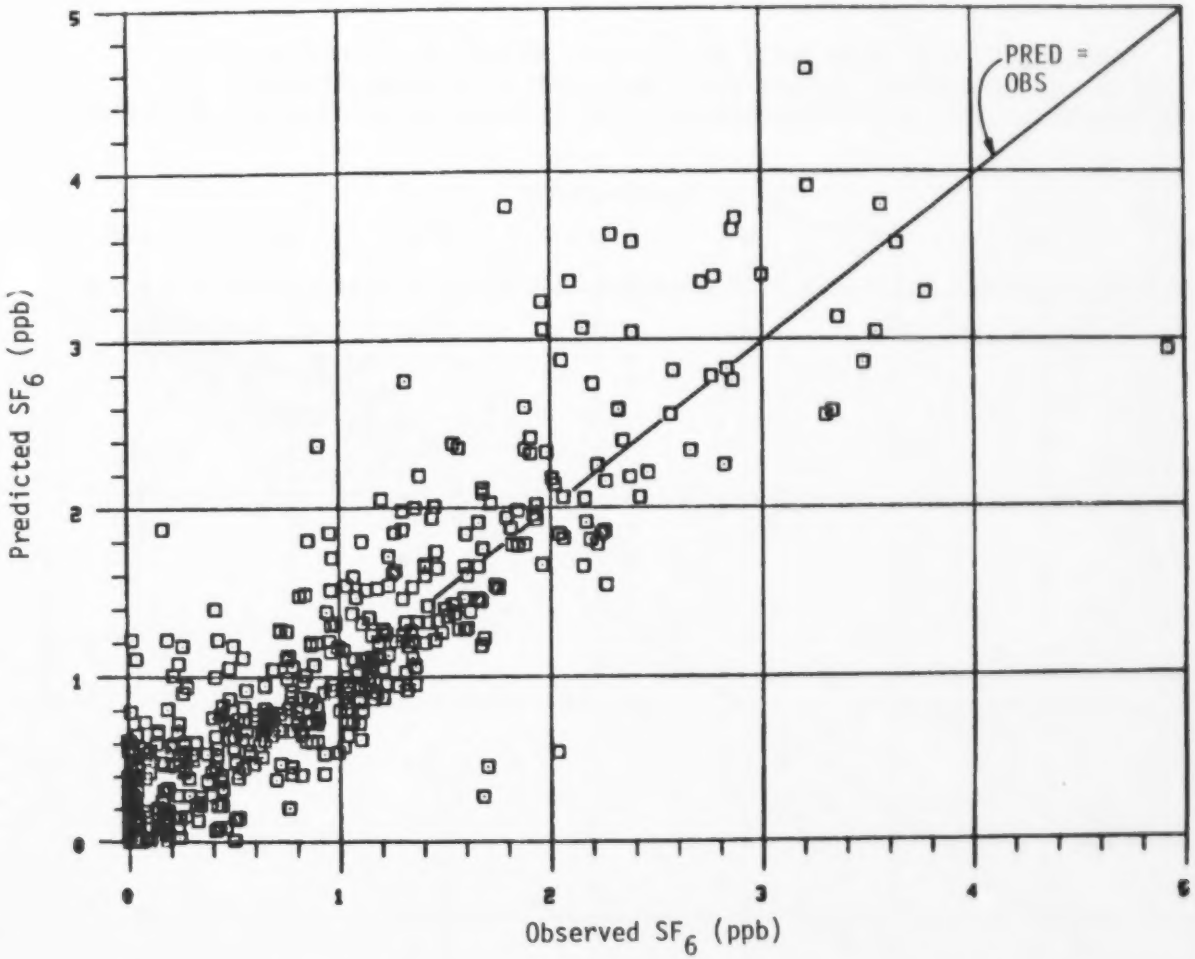

FIGURE 19. COMPARISON OF OBSERVED SF_6 CONCENTRATIONS WITH THOSE PREDICTED BY THE ROADWAY MODEL WITH WAKE TURBULENCE EFFECTS PARAMETERIZED: RESULTS DISPLAYED FOR STABLY STRATIFIED FLOWS ONLY (580 DATA POINTS)

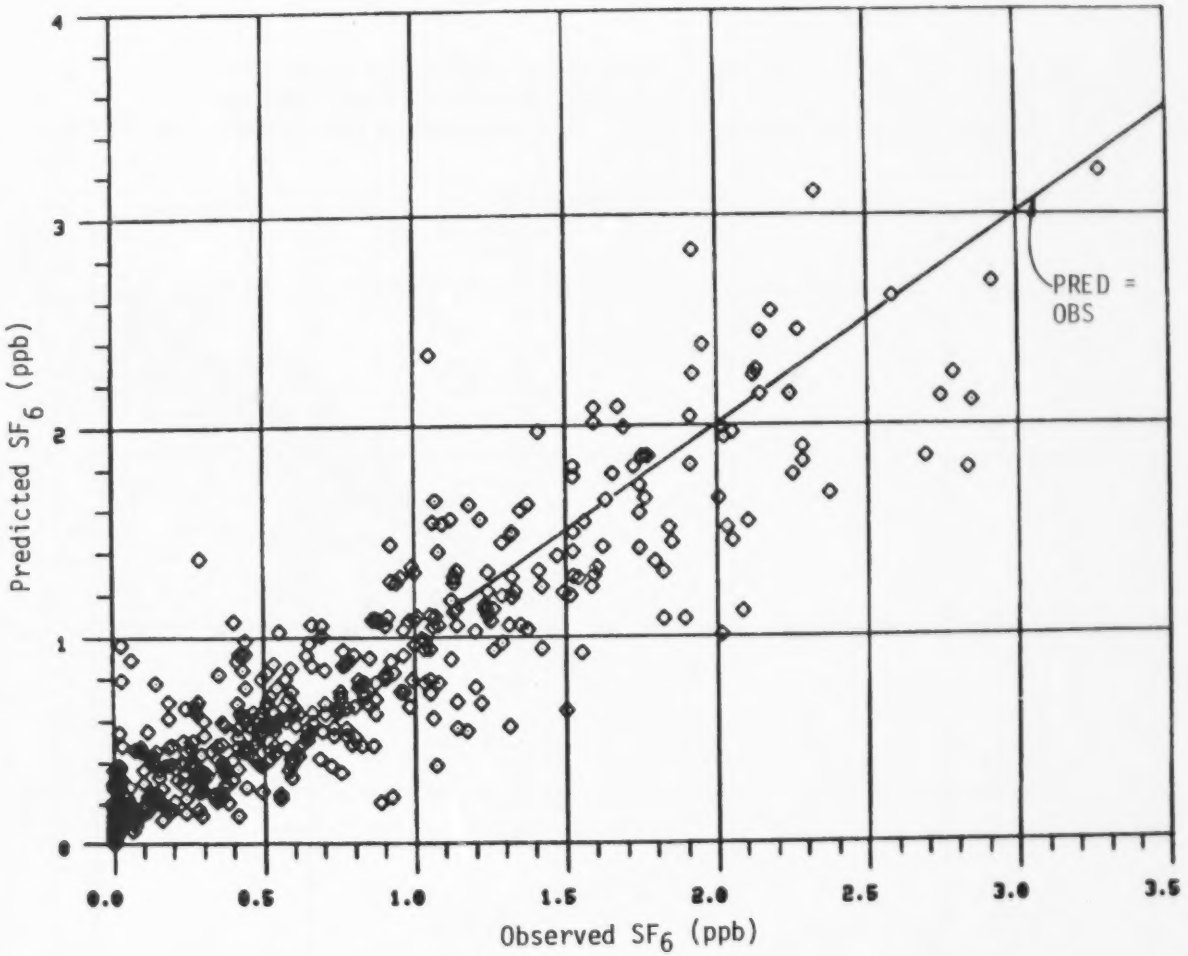

FIGURE 20. COMPARISON OF OBSERVED SF_6 CONCENTRATIONS WITH THOSE PREDICTED BY THE ROADWAY MODEL WITH WAKE TURBULENCE EFFECTS PARAMETERIZED: RESULTS DISPLAYED FOR UNSTABLY STRATIFIED FLOWS ONLY (520 DATA POINTS)

stratified flows and to underpredict during unstable situations. These tendencies are also apparent from the following performance statistics:

- Stable cases only
  Number of data points N = 580
  Average predicted concentrations $\overline{P}$ = 0.85 ppb
  Average observed concentrations $\overline{O}$ = 0.76 ppb
  σ = 0.38 ppb
  ρ = 0.91
  PRED = 0.13 + 0.95 · OBS.
- Unstable cases only
  N = 520
  $\overline{P}$ = 0.68 ppb
  $\overline{O}$ = 0.65 ppb
  σ = 0.28 ppb
  ρ = 0.91
  PRED = 0.14 + 0.83 · OBS.

The fact that the intercept of the regression line for the cases with the wake scheme employed is larger than that obtained with the scheme omitted indicates that the wake parameterization is spreading material over too large an area. Another feature of the model results is the lower slope of the regression line achieved. Contributing to this deficiency is the set of points predicted for Day 275. For some unknown reason, the highest observed values on one of the experiments of this day are consistently higher than the predicted values by a factor of two. The other experiment shows a similar underestimation.

A quantity of great concern in applied air pollution studies is the expected peak concentration. Figure 21 displays a scatter plot of the predicted versus observed peak values obtained in the 55 experiments. The sloping dashed lines in the figure delineate the ± 25 percent error bounds. Over 75 percent of the calculated peak values fall within these bounds.

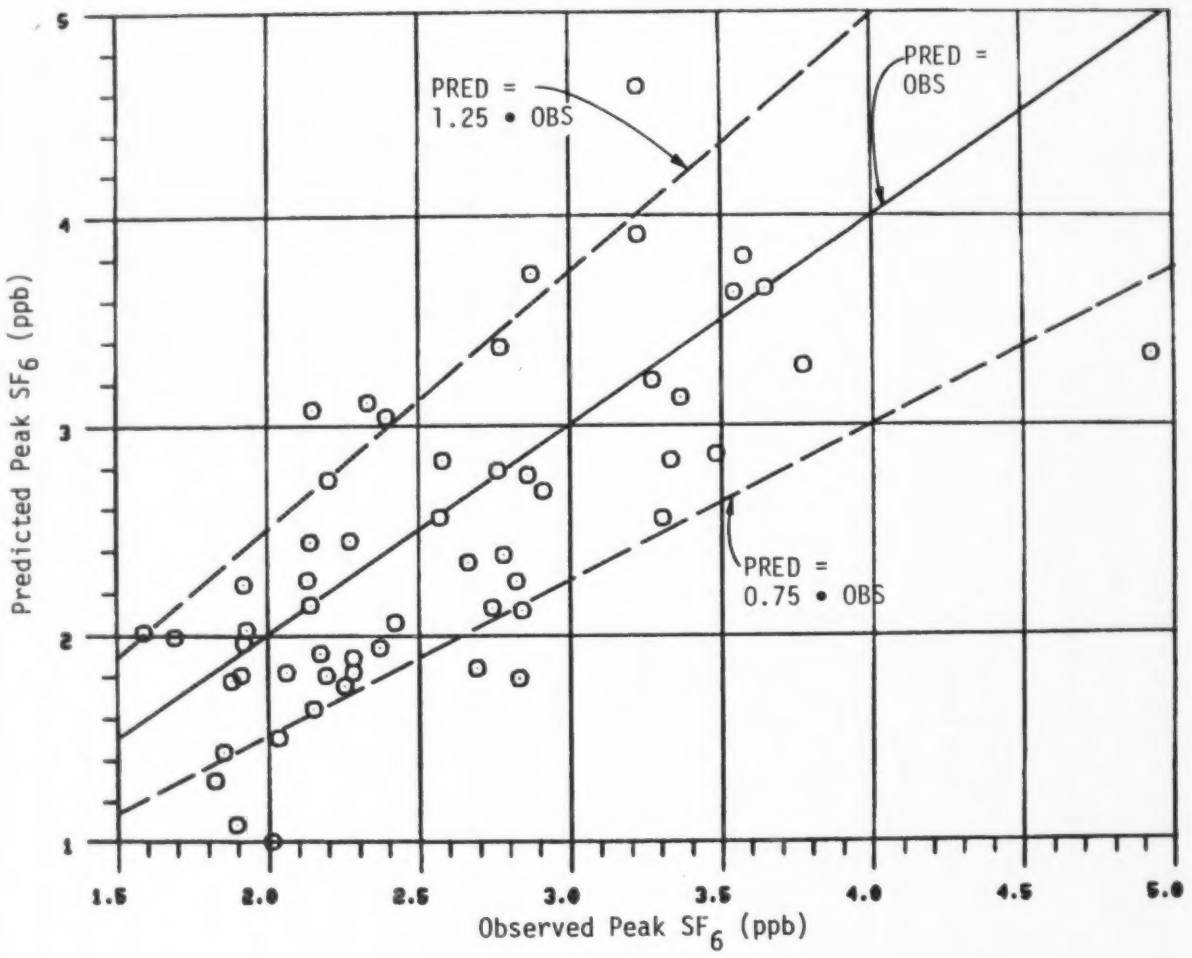

FIGURE 21. COMPARISON OF OBSERVED PEAK SF_6 CONCENTRATION FOR EACH OF THE 55 GM EXPERIMENTS WITH THE VALUES PREDICTED BY THE MODEL (WAKE EFFECTS INCLUDED)

The performance statistics of the model are summarized in Table 2, and plots of the fractional error distributions found for several of the validation studies are given in Figure 22. The basic model requires about 36,000 words of core storage and it used about 10 minutes of CPU time on the UNIVAC 1110 to simulate all 55 of the GM experiments. Shorter execution times can be achieved by relaxing the error bounds on the predicted concentrations (see Table 2). The computer memory requirement increases by 3 words for each additional monitor site added, regardless of the distance of the monitor from the roadway. The machine time required by the model increases very slightly as additional sampling sites are added to a given area. However, if the area itself is extended, the machine time requirement increases. We have not established the quantitative dependence of the machine time requirement on the size of the sampling domain.

TABLE 2. MODEL PERFORMANCE STATISTICS

Conditions	N	$\bar{P}$	$\bar{O}$	σ	ρ	Error Distribution--percentage of predicted value with error ≤: 25%	50%	100%	Regression Line--PRED = α + β · OBS α	β
1. All experiments, wake "on"	1100	0.76	0.71	0.33	0.91	47%	68%	83%	0.12	0.91
2. Day 295 omitted, wake "on"	1020	0.74	0.70	0.30	0.92	48	70	85	0.11	0.90
3. Same as No. 1 but with relaxed error (execution time = 3 min; Case 1 = 10 min)	1100	0.76	0.71	0.38	0.88	42	65	81	0.13	0.90
4. All experiments, wake "off"	1100	0.96	0.71	0.80	0.79	36	57	80	0.07	1.27
5. Day 295 omitted, wake "off"	1020	0.88	0.70	0.53	0.87	37	59	82	0.07	1.16

N = total data points.

$\bar{P}$ = Average predicted SF_6 (ppb).

$\bar{O}$ = Average observed SF_6.

σ = rms error.

ρ correlation coefficient.

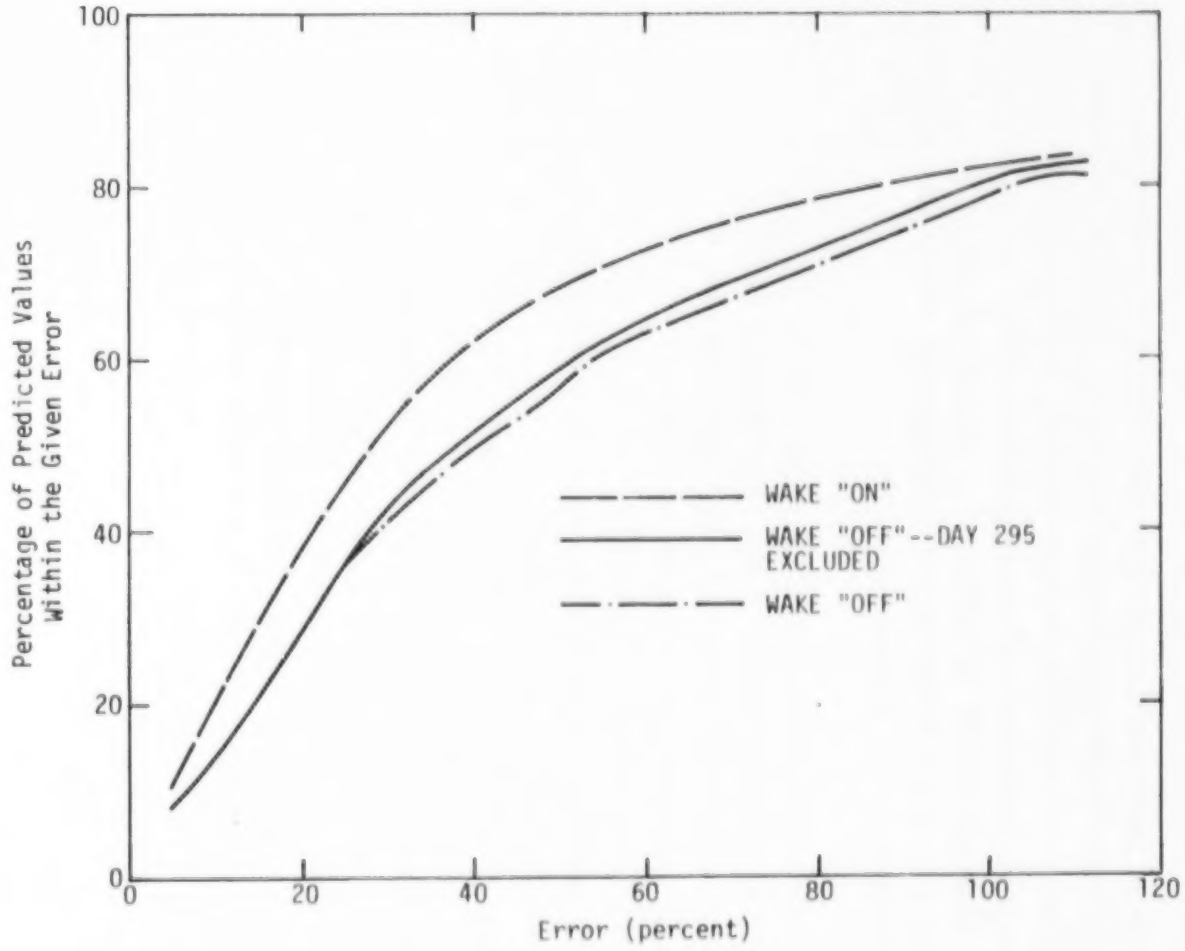

FIGURE 22. DISTRIBUTION OF FRACTIONAL ERROR. The curve labeled "wake 'on'" includes wake parameterization; "wake 'off'" simulations ignore wake effects.

VI SUMMARY

We have developed a model of air pollutant transport, dispersion, and removal processes based on Lagrangian principles. The model requires as inputs estimates of the local friction velocity, the Monin-Obukhov length, the surface roughness, and source emission rates. In applications to pollutant dispersal within 100 meters of a roadway, we showed that the model performs very well provided that the Richardson's number does not exceed approximately 0.25. We also found that

- Vehicle wake turbulence plays a dominant role in dispersing material within 10 meters of roadways when the wind speeds are less than about 1 m/sec and the vehicle speeds are about 20 m/sec or larger.
- The dispersive effects of wake turbulence are greatly reduced when vehicles are closely spaced and the wind is parallel to the roadway.
- Except for situations in which wind speeds are less than 1 m/sec, spatial and temporal variations in material concentration are dominated by ambient turbulence. A correlation coefficient of 0.87 was obtained under these conditions with wake effects ignored entirely. However, the rms error of the estimates is greatly improved if wake effects are taken into account.

APPENDIX A

A SCHEME FOR SIMULATING PARTICLE PAIR MOTIONS IN TURBULENT FLUID

Robert G. Lamb*

Meteorology and Assessment Division
Environmental Sciences Research Laboratory
Environmental Protection Agency
Research Triangle Park, North Carolina 27711

Preprint. Submitted for publication to the
Journal of Computational Physics, 1978

* On assignment with the EPA from NOAA, U.S. Department of Commerce.

APPENDIX A

A SCHEME FOR SIMULATING PARTICLE PAIR MOTIONS IN TURBULENT FLUID

ABSTRACT

A technique is developed and tested for simulating the random motion of particles in turbulent fluid. The technique is applicable to single particles or to pairs of particles whose motions are correlated. The method is intended for use in determining one- or two-particle Lagrangian turbulence statistics from instantaneous velocity fields generated by numerical turbulence models. The technique can also be used as the basis of the Monte Carlo type of models of turbulent diffusion. It requires as inputs the mean, variance, and Lagrangian integral time scale of the turbulence, and for particle pair simulations, it additionally requires the energy dissipation rate of the turbulence.

1. INTRODUCTION

In numerical studies of material dispersion in turbulent fluid, only a portion of the spectrum of fluid motions can be described in a deterministic manner. These motions comprise the largest scales of fluid motion, and their combined effect is represented by the so-called "mean" velocity in the calculation process. The remaining, small scales of motion are regarded as "turbulence" and are treated in various ways. The most common of these in air pollution modeling studies is the eddy diffusivity hypothesis. In this approach, the effects of small-scale velocity fluctuations on the mean material concentration $\bar{c}$ are parameterized by a semi-empirical eddy diffusivity $\underline{K}$ in an equation of the form:

$$\frac{\partial \bar{c}}{\partial t} + \bar{\underset{\sim}{v}} \cdot \nabla \bar{c} = \nabla \cdot \underset{\sim}{K} \nabla \bar{c} + S \quad , \tag{A-1}$$

where $\bar{\underset{\sim}{v}}$ is the "mean" wind vector referred to above and S is the source strength function.

There are numerous situations in which either accurate expressions for $\underset{\sim}{K}$ are unavailable or the eddy diffusivity hypothesis itself is inconsistent with the observed character of material diffusion. An example of the former is the modeling of air pollution on scales of 1000 km or larger. In this case, the "turbulence" comprises eddy sizes up to about 100 km, i.e., roughly the average separation of wind monitoring stations. An eddy diffusivity representative of this portion of the velocity spectrum is not available. An example of a situation in which the eddy diffusivity hypothesis is inconsistent with the character of the diffusion process is unstable boundary layers. Deardorff and Willis (1975) have shown that in free convection the vertical component K_{zz} of $\underset{\sim}{K}$, which intrinsically is a positive quantity, would have to assume negative values to describe the diffusion phenomena observed.

The problems of K-theory can be circumvented by working with Lagrangian diffusion theory. The Lagrangian counterpart of Eq. (A-1) for $\bar{c}$ at a specified point $\underset{\sim}{x}$ and time t is expressed as follows:

$$\bar{c}(\underset{\sim}{x},t) = \int_0^t \iint p(\underset{\sim}{x},t|\underset{\sim}{x}';t')S(\underset{\sim}{x}';t') \, d\underset{\sim}{x}' \, dt' \quad . \tag{A-2}$$

The difficulty with the Lagrangian approach is determining the form of the kernel $p(\underset{\sim}{x},t|\underset{\sim}{x}';t')$, which is the probability density that a material particle released at $\underset{\sim}{x}'$ at time t' will be found at $\underset{\sim}{x}$ at time t. Until recently, the only method of implementing Eq. (A-2) was to assume a form for p. The Gaussian puff and plume formulas are examples of models derived from Eq. (A-2) under the assumption that p has the Gaussian form (see Lamb and Seinfeld, 1973).

Within the last few years, numerical turbulence models have been developed [e.g., Deardorff (1974)] that make it possible to derive Lagrangian turbulence properties such as p computationally. In these models, which explicitly resolve large portions of the spectrum of turbulent motions, particles can be released and tracked at will to obtain the ensembles of particle trajectories required to derive Lagrangian information. Each realization of the ensemble of trajectories needed to compute p is given by:

$$\underset{\sim}{x}(t;\underset{\sim}{x}_0) = \int_0^t \left\{ \tilde{\underset{\sim}{u}}[\underset{\sim}{x}(t';\underset{\sim}{x}_0),t'] + \underset{\sim}{u}'[\underset{\sim}{x}(t';\underset{\sim}{x}_0),t'] \right\} dt' + \underset{\sim}{x}_0 \quad , \tag{A-3}$$

where $\underset{\sim}{x}_0$ denotes the particle release point (at t = 0); $\tilde{\underset{\sim}{u}}(\underset{\sim}{x},t)$ is the resolvable portion of the Eulerian velocity at $(\underset{\sim}{x},t)$, given by the turbulence model; and $\underset{\sim}{u}'(\underset{\sim}{x},t)$ is a random velocity that represents the combined effect of all fluctuations in the instantaneous velocity field that the turbulence model cannot explicitly resolve. In general, $\underset{\sim}{u}'$ represents all velocity variations smaller than the model's grid dimensions. This appendix describes a technique for generating stochastic velocity fields $\underset{\sim}{u}'$ suitable for use in calculating Lagrangian turbulence properties from numerical turbulence data. [For convenience, we shall hereafter refer to $\underset{\sim}{u}'$ as the subgrid-scale (SGS) velocity.]

Approximation of the kernel p can also be obtained using so-called Monte Carlo techniques. With these methods (see Chapter II of this report), p is estimated from an ensemble of particle trajectories created from computer-generated random velocity fields whose statistics are made to satisfy given Eulerian statistical properties of the flow, such as velocity variance profiles, energy dissipation rate profiles, and so on.

For generality, we developed a scheme for generating pairs of correlated velocity functions $\underset{\sim}{u}'_1$, $\underset{\sim}{u}'_2$. Such functions are required to simulate the trajectories $\underset{\sim}{x}_1(t;\underset{\sim}{x}_{10})$ and $\underset{\sim}{x}_2(t;\underset{\sim}{x}_{20})$ of a pair of particles

simultaneously released at points $\underset{\sim}{x}_{10}$, $\underset{\sim}{x}_{20}$ located close enough together that the motions of the particles are correlated for a time. Particle pair trajectory simulations are needed to determine the two particle displacement probability density function $p_2(\underset{\sim}{x},t;\underset{\sim}{x}';t'|\underset{\sim}{x}_{10},t_1;\underset{\sim}{x}_{20},t_2)$ that a pair of particles released at the space-time points $(\underset{\sim}{x}_{10}, t_1)$, $(\underset{\sim}{x}_{20}, t_2)$ will be found at $(\underset{\sim}{x},t)$, $(\underset{\sim}{x}';t')$, respectively. The function p_2 is required to calculate the mean square concentration $\overline{c^2}(\underset{\sim}{x},t)$, viz,

$$\overline{c^2}(\underset{\sim}{x},t) = \int\int\int\int_0^t\int_0^t p_2(\underset{\sim}{x},t;\underset{\sim}{x},t|\underset{\sim}{x}';t';\underset{\sim}{x}'';t'')S(\underset{\sim}{x}';t')S(\underset{\sim}{x}'';t'')\, dt'\, dt''\, d\underset{\sim}{x}'\, d\underset{\sim}{x}'' \quad . \tag{A-4}$$

Shu, Lamb, and Seinfeld (1978) have used this equation in conjunction with p_2 estimates, derived in the manner outlined above from Deardorff's (1974) numerical simulation of the convective planetary boundary layer, to model nonlinear chemical reactions among the constituents of a point source plume and species in the ambient air. Lamb (1976) proposed the concept of a macroturbulence through which historical meteorological data can be used to determine a kernel p_2, which, when combined with Eq. (A-4) yields estimates of air pollution episode probabilities.

Deardorff and Peskin (1970), Riley and Patterson (1974), Lamb, Chen, and Seinfeld (1975), and Lamb (1978b) have computed single-particle displacement statistics using Eq. (A-3) and velocity data $\hat{\underset{\sim}{u}}$ from numerical turbulence models. In all of these studies, the effect of the subgrid-scale velocity $\underset{\sim}{u}'$ were found to be negligible, and they were generally ignored. While it is true that the effects of $\underset{\sim}{u}'$ on the displacement statistics of a single particle are small, if $\underset{\sim}{u}'$ constitutes only a small fraction of the total energy spectrum of fluid motion, the subgrid-scale velocity component $\underset{\sim}{u}'$ plays a dominant role in determining the joint displacement statistics of a pair of particles initially separated by a distance smaller than the dimensions of the grid on which the model data $\underset{\sim}{u}$ are available. This is true even when $\underset{\sim}{u}'$ represents only a small fraction of the total fluid kinetic energy. For this reason, the parameterization of the subgrid velocity field is essential in the

calculation of mean square concentration distributions. Thus, the main uses that we foresee for the two-particle scheme described here are in modeling the mean square concentration by Lagrangian methods, i.e. by using Eq. (A-4) in conjunction with Eulerian velocity data. The scheme will also be of value in implementing Eq. (A-2) when the available velocity data are on such a coarse grid that the subgrid-scale portion of the energy spectrum is significant; and it can be used as well in conjunction with Eq. (A-2) as the basis of Monte Carlo diffusion models.

2. DESIGN OF THE PARAMETERIZATION SCHEME

The basic approach to developing an approximation for the subgrid-scale particle velocities $\underset{\sim}{u}_1'$ and $\underset{\sim}{u}_2'$ is to formulate a rule for generating random functions such that the statistical properties of those functions are equivalent to those that the SGS velocities are known to possess. For example, the mean square subgrid-scale velocity $\overline{u'^2}$ is usually known. Thus, the random functions chosen to represent $\underset{\sim}{u}_1'$ and $\underset{\sim}{u}_2'$ must satisfy $\overline{u_1'^2} = \overline{u_2'^2} = \overline{u'^2}$. The Lagrangian integral time scale of the SGS velocities and certain mean values of particle displacements that they induce may also be known. In this case, the selected random functions $\underset{\sim}{u}_1'$ and $\underset{\sim}{u}_2'$ must have statistical properties that are consistent with all of these known quantities. We outline below the SGS velocity and displacement statistics that are generally known and that serve as constraints on the formulation of the parameterization scheme. For simplicity, we treat only the x-component of the SGS velocity and displacement and ignore cross-correlations among the three vector components. Extensions of the scheme to more general situations are straightforward.

a. Constraints on the Subgrid-Scale Particle Displacements

By definition the mean subgrid-scale velocity u' is zero locally; and although it does not necessarily follow from this definition that the mean SGS particle displacements are zero, nevertheless, we assume that

$$\bar{x}_1(t) = x_{10} \quad , \quad \bar{x}_2(t) = x_{20} \quad , \tag{A-5}$$

where x_{10} and x_{20} denote the release points of particles 1 and 2. This assumption will generate an error roughly proportional to the magnitude of the shear in the deterministic flow speed component $\bar{u}$ at the points x_{10}, x_{20} of release. The mean square SGS particle displacement and separations can be expressed in the following forms:

$$\overline{x_1^2}(t) = \sigma^2(t) + x_{10}^2 \quad , \tag{A-6a}$$

$$\overline{x_2^2}(t) = \sigma^2(t) + x_{20}^2 \quad , \tag{A-6b}$$

$$\overline{\left[x_1(t) - x_2(t)\right]^2} = \overline{\ell^2}(t) + (x_{10} - x_{20})^2 \quad . \tag{A-7}$$

Implicit in Eq. (A-6) is the assumption that x_{10} and x_{20} are sufficiently close together that $\sigma^2(t) = \sigma_2^2(t) = \sigma^2(t)$. For the moment, we assume that $\sigma^2(t)$ and $\ell^2(t)$ are known functions.

To specify the random displacements x_1 and x_2 uniquely, we would have to specify the entire infinite hierarchy of joint moments of these variables. In practical situations, at best only the first- and second-order moments are known. Thus, in developing the SGS parameterization, it suffices to incorporate only Eqs. (A-5) through (A-7) as constraints.

b. General Form of the Displacement Parameterization

Let x_n be the displacement of the n-th particle of a pair (n = 1, 2) produced by our simulation of the turbulence velocity u'. The constraints of Eqs. (A-5) through (A-7) on the statistics of x_n can be satisfied if x_n is of the following form:

$$x_n - x_{n0} = a\xi + bx_n \quad , \quad n = 1, 2 \quad ; \tag{A-8}$$

where a and b are functions of travel time and ξ and x_n are computer-generated random numbers. To satisfy Eq. (A-5), we must have

$$\bar{\xi} = \bar{x}_n = 0 \quad . \tag{A-9}$$

It is also convenient to have ξ and x_n statistically independent and x_1 and x_2 independent of each other. In this case,

$$\overline{\xi x_n} = \bar{\xi}\bar{x}_n = 0 = \overline{x_1 x_2} \quad . \tag{A-10}$$

To satisfy Eq. (A-6), we need

$$\overline{(x_n - x_{n0})^2} = a^2\overline{\xi^2} + b^2\overline{x_n^2} = \sigma^2 \quad , \tag{A-11}$$

and to satisfy Eq. (A-7), we must have

$$\overline{(x_1 - x_2)^2} - (x_{10} - x_{20})^2 = b^2\overline{x_1^2} + b^2\overline{x_2^2} = \overline{\varepsilon^2} \quad . \tag{A-12}$$

If we make

$$\overline{\xi^2} = \sigma^2 \tag{A-13a}$$

$$\overline{x_1^2} = \overline{x_2^2} = \sigma^2 \quad , \tag{A-13b}$$

then it follows that Eqs. (A-5) through (A-7) will be satisfied by Eq. (A-8) if, in addition to Eqs. (A-9), (A-10), and (A-13) we select a and b such that

$$a^2 = 1 - \left(\overline{\xi^2}/2\sigma^2\right) \quad , \tag{A-14a}$$

$$b^2 = 1 - a^2 \quad . \tag{A-14b}$$

c. General Form of the Velocity Parameterization

The algorithm for generating u' is obtained by differentiating Eq. (A-7):

$$u'_n = a\dot{\xi} + \xi\dot{a} + b\dot{\chi}_n + \chi_n\dot{b} \quad . \tag{A-15}$$

With a and b given by Eqs. (A-14a) and (A-14b), respectively, and ξ and χ_n satisfying conditions in Eqs. (A-9), (A-10), and (A-13), Eq. (A-15) constitutes the basis of our parameterization of the subgrid-scale velocity field Next, we must specify the forms of ξ, χ_n, σ^2, and $\overline{\xi^2}$.

In view of conditions in Eq. (A-13), our choice of forms for ξ and χ_n will be guided by our knowledge of σ, which until now we have regarded as a given function. In actuality, we have very little information about the form of σ. We know only that for small times,

$$\sigma^2(t) = \overline{u'^2}t^2 \quad , \quad \text{small } t \quad , \tag{A-16}$$

where $\overline{u'^2}$ is the mean square subgrid-scale velocity fluctuation and t is travel time. The behavior of σ at large times is not known. Lamb (1971) showed that if the turbulence is stationary and the Lagrangian velocity spectrum is a band-pass spectrum, similar to that which the Eulerian spectrum of the SGS velocity is known to be, then in the limit of large travel times the mean square particle displacement σ approaches a constant value. This is in marked contrast to the effect that a white noise velocity spectrum would produce, namely $\sigma^2 \sim t$ in the limit of large travel times. Whether the SGS velocities produce a constant, a linearly increasing, or an altogether different dispersion σ^2 in the limit of large travel

times is not known, but we expect that the details of the variations in the long-time regime are not crucial. Even if particles are released near a boundary where the SGS velocities constitute a significant fraction of the total turbulence, by the time the dispersion enters the long-time regime the particles will have moved into a region of the fluid where the resolvable scale, rather than the SGS, motions dominate the particle displacements. Proceeding under this assumption, we adopt expressions for the velocities $\dot{\xi}$ and $\dot{\chi}_n$ that are consistent with Eqs. (A-16) and (A-9) and with estimates of the Lagrangian integral time scale $\mathcal{T}$ of the SGS velocity field. The long term statistical behavior of ξ and χ_n that result from these specifications will be regarded as best estimates of σ^2 [cf. Eq. (A-13)].

In the context of the Monte Carlo type of models of diffusion, the previous comments do not apply because there u' represents the entire spectrum of turbulent motion. In this case Eq. (A-16) holds for small t and $\sigma^2 \sim t$ applies in the limit $t \to \infty$. The scheme described here replicates both these regimes.

Since the statistical properties of ξ and χ_n are identical, for simplicity we treat only ξ in the following discussion. A suitable expression for $\dot{\xi}$ is the Markov-1 form

$$\dot{\xi}(t_n) = \alpha\dot{\xi}(t_{n-1}) + \beta\rho_\xi(t_n) \quad , \tag{A-17}$$

where $t_n = n\Delta t$, Δt is the time step used in the diffusion simulation, α and β are constants, and $\rho_\xi(t_n)$ is a random variable with the following properties:

$$\bar{\rho}_\xi(t) = 0 \tag{A-18a}$$

$$\overline{\rho_\xi(t_n)\dot{\xi}(t_m)} = 0 \quad , \quad n \neq m \quad , \tag{A-18b}$$

$$\overline{\rho_\xi(t_n)\rho_\xi(t_m)} = 0 \quad , \quad n \neq m \quad . \tag{A-18c}$$

The first of these is necessary to satisfy Eq. (A-9).

Through straightforward analyses, we find that with $\dot{\xi}$ given by Eq. (A-17), its autocorrelation is

$$\overline{\dot{\xi}(t_n)\dot{\xi}(t_{n-m})} = \alpha^m \overline{\dot{\xi}^2}(t_{n-m}) \quad , \tag{A-19}$$

and its mean square varies temporally as

$$\overline{\dot{\xi}^2}(t_n) = \alpha^2 \overline{\dot{\xi}^2}(t_{n-1}) + \beta^2 \overline{\rho_\xi^2}(t_n) \quad . \tag{A-20}$$

Consider for the moment the case of stationary, homogeneous turbulence:

$$\overline{\dot{\xi}^2}(t) = \overline{u'^2}(t) = \text{Constant} \quad , \tag{A-21}$$

where $\overline{u'^2}$ is the mean square SGS velocity fluctuation. To ensure that Eq. (A-21) is satisfied when Eq. (A-17) is used to describe particle velocities in stationary, homogeneous turbulence, we must set [see Eq. (A-20)]

$$\alpha^2 + \beta^2 = 1 \quad , \tag{A-22}$$

$$\overline{\rho_\xi^2}(t) = \overline{u'^2} \tag{A-23}$$

and the initial values of $\dot{\xi}$ must be selected such that

$$\overline{\dot{\xi}^2}(0) = \overline{u'^2} \quad . \tag{A-24}$$

The Lagrangian integral time scale T_ξ of $\dot{\xi}$, which is defined by

$$T_\xi = \frac{1}{\overline{u'^2}} \sum_{m=0}^{\infty} \dot{\xi}(t_n)\dot{\xi}(t_{n+m})\Delta t \quad , \tag{A-25}$$

acquires a particularly simple value in stationary, homogeneous turbulence, namely [see Eqs. (A-19) and (A-21)],

$$T_\xi = \Delta t \sum_{m=0}^{\infty} \alpha^m = \frac{\Delta t}{1 - \alpha} \tag{A-26}$$

Thus, in applications to stationary, homogeneous SGS velocity fields with prescribed values of T_ξ and $\overline{u'^2}$, the parameterization scheme must satisfy for given Δt:

$$\alpha = 1 - \frac{\Delta t}{T_\xi} \quad , \tag{A-27}$$

$$\beta = (1 - \alpha^2)^{1/2} \quad , \tag{A-28}$$

and ρ_ξ and $\dot{\xi}(0)$ must satisfy Eqs. (A-23) and (A-24).

In many cases of applied interest, the SGS field is stationary but not homogeneous. In this case,

$$\overline{\dot{\xi}^2}(t_n) \neq \overline{\dot{\xi}^2}(t_m) \quad , \quad n \neq m \quad . \tag{A-29}$$

If we were to apply the parameterization scheme to problems of this type, we could continue to use Eqs. (A-24), (A-27), and (A-28) to specify $\dot{\xi}(0)$, α, and β, but we would have to require that ρ_ξ satisfy [see Eq. (A-20)]

$$\overline{\rho_\xi^2}(t_{n+1}) = \frac{\overline{u'^2}(x_{n+1}) - \alpha^2\overline{u'^2}(x_n)}{\beta^2} \quad , \tag{A-30}$$

where $\overline{u'^2}(x_m)$ denotes the mean square SGS velocity at the location x_m of a particle at time $t = m\Delta t$ on any given realization. Placing this condition as a constraint on the random variable ρ_ξ is undesirable because, during the execution of the scheme on the computer, Eq. (A-30) would require a square root calculation, which is time consuming; and in regions of highly inhomogeneous SGS fields, Eq. (A-30) might require (for a given Δt) that $\overline{\rho_\xi^2} < 0$. For these reasons, we adopt the following approximation:

$$\overline{\rho_\xi^2}(t_n) = \overline{u'^2}(x_n) \quad . \tag{A-31}$$

It can be shown that the error incurred through the use of this approximation in inhomogeneous turbulence is negligible if

$$\Delta t << \left(\left| \nabla \overline{u'^2}^{1/2} \right| \right)^{-1} \quad . \tag{A-32}$$

For example, in the unstable surface layer where $\overline{w'^2} \sim (z/L)^{2/3}$ [see Panofsky et al. (1977)], the right side of this expression has a value of about 100 sec at $z = 10$ m when $L = -25$ m and $u_* = 0.1$ m/sec. In short Eq. (A-17) can be applied to inhomogeneous SGS velocity fields provided that the time step Δt used in this equation satisfies Eq. (A-32) where $\overline{u'^2}$ denotes the mean square SGS velocity as a function of space.

When the parameterization scheme is implemented, a random number generator is used to produce values of ρ_ξ. The mean and variance of this function are specified by Eqs. (A-18) and (A-31), respectively. It should be kept in mind that the right-hand side of Eq. (A-31) is a known, local property of the SGS velocity field.

A Gaussian random number generator can be used to produce ρ_ξ in the Monte Carlo type of models applied to neutrally stratified flows because

turbulent velocity fluctuations are known to be normally distributed in this case (Batchelor, 1953). The Gaussian generator should also be appropriate in simulating subgrid-scale turbulence in both neutrally and unstably stratified flows provided that the grid size is much smaller than the scale of the energy-containing eddies. However, the joint distribution of turbulence velocities at two sufficiently close points is not normally distributed under any conditions (Batchelor, 1953). Thus, the use of jointly normal random number generators in the parameterization scheme will result in errors in the joint statistics of the particle pair displacements, but this error is probably no larger than that incurred from other assumptions in the scheme.

Generating random numbers with a Gaussian distribution requires more computer time than that needed to generate uniformly distributed random numbers. Therefore, it is advantageous to use a uniform random number to index a table of numbers configured in such a way that the numbers retrieved from the table have a Gaussian distribution with zero mean and unit variance. This technique requires less than half of the machine time required to generate Gaussian numbers using conventional algorithms.

In conclusion, $\dot{\xi}(t_n)$ is given by Eq. (A-17) with α and β specified by Eqs. (A-27) and (A-28), respectively. The random variable ρ_ξ has a Gaussian distribution with zero mean and variance given by Eq. (A-31). If the time step Δt satisfies Eq. (A-32), Eq. (A-17) can be applied to inhomogeneous SGS velocity fields.

The equivalence of the statistical properties of $\dot{\xi}$ and $\dot{x}_n$ suggests that an expression similar to Eq. (A-17) should be suitable for producing $\dot{x}_n$. In particular, if

$$\dot{x}_n(t_m) = \alpha \dot{x}_n(t_{m-1}) + \beta \rho_n(t_m) \quad , \qquad \text{(A-33)}$$

where α and β are given by Eqs. (A-27) and (A-28), respectively, and

$$\overline{\rho_n^2}(t_m) = \overline{u'^2}(x_m) \quad , \tag{A-34}$$

$$\overline{\dot{x}_n^2}(0) = \overline{\rho_n^2}(0) = \overline{u'^2}(x_{n0}) \quad , \tag{A-35}$$

then all of the conditions imposed on $\dot{x}_n$, namely Eqs. (A-9), (A-10), and (A-13b), are satisfied. Note that $T_\chi = T_\xi = T$, where T is the Lagrangian integral time scale of the SGS velocity. The expressions for ξ and x_n follow immediately from those of $\dot{\xi}$ and $\dot{x}_n$:

$$\xi(t_n) = \xi(0) + \sum_{m=0}^{n-1} \dot{\xi}(t_m)\Delta t \quad , \tag{A-36}$$

$$x_n(t_m) = x_n(0) + \sum_{k=0}^{m-1} \dot{x}_n(t_k)\Delta t \quad . \tag{A-37}$$

These equations together with Eqs. (A-15), (A-17), and (A-33) constitute the basis of our parameterization scheme. All that remains to render these equations operational is to express the functions a and b in terms of available quantities and to check whether the scheme produces the proper particle behavior near reflective boundaries.

d. The Velocity Parameterization at Reflective Boundaries

The Markov form of the velocity parameterization we have chosen imparts a "memory" of approximate length T to the motion of each particle. Consequently, a particle that has a positive velocity, say, just prior to its striking a reflective boundary, is more likely to have a positive velocity after impact than a negative one; and hence it is more likely to strike the boundary a second time than to move away. As a result, the particle will linger at the boundary. This phenomenon is manifested in diffusion simulations by fictitiously large particle concentrations at all reflective surfaces.

Actually, turbulent eddies that carry particles into a wall are most likely dissipated by viscous forces near the wall and, consequently, the memory they impart to particles is lost. We can approximate this effect in the parameterization scheme by modifying the expression for ξ, $\dot{\xi}$, χ_n, and $\dot{\chi}_n$ as follows:

$$\left.\begin{aligned} \xi(t_m) &= \chi_n(t_m) = 0 \\ \dot{\xi}(t_m) &= \rho_\xi(t_m) \\ \dot{\chi}_n(t_m) &= \rho_n(t_m) \end{aligned}\right\} \quad \text{if reflection occurred during } t_{m-1} \leq t < t_m \quad , \tag{A-38}$$

where ρ_ξ and ρ_n are Gaussian random numbers with zero means and variances $\overline{\rho_\xi^2} = \overline{\rho_n^2} = \overline{u'^2}(\chi_m)$, where $\overline{u'^2}(\chi_m)$ denotes the mean square SGS velocity at the particle's location at time t. Equation (A-38) is used only after reflection. At all other times, Eqs. (A-17), (A-33), and (A-37) are used. Tests of this boundary modification have shown that it eliminates the erroneous accumulation of particles at the boundaries.

e. Specification of the Parameters a and b

When two particles are separated by a distance that is larger than the largest turbulent eddies, the random motions of those particles are uncorrelated. In this case, it is easy to show that $\overline{\ell^2} = \sigma_1^2 + \sigma_2^2$ (= σ^2 in the present situation). At the other extreme where the particles are released at virtually the same time and locations, they never separate (under the action of turbulence alone), and thus, $\overline{\ell^2}$ remains zero for all time. These two limiting cases indicate that a, as given by Eq. (A-14a), ranges in value from unity for particles whose motions are totally correlated to zero for those whose velocities are statistically independent. These observations indicate that in the limit of large travel times, as the mean particle separation becomes large compared with the grid size, the function a approaches zero. In order to determine the initial value of a and the manner in which it approaches its final value, we need explicit expressions for σ^2 and $\overline{\ell^2}$.

Like σ, $\overline{\ell^2}$ is a parameter about which we have little information. Using Kolmogorov's similarity hypothesis, Batchelor (1950) showed that if the initial separation ℓ_0 of two particles lies in the inertial subrange, then for small times:

$$\overline{\ell^2} = \frac{10}{3} c_1 \ell_0^{2/3} \epsilon^{2/3} t^2 \quad , \quad t \ll \ell_0^{2/3} \epsilon^{-1/3} \quad , \tag{A-39}$$

where c_1 is a constant on the order of 1, ϵ is the energy dissipation rate of the turbulence, and t is travel time. In Deardorff's (1974) turbulence model, $\Delta = (\Delta x \Delta y \Delta z)^{1/3}$ (where Δx, Δu, and Δz are the grid cell dimensions) lies in the inertial subrange; so Eq. (A-39) should apply for all ℓ_0 less than Δ but large enough that viscous effects are unimportant.

Deardorff and Drake (1975) suggest the semi-empirical formula

$$\epsilon = E^{3/2}\left(\frac{0.7G}{\Delta}\right) \tag{A-40}$$

$$G = 1 + \frac{2}{\left(\frac{z}{\Delta z} + \frac{3}{2}\right)^2 - 3.3} \quad , \quad z \geq \frac{\Delta z}{2} \quad , \tag{A-41}$$

where z is elevation above ground and E is the SGS kinetic energy. By combining Eqs. (A-14a), (A-16), (A-39), and (A-40) and by assuming isotropy of the SGS velocity field, i.e., $\overline{u'^2} = 2/3E$, we obtain

$$a_0 = a(t_0) = 1 - (0.7G)^{2/3}\left(\frac{\ell_0}{\Delta}\right)^{2/3} \quad . \tag{A-42}$$

For convenience, we have chosen $c_1 = 2/5$. It is interesting that the initial value of a is independent of E. The indicated dependence of a_0 on ℓ_0 is consistent with the fact that $a_0 \to 1$ as $\ell_0 \to 0$, but Eq. (A-42) cannot be valid for $\ell_0 >> \Delta$ because it yields large negative values for a. Although it is possible that a could achieve a small negative value, in our applications of the parameterization scheme we assume that $0 \leq a \leq 1$.

In addition to deriving Eq. (A-39), Batchelor obtained an expression for the temporal variation of $\overline{\ell^2}$ during the intermediate time period $t >> \ell_0^{2/3} \epsilon^{-1/3}$ with t small enough that the particle separation is small compared with the scale of the energy-containing eddies of the turbulence. We could utilize this information to help describe the behavior of a(t) between its initial and final values, but this approach would be of very limited use. Because it is applicable only in the range $\ell_0 << \overline{\ell^2}^{1/2} << \Delta$, this additional information would be of value only when ℓ_0 is several orders of magnitude smaller than Δ. Rather than piece together an expression for a(t), we adopt a single, ad hoc formulation that is consistent with available information.

Specifically, we note from Eq. (A-42) that the slope of a(t) is zero at t = 0. Also, we expect that $\Delta^{2/3}\epsilon^{-1/2}$ must be proportional to the characteristic time scale of a(t). This information and the known initial and final values of a(t) can all be taken into account by the following simple formulas:

$$a(t) = a_0 \exp(-A) \quad , \tag{A-43a}$$

$$A = \int_0^t \frac{t'}{T^2(t')\, dt'} \quad , \tag{A-43b}$$

$$T(t) = \frac{\lambda\Delta}{E^{1/2}(t)} \quad , \tag{A-43c}$$

where E(t) is the SGS kinetic energy at the centroid of the particle pair at time t, and λ is a constant. Observational studies of mean square concentration fluctuations $\overline{c^2}$ in turbulent pipe flows indicate that $\overline{c^2}/\bar{c}^2$ is self-similar over a considerable region downstream of the source. Lamb (1977) speculates that this is a characteristic feature of dispersion in decaying turbulence and has shown that it implies that $\overline{\ell^2}/\sigma^2$ = constant. [To simulate this condition with our parameterization, we would need a = constant, which in turn would require that the constant in Eq. (A-43c) have a very large value. In a future study, we plan to investigate the value of λ in some detail.

If the scheme developed here were used in a Monte Carlo model of diffusion in the planetary boundary layer, in place of Eq. (A-40) one would need the $\varepsilon(z)$ profile appropriate for boundary layer turbulence (see Wyngaard and Cote, 1971); and in place of $\overline{u'^2} = 2/3E$, one might use the $\overline{u'^2}(z)$ profiles given by Panofsky et al. (1977). This approach is described in this report in Chapter IV.

f. Recapitulation

For convenience, we summarize below the complete parameterization scheme for the two-particle subgrid-scale velocities u_1' and u_2'.

$$u_n'(t_m) = a(t_m)\dot{\xi}(t_m) + \xi(t_m)\dot{a}(t_m) + b(t_m)\dot{\chi}_n(t_m) + \chi_n(t_m)\dot{b}(t_m) \quad , \quad n = 1, 2 \quad ;$$

$$\dot{\xi}(t_m) = \begin{cases} \rho_\xi(t_m) \quad , & \text{if a reflection of either particle occurred during } t_{m-1} \le t < t_m; \\ \alpha\dot{\xi}(t_{m-1}) + \beta\rho_\xi(t_m) \quad , & \text{otherwise.} \end{cases}$$

$$\xi(t_m) = \begin{cases} 0 \quad , & \text{if reflection of either particle occurred during } t_{m-1} \le t < t_m; \\ \xi(t_{m-1}) + \dot{\xi}(t_{m-1})\Delta t \quad . \end{cases}$$

$$\dot{\chi}_n(t_m) = \begin{cases} \rho_n(t_m) \quad , & \text{if a reflection of particle n occurred during } t_{m-1} \le t < t_m; \\ \alpha\dot{\chi}_n(t_{m-1}) + \beta\rho_n(t_m) \quad , & \text{otherwise.} \end{cases}$$

$$\chi_n(t_m) = \begin{cases} 0 \quad , & \text{if reflection of particle n occurred during } t_{m-1} \le t < t_m; \\ \chi_n(t_{m-1}) + \dot{\chi}_n(t_{m-1})\Delta t. \end{cases}$$

Initial values are $\dot{\xi}(0) = \rho_\xi(0)$, $\xi(0) = 0$, $\dot{\chi}_n(0) = \rho_n(0)$, and $\chi_n(0) = 0$. Here, $\rho_n(t)$ $(n = 1, 2)$ and $\rho_\xi(t)$ are Gaussian random numbers with zero means and mean square $\overline{\rho_\xi^2}(t)$, and so on equal to the mean square subgrid-scale velocity $\overline{u'^2}$ at the location of the particle at time t. The parameters α and β are given by Eqs. (A-27) and (A-28), a and $\mathring{a}$ are given by Eq. (A-43), and b and $\mathring{b}$ are specified by Eq. (A-14b).

3. RESULTS OF TEST CALCULATIONS

In Figure A-1, we show that the scheme gives the correct temporal variation in the rms separation of particle pairs when we set the parameter $a(t) = a_0 =$ constant [see Eq. (A-14a)]. In this case Eq. (A-14a) gives $\overline{\ell^2} \sim \sigma^2$. This relationship is clearly satisfied by the rms particle separation values shown in Figure A-1 that were determined from the simulation. Also, by comparing the curves given in Figure A-1 for the case $a_0 = 0$, i.e., uncorrelated motion of the particle pairs, with the σ_x profiles shown in Figure 6 (Chapter III), one can see that the parameterization scheme reproduces correctly the limiting relationship

$$\lim_{t \to \infty} \overline{\ell^2}(t) = 2\sigma^2(t) \quad .$$

The reader is referred to Chapter III for results of single particle displacement statistics and concentration fields simulated using the technique developed here.

4. CONCLUSION

We have developed a method of generating pairs of random velocity fields suitable for simulating particle pair motions in turbulent fluid. The scheme can be used to simulate the effects of subgrid-scale turbulence in situations in which one is interested in determining Lagrangian turbulence statistics from instantaneous velocity fields obtained from a numerical turbulence model; or the scheme can be used as the basis of a

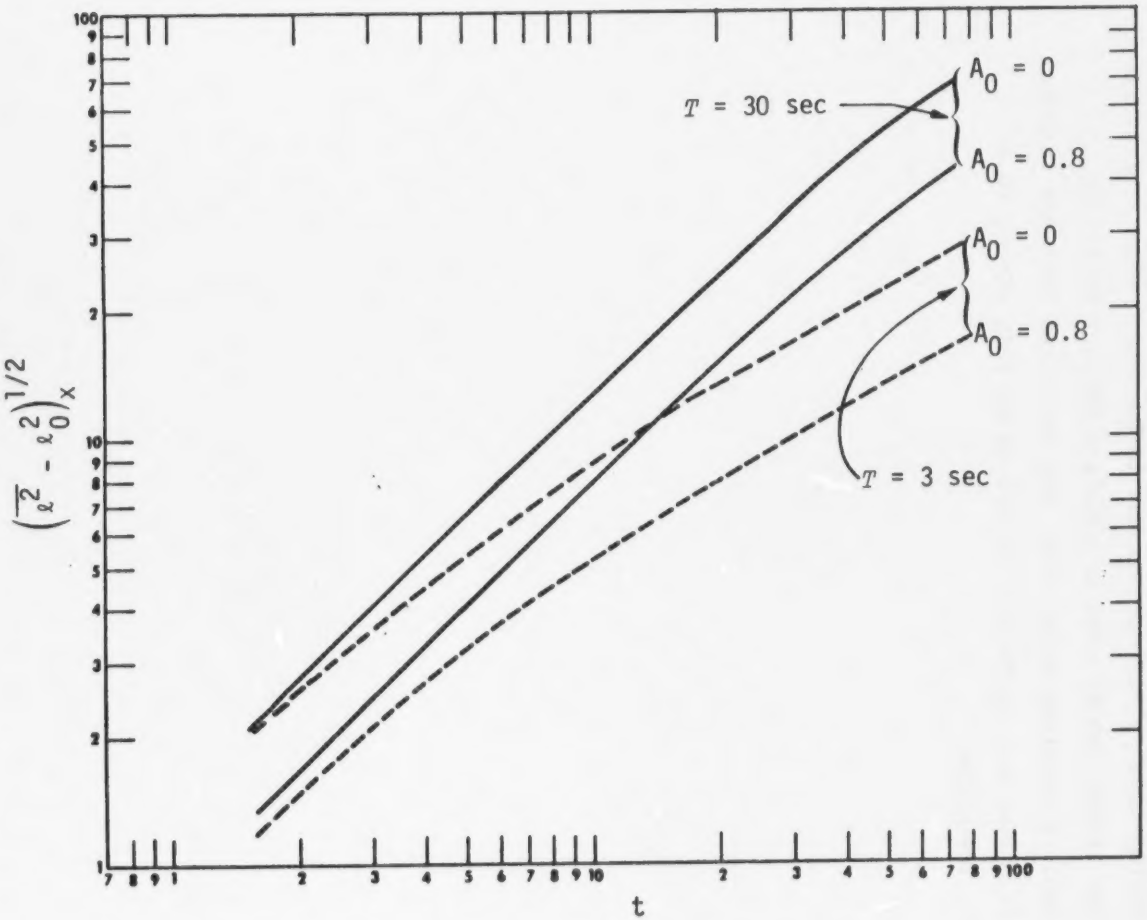

FIGURE A-1. STREAMWISE COMPONENT $(\overline{\ell^2} - \ell_0^2)_x^{1/2}$ OF THE rms SEPARATION OF SIMULATED PARTICLE MOTIONS UNDER THE CONDITIONS $\bar{u} = 3.0$, $\overline{u'^2} = 1$, AND $\overline{w'^2} = 0.6$ (MKS UNITS) FOR TWO VALUES OF THE PARAMETER a_0

Monte Carlo model of turbulent dispersion, in situations in which one attempts to determine Lagrangian turbulence statistics from Eulerian statistics. The inputs to the scheme include the profiles of mean wind and variances of the turbulence velocities, the Lagrangian integral time scale, and the energy dissipation rate of the turbulence. With very simple modifications, the scheme can be used to simulate buoyant particles, particles with nonzero settling velocities, and particles that are absorbed or resuspended from boundary surfaces. We are using this scheme in all of the roles described here.

APPENDIX B

USER'S GUIDE TO THE LAGRANGIAN HIGHWAY MODEL

APPENDIX B
USER'S GUIDE TO THE LAGRANGIAN HIGHWAY MODEL

The theoretical aspects of the highway model are discussed in the main text of this document. This appendix presents a short discussion of the use of the model. Although the computer program was coded using American National Standards Institute (ANSI) FORTRAN IV, there are some machine-dependent portions that the user must check to ensure that the program will work properly on his computer system. These are discussed in Section 3.

1. DESCRIPTION OF THE INPUT CARDS

Five sets of input cards must be used to run the computer program:

- Overall control cards
- Monitor site cards
- Meteorological data cards
- Source location card
- Miscellaneous data cards.

These sets are discussed in turn below.

a. Overall Control Cards

Four control cards must be placed at the beginning of the input deck. Card No. 1 contains the number of simulations to be performed. Two parameters are entered on this card: the first is the number of the first experiment (usually 1), and the second is the number of the last experiment. Thus the user wishing to perform three simulations must specify 1 and 3 in Columns 5 and 10 on Card 1. The two variables are entered as five-digit integer variables. The format for the Card 1 is given in Table B-1.

TABLE B-1. FORMAT FOR CARD 1

Variable	Column	Format	Description
NSTART	1-5	I5	The number of the first simulation
NSTOP	6-10	I5	The number of the last simulation

Card 2, the second card in the input deck, contains the title of the simulations. The title may be up to 72 characters.

Cards 3 and 4 in the input deck contain 21 variables (12 on the first and 9 on the second). Each variable and the format for that variable are described in Table B-2.

b. Monitor Site Cards

The calculated P1 and P2 kernels (and ultimately the concentration of pollutant at each monitor site) are stored for each monitor site. Therefore a simulation is not performed unless there is at least one monitor site. The maximum number of monitors is 100. The format for the monitor site cards is given in Table B-3. One card is entered for each monitor site, and these cards are placed after Card 4. Although the program can handle up to four lanes, the computer cost increases with the number of lanes. If the lanes are located symmetrically about the center of the roadway, the user can create pseudo-stations to reduce the number of lanes to be treated. (This procedure is discussed in the main text.) The pseudo-sites will monitor the P1 and P2 calculations for the extra lanes.

c. Meteorological Data Cards

Meteorological data are read from two cards. The first, Card 6A, is described in Table B-4.

TABLE B-2. FORMAT FOR CARDS 3 AND 4

(a) Card 3

Variable	Column	Format	Description
LFILE	1	I1	Option to save data on an external file
LGRID	2	I1	Option to print calculated results on a grid
LPRNT	3	I1	Option to print input data
NPLT	4	I1	Option to plot particle trajectories
LMET	5	I1	Option to print calculated meteorological data
NDATA	6	I1	Flag for comparison of calculated data and observed data
NX	11-15	I5	Number of cells in the x-direction
NZ	16-20	I5	Number of cells in the z-direction
XMAX	21-25	F5.0	Length of the region in the x-direction (in meters)
ZMAX	26-30	F5.0	Length of the region in the z-direction (in meters)
STRTIM	31-35	F5.0	Starting time of the simulation
ENDTIM	36-40	F5.0	Ending time of the simulation

TABLE B-2 (Concluded)

(b) Card 4

Variable	Column	Format	Description
NMON	1-5	I5	Number of monitors
NSAMP	6-10	I5	Sampling number of convergence test (recommended value is 7)
NITER	11-15	I5	Number of 100 iterations used for sampling (recommended value is 7)
NRLMX	16-20	I5	Maximum number of iterations for each simulation
TOL	21-30	F10.0	Error tolerance at each monitor site
SMPDIM	31-40	F10.0	Sampling dimensions of each monitor
SEPR	41-50	F10.0	Separation between the two paired particles
MONSGS	54	L1	Option to activate printing of particle statistics
MONWAK	55	L1	Option to activate printing of particle statistics caused by the wake turbulence

TABLE B-3. FORMAT FOR THE MONITOR SITE CARDS (CARDS 5)

Variable	Column	Format	Description
NAMMON(I)	1-4	A4	Name of the i-th monitor (if any
XMON(I)	6-15	F10.2	Location of the i-th monitor in the x-direction
ZMON(I)	16-25	F10.2	Location of the i-th monitor in the z-direction

TABLE B-4. FORMAT FOR THE FIRST METEOROLOGICAL DATA CARD (CARD 6A)

Variable	Column	Format	Description
ZØ	1-5	F5.0	Surface roughness
ZI	6-10	F5.0	Inversion height
ANEHMT	11-20	F10.1	Anemometer height
OBUKOV	21-30	F10.1	Monin-Obukhov length
USTAR	31-40	F10.1	Friction velocity
WNDSPD	41-50	F10.1	Mean wind speed
WNDANG	51-60	F10.1	Mean wind angle perpendicular to the roadway
DTDZ	61-70	F10.1	Vertical temperature gradient

The user may enter experimental data to compare with model predictions by including Card 6B (see Table B-5) and an external file called TAPE 10. The meteorological parameters read from the external file will replace the meteorological parameters read on Card 6A.

d. Source Location Card

The location and description of the roadway is entered on Cards 7, after the meteorological data. The format for Cards 7 is given in Table B-6. All distances and heights on Cards 7 are entered in units of meters.

e. Miscellaneous Data Cards

Three cards are required for miscellaneous data, as described in Table B-7. The data entered on Card 7 control the simulation time. Card 9 contains parameters that describe the wake turbulence profile. Card 10 contains descriptions of the vehicles found on each lane.

2. SAMPLE INPUT DECK

A sample input deck is presented in Table B-8. In this example, the input data are those used in the simulations of the GM experiments. Users may wish to use these data for their initial simulations.

3. COMPUTER-DEPENDENT PARAMETERS AND SUBROUTINES

The Highway Program requires approximately 44,000 decimal words to load on the CDC 7600 computer. This number may vary among computer systems, and some users may find the program too large for their system. However, certain routines that handle input-output options can be eliminated by making them dummy routines. Consider, for example, routine SGSMON, which is coded as follows:

TABLE B-5. FORMAT FOR THE SECOND METEOROLOGICAL DATA CARD (CARD 6B)

Variable	Column	Format	Description
(TITLE(I),I=12,14)	4-15	3A4	Title of the experiment
OBUKOV	16-25	F10.2	Observed Monin-Obukhov length
USTAR	26-35	F10.2	Observed friction velocity
WNDSPD	36-45	F10.2	Observed wind speed
WNDANG	46-55	F10.2	Observed mean wind angle perpendicular to the roadway
DTDZ	56-66	E11.2	Observed vertical temperature gradient
Next card:			
(STREN(I),I=1,4)	1-44	4E11.2	Source strength from each lane of the roadway
Next cards:			
(SF6(I),I=1,20)	1-72	9F8.3	Observed concentrations (up to nine on each card)

TABLE B-6. FORMAT FOR THE SOURCE LOCATION CARD (CARD 7)

Variable	Column	Format	Description
NLANE	1-10	I10	Number of lanes on the roadway (maximum = 4)
LANILO	11-20	F10.1	Location of the first lane (in meters from the origin)
DELTAL	21-30	F10.1	Distance between the centers of the lanes
TRUCKH	31-40	F10.1	Height of source emissions from a truck
AUTOH	41-50	F10.1	Height of source emissions from an automobile

TABLE B-7. FORMAT FOR THE MISCELLANEOUS DATA CARDS (CARDS 8, 9, AND 10)

(a) Card 8

Variable	Column	Format	Description
DELTAT	1-5	F5.0	Time step (in seconds)
BETA	6-10	F5.0	Time decay multiplier of AØ
TIMSCL	11-20	F10.1	Lagrangian integral time scale
AØ	21-30	F10.1	Boundary layer initial particle separation coefficient

(b) Card 9

Variable	Column	Format	Description
TIMWAK	1-5	F5.0	Lagrangian integral time scale of the wake component
AØWAKE	6-10	F5.0	Boundary layer initial particle separation coefficient due to the wake turbulence
BETAWK	11-20	F10.0	Time decay multiplier of AØWAKE
UWKCOF	21-30	F10.0	Coefficient of the u-component of the wake turbulence
WWKCOF	31-40	F10.0	Coefficient of the w-component of the wake turbulence

(c) Card 10*

Variable	Column	Format	Description
VEHWD(I)	1-5	F5.0	Width of the vehicle in the i-th lane
VEHSPD(I)	6-10	F5.0	Speed of the vehicle in the i-th lane
DRGCOF(I)	11-20	F10.1	Drag coefficient of the vehicle in the i-th lane

* One Card 10 is entered for each lane specified in Card 7.

TABLE B-8. SAMPLE INPUT DECK USED IN THE GM SIMULATIONS

```
    1   63
                                GM EXPERIMENT NO.
111111      100    30 350.   90.1000.1100.
   69     7  100 3000      .05        3.0        0.0      FF
11          104.4        9.38
12          104.4        3.31
13          104.4        0.31
21          132.3        9.30
22          132.3        3.63
23          132.3        0.36
31          147.1        9.38
32          147.1        3.03
33          147.1        0.36
41          163.6        9.63
42          163.6        3.61
43          163.6        0.31
31          174.8        9.30
32          174.8        3.48
33          174.8        0.36
61          189.8        9.60
62          189.8        3.84
63          189.8        0.38
73          209.8        0.36
83          239.8        0.36
11P         101.0        9.38
12P         101.0        3.31
13P         101.0        0.31
21P         129.1        9.30
22P         129.1        3.63
23P         129.1        0.36
31P         143.7        9.38
32P         143.7        3.03
33P         143.7        0.36
41P         160.2        9.63
42P         160.2        3.61
43P         160.2        0.31
31P         171.4        9.30
32P         171.4        3.48
33P         171.4        0.36
61P         186.4        9.60
62P         186.4        3.84
63P         186.4        0.38
73P         206.4        0.36
83P         236.4        0.36
41           83.8      9.38
42           83.8      3.31
43           83.8      0.31
444         113.9      9.3
434         113.9      3.6
464         113.9      0.6
32          136.0      9.3
33          136.0      3.3
33          136.0      0.3
60          241.2      0.3
44           82.4      9.38
44           82.4      3.3
43           82.4      0.3
64          110.3      9.3
63          110.3      3.6
66          110.3      0.3
67          125.1      9.3
68          125.1      3.3
69          125.1      0.3
70          141.6      9.3
```

TABLE B-8 (Concluded)

```
    1   63
                                  GM EXPERIMENT NO.
111111       100    30 330.  90.1000.1100.
   69     7  100 3000      .05        3.0        0.0      FF
61          141.6      3.3
61          141.6      0.3
63          132.8      9.3
64          132.8      3.3
63          132.8      0.3
66          167.8      9.3
67          167.8      3.3
68          167.8      0.3
80          237.8      0.3
  .03 300.        10.3      -2.72        .20        1.9       2.32      .0028
         1     136.1        18.6         1.         1.         .8
  0.8  1.0       30.          0.
  0.0  0.8        1.0    0.008       0.008
  2.3 22.2     .3
```

```
SUBROUTINE SGSMON
COMMON . . .
.
.
.
RETURN
END
```

This routine can be made into a dummy by simply eliminating the code between the second card and the RETURN card:

```
SUBROUTINE SGSMON
RETURN
END
```

If the user is interested only in the predicted results, the following routines can be made into dummy routines:

METRRT
WAKMON } should be kept for testing purposes
SGSMON
ERPRNT
WRITGD
GRID
CONVT
PLTRAJ
FRAME
AXES
MNSTAT--used only if experimental data are entered

An option of the Highway Program is an off-line plot (CALCOMP) of the first 20 realizations of the first 100 particle trajectories. If this option is used, standard CALCOMP routines must be supplied by the user:

NUMBER
LINE
PLOT
SYMBOL
PLOTS

If the user does not have the facility for off-line plotting, he must create dummy routines for each of the above.

The Highway Program requires the use of a random number generator to generate a number between 0 and 1. This is done through the use of the system routine for the random number generator. On the CDC computer the random number generator function is called RANF(Ø). This function varies between computer systems. Therefore, the user must rewrite the statement

RANUM(X)=RANF(X)*GMAX

found in subroutines SGSSET and ADVECT. The card should be changed to

RANUM(X)=(user's random number function)*GMAX

REFERENCES

Batchelor, G. K. (1953), The Theory of Homogeneous Turbulence (University Press, Cambridge, United Kingdom).

_____ (1950), "The Application of the Similarity Theory of Turbulence to Atmospheric Diffusion," Quart. J. Roy. Meteor. Soc., Vol. 76, pp. 133-146.

Binkowski, F. S. (1978), "Consistency of a Semi-empirical Theory for Turbulence in the Atmospheric Surface Layer," Atmos. Environ., in press.

Cadle, S. H., et al. (1976), "Results of the GM Sulfate Dispersion Experiment," GMR-2107, General Motors Corporation, Warren, Michigan.

Chock, D. P. (1977), "General Motors Sulfate Dispersion Experiment: Assessment of the EPA HIWAY Model," J. Air Poll. Contr. Assoc., Vol. 27, No. 1, pp. 39-45.

Danard, M. B. (1972), "Numerical Modeling of Carbon Monoxide Concentrations Near Highways," J. Appl. Meteor., Vol. 11, pp. 947-957.

Deardorff, J. W. (1974), "Three-Dimensional Numerical Study of the Height and Mean Structure of a Heated Planetary Boundary Layer," Bound. Layer Meteor., Vol. 7, pp. 81-106.

Deardorff, J. W., and M. A. Drake (1975), "Boundary Layer Data from a Numerical Integration in Three Dimensions," National Center for Atmospheric Research, Boulder, Colorado.

Deardorff, J. W., and R. L. Peskin (1970), "Lagrangian Statistics from Numerically Integrated Turbulent Shear Flow," Phys. Fluids, Vol. 13, pp. 584-595.

Deardorff, J. W., and G. E. Willis (1975), "A Parameterization of Diffusion into the Mixed Layer," J. Appl. Meteor., Vol. 14, pp. 1451-1458.

Draxler, R. R. (1976), "Determination of Atmospheric Diffusion Parameters," Atmos. Environ., Vol. 10, pp. 99-105.

Egan, B. A., A. Epstein, and M. Keefe (1973), "Development of Procedures To Simulate Motor Vehicle Pollution Levels," Department of Highways and Traffic, Washington, D.C. (NTIS PB-233-938).

Eskridge, R. E., and K. L. Demerjian (1977), "A Highway Model for the Advection, Diffusion and Chemical Reaction of Pollutants Released by Automobiles," Preprint Volume, Joint Conference on Applications on Air Pollution Meteorology, American Meteorological Society, 29 November-2 December 1977, Salt Lake City, Utah.

Lamb, R. G. (1978a), "Mathematical Principles of Turbulent Diffusion Modeling," Lectures presented at the International School of Atmospheric Physics, 13-27 February, 1978, Erice, Sicily, Environmental Protection Agency, Research Triangle Park, North Carolina, in press.

_____ (1978b), "A Numerical Simulation of Dispersion from an Elevated Point Source in the Convective Planetary Boundary Layer," Atmos. Environ., Vol. 12, pp. 1297-1304.

_____ (1977), "Continued Research in Mesoscale Air Pollution Simulation Modeling--Vol. VI: Further Studies in Modeling Microscale Phenomena," EF77-143, Systems Applications, Incorporated, San Rafael, California.

_____ (1976), "The Calculation of Long-Term Atmospheric Pollutant Concentration Statistics Using the Concept of a Macro-Turbulence," Preprint Volume, Third Symposium on Atmospheric Turbulence, Diffusion, and Air Quality, American Meteorological Society, Raleigh, North Carolina.

_____ (1973), "Note on the Application of K-Theory to Diffusion Problems Involving Nonlinear Chemical Reactions," Atmos. Environ., Vol. 7, pp. 257-263.

_____ (1971), "Numerical Modeling of Urban Air Pollution," Ph.D. Thesis, University of California, Los Angeles, California (available from University Microfilm, Ann Arbor, Michigan).

Lamb, R. G., and J. H. Seinfeld (1973), "Mathematical Modeling of Urban Air Pollution: General Theory," Environ. Sci. Technol., Vol. 7, pp. 253-261.

Lamb, R. G., and W. R. Shu (1978), "A Model of Second-Order Chemical Reactions in Turbulent Fluid," Atmos. Environ., Vol. 12, pp. 1685-1694.

Lamb, R. G., W. H. Chen, and J. H. Seinfeld (1975), "Numerico-Empirical Analyses of Atmospheric Diffusion Theories," J. Atmos. Sci., Vol. 32, pp. 1794-1807.

Monin, A. S., and A. M. Yaglom (1971), Statistical Fluid Mechanics (MIT Press, Cambridge, Massachusetts).

Morse, P. M., and H. Feshback (1953), Methods of Theoretical Physics, p. 795 (McGraw-Hill Book Company, New York, New York).

Panofsky, H. A., et al. (1977), "The Characteristics of Turbulent Velocity Components in the Surface Layer Under Convective Conditions," Bound. Layer Meteor., Vol. 11, pp. 355-361.

Ragland, K. W. (1973), "Multiple Bay Model for Dispersion of Air Pollutants from Area Sources," Atmos. Environ., Vol. 7, pp. 1017-1032.

Ragland, K. W., and J. J. Pierce (1975), "Boundary Layer Model for Air Pollutant Concentrations Due to Highway Traffic," J. Air Poll. Contr. Assoc., Vol. 25, No. 1, pp. 48-51.

Riley, J. J., and G. S. Patterson, Jr. (1974), "Diffusion Experiments with Numerically Integrated Isotropic Turbulence," Phys. Fluids, Vol. 17, pp. 292-297.

Shu, W. R., R. G. Lamb, and J. H. Seinfeld (1978), "A Model of Second-Order Chemical Reactions in Turbulent Fluid--Part II: Application to Atmospheric Plumes," Atmos. Environ., Vol. 12, pp. 1695-1706.

Taylor, G. I. (1921), "Diffusion by Continuous Movements," Proc. London Math. Soc., Vol. 20, pp. 196-212.

Teske, M. E., and W. S. Lewellen (1978), "Prediction of Estimated Highway Emissions by a Second-Order Closure Model," Draft Report, Environmental Protection Agency, Research Triangle Park, North Carolina.

Wyngaard, J. C., and O. R. Cote (1971), "The Budgets of Turbulent Kinetic Energy and Temperature Variance in the Atmospheric Surface Layer," J. Atmos. Sci., Vol. 28, pp. 190-201.

Zimmerman, J. R., and R. S. Thompson (1975), "User's Guide for HIWAY, a Highway Air Pollution Model," EPA-650/4-74-008, Environmental Protection Agency, Research Triangle Park, North Carolina.